VOL. 107 NO. GT11. NOV. 1981

JOURNAL OF THE GEOTECHNICAL ENGINEERING DIVISION

PROCEEDINGS OF
THE AMERICAN SOCIETY
OF CIVIL ENGINEERS

VOL.107 NO.GT11. NOV. 1981

JOURNAL OF THE GEOTECHNICAL ENGINEERING DIVISION

PROCEEDINGS OF THE AMERICAN SOCIETY OF CIVIL ENGINEERS

ISSN 0093-6405

William F. Marcuson III, Editor
U.S. Army Engineers

AMERICAN SOCIETY OF CIVIL ENGINEERS

CONTENTS

The Journal of the Geotechnical Engineering Division (ISSN 0093-6405) is published monthly by the American Society of Civil Engineers. Publications office is at 345 East 47th Street, New York, N.Y. 10017. Address all ASCE correspondence to the Editorial and General Offices at 345 East 47th Street, New York, N.Y. 10017. Allow six weeks for change of address to become effective. Subscription price to members is $16.00. Nonmember subscriptions available; prices obtainable on request. Second-class postage paid at New York, N.Y. and at additional mailing offices. GT.

POSTMASTER: Send address changes to American Society of Civil Engineers, 345 East 47th Street, New York, NY 10017.

The Society is not responsible for any statement made or opinion expressed in its publications.

DISCUSSION

Proc. Paper 16614

INFORMATION RETRIEVAL

The key words, abstract, and reference "cards" for each article in this Journal represent part of the ASCE participation in the EJC information retrieval plan. The retrieval data are placed herein so that each can be cut out, placed on a 3 × 5 card and given an accession number for the user's file. The accession number is then entered on key word cards so that the user can subsequently match key words to choose the articles he wishes. Details of this program were given in an August, 1962 article in CIVIL ENGINEERING, reprints of which are available on request to ASCE headquarters.

*Discussion period closed for this paper. Any other discussion received during this discussion period will be published in subsequent Journals.

STATEMENT OF OWNERSHIP

The *Journal of the Geotechnical Engineering Division* is edited and published by the American Society of Civil Engineers, with general business offices at 345 East 47th Street, New York, N.Y. 10017. The Manager of Technical and Professional Publications is Richard R. Torrens.

This Journal is owned wholly by the American Society of Civil Engineers, a nonprofit educational and professional organization with about 78,000 members. There are no individual owners or stockholders.

	Average No. Copies Each Issue During Preceding 12 Months	Single Issue Nearest To Filing Date
Total no. copies printed (net press run)	10,767	10,626
Paid mail circulation	8,477	8,887
Sales through dealers and counter sales	None	None
Free distribution	None	None
Total distribution	8,477	8,887
Left Over (extra for new orders, office use, etc.)	2,290	1,739
Total	10,767	10,626

I certify that the above statements made by me are correct and complete.—Richard R. Torrens, Manager of Technical and Professional Publications.

16635 NONLINEAR LATERAL DYNAMIC STIFFNESS OF PILES

KEY WORDS: **Dynamic response; Dynamics; Foundations; Lateral loads (piles);** Piles; Soil dynamics; **Soil properties; Soil-structure interaction;** Stiffness; Vibration

ABSTRACT: The effect of nonlinear soil behavior (without slippage of gapping) on the dynamic response of piles subjected to lateral loads is explored, using a finite element model for the soil region adjoining the pile, a consistent boundary matrix at some distance to reproduce radiation effects, and an iterative, equivalent linearization technique to estimate the variation of soil properties with level of strain. Results obtained with this procedure are compared with those that would result from application of the p-y curves and the differences are discussed.

REFERENCE: Angelides, Demosthenes C. (Sr. Consulting Struct. Engr., Research and Development Div., McDermott Inc., P.O. Box 60035, New Orleans, La. 70160), and Roesset, Jose M., "Nonlinear Lateral Dynamic Stiffness of Piles," *Journal of the Geotechnical Engineering Division,* ASCE, Vol. 107, No. GT11, **Proc. Paper 16635**, November, 1981, pp. 1443-1460

16634 COUPLED HEAT AND WATER FLOWS AROUND BURIED CABLES

KEY WORDS: Backfills; **Buried cables; Computer analysis;** Diffusion; **Field tests; Heat transfer;** Numerical analysis; **Soil moisture;** Temperature distribution; **Temperature gradients**

ABSTRACT: Theoretical and experimental studies of heat flow and moisture movement under thermal gradients are described with particular emphasis on flows around buried electrical transmission cables. A one-dimensional finite difference computer program for analysis of coupled heat and water flows in layered systems based on the Philip and DeVries theory is developed. Theoretical analysis indicate that the most important parameters affecting rate and amount of moisture migration away from buried heat sources are the sources temperature and the soil type. A field test was conducted to evaluate the heat and moisture flow predictive methods. The results showed that water content predictions using the coupled flow computer program match poorly with the actual values, and that predicted values are very sensitive to the soil properties used. A finite element two-dimensional computer program is used to predict the variation of temperature distributions around the buried cable with time after initiation of cable heating. The results show very good agreement between measured and predicted temperature contours.

REFERENCE: Abdel-Hadi, Omar N. (Geotechnical Engr., Geotechnical Consultants, Inc., San Francisco, Calif.), and Mitchell, James K., "Coupled Heat and Water Flows Around Buried Cables," *Journal of the Geotechnical Engineering Division,* ASCE, Vol. 107, No. GT11, **Proc. Paper 16634**, November, 1981, pp. 1461-1487

16628 TOLERABLE SETTLEMENT OF BUILDINGS

KEY WORDS: **Allowable settlement; Buildings;** Damage; Field investigations; Foundation settlement; **Settlement (structural);** Soil mechanics; **Subsidence**

ABSTRACT: Current practices and concepts for establishing the tolerable settlement of buildings are reviewed. The role of differential settlement is emphasized. Most current tolerance limits are shown to be based on the works of Skempton, MacDonald, Polshin, and Tokar. These criteria are compared with field observations of settlement and damage. A simple beam analogy, which was proposed by Burland and Wroth, is used to illustrate factors that influence tolerable settlement. The effects of the critical tensile strain of the structural materials, the L/H ratio of the building, the relative stiffness of the structure in shear and bending, the longitudinal stiffness of the foundation, and the shape of the settlement pattern are demonstrated. Different criteria are required for different types of structures. The allowable settlement is smallest for cases in which the settlement curve is concave downward.

REFERENCE: Wahls, Harvey E. (Prof. of Civ, Engrg., North Carolina State Univ., Raleigh, N. C.), "Tolerable Settlement of Buildings," *Journal of the Geotechnical Engineering Division,* ASCE, Vol. 107, No. GT11, **Proc. Paper 16628**, November, 1981, pp. 1489-1504

16636 INSTABILITY OF AMUAY CLIFFSIDE

KEY WORDS: **Case reports;** Clays; **Cliffs;** Field investigations; **Laboratory tests; Landslides;** Perched water; Pore pressure; **Stability analysis**

ABSTRACT: This paper presents a case study of cliffside instability. Geotechnical analyses employing field measurements and laboratory test results obtained over a 30-yr period indicate that rising pore pressures trigger slides along the cliff. Visual observation, surveys, and field exploration show that most of the landslides have wedge-type failure geometry. Shear occurs through a nearly horizontal stratum of weak clay, brown fat clay. The strength of the fat clay decreases with deformation. Fluids generated by domestic and industrial activities have resulted in a perched water layer above the stratum of fat clay. For more than two decades, the pore pressure on top of the fat clay has risen. A wedge type of stability analysis can give the correct factor of safety — i.e., 1.0 — for the slides which have occurred.

REFERENCE: Lambe, T. William (Prof., Dept. of Civ. Engrg., Massachusetts Inst. of Tech., Cambridge, Mass. 02139), Silva, Francisco, and Marr, W. Allen, "Instability of Amuay Cliffside," *Journal of the Geotechnical Engineering Division,* ASCE, Vol. 107, No. GT11, **Proc. Paper 16636,** November, 1981, pp. 1505-1520

16663 FRICTION CAPACITY OF PILES DRIVEN INTO CLAY

KEY WORDS: **Clay soils; Friction resistance; Penetration;** Pile foundations; **Pile friction;** Pile loading tests; Static pile formula

ABSTRACT: Several studies on axial pile capacity in clays have shown that the average frictional resistance, expressed as a fraction of the average undrained shear strength or average effective overburden pressure, decreases with increasing pile penetration. Procedures to compute shaft friction are reviewed, and the effect of pile length on the development of shaft friction on piles in clay is examined in terms of the relative pile-soil stiffness and lateral pile movements during installation. Correlations are developed to relate shaft friction coefficients α β λ to pile length, relative pile-soil stiffness, and soil stress history. Procedures are recommended to compute the friction capacity of piles in clay.

REFERENCE: Kraft, Leland M. (Mgr., Special Projects Group, McClelland Engrs, Inc., Houston, Tex.), Focht, John A., Jr., and Amerasinghe, Srinath F., "Friction Capacity of Piles Driven into Clay," *Journal of the Geotechnical Engineering Division,* ASCE, Vol. 107, No. GT11, **Proc. Paper 16663,** November, 1981, pp. 1521-1541

16653 THEORETICAL T-Z Curves

KEY WORDS: **Axial loads;** Field data; Laboratory tests; Piles; **Pile settlement; Predicting; Responses;** Settlement analysis; Stress; Subgrades

ABSTRACT: Most procedures to compute the t-z (stress-displacement) response for axial pile loading are empirical, based mostly on data for pile diameters less than 18 in. (0.15 m) and pile penetrations less than 100 ft (30 m). These procedures may not be appropriate for pile and soil conditions that differ from those on which the procedures were developed. Therefore, a theoretical procedure is developed to generate t-z curves for predicting pile movements under axial load. The procedure uses an approximate one-dimensional, elastic continuum approach to define the t-z response up to the maximum t response and laboratory simulation to define the post-peak response. The procedure was used with several case studies. Predicted response of the pile under axial loading was in good agreement with the measured response.

REFERENCE: Kraft, Leland M., Jr. (Mgr., Special Projects Group, McClelland Engrs., Inc., Houston, Tex. 77081), Ray, Richard P., and Kagawa, Takaaki, "Theoretical t-z Curves," *Journal of the Geotechnical Engineering Division,* ASCE, Vol. 107, No. GT11, **Proc. Paper 16653,** November, 1981, pp. 1543-1561

16652 SEEPAGE FROM FREEWATER ABOVE TAILINGS

KEY WORDS: Complex variables; **Dams (earth);** Mine wastes; **Mining;** Models; **Seepage; Soil mechanics;** Tailings

ABSTRACT: A proposed model for seepage discharge into a porous embankment from free water above impermeable tailings is described. It is assumed that the discharge is controlled by saturated seepage in an entry zone adjacent to the free water interface. The isotropic entry zone has been analysed by complex variable methods and a general solution obtained for seepage discharge quantities. Application of the solution to anisotropic embankments is described. The significance of the theoretical results for design is discussed and a simple formula proposed for estimating the discharge.

REFERENCE: Isaacs, Lewis T. (Sr. Lect., Dept. of Civ. Engrg., Univ. of Queensland, Brisbane, Australia), and Hunt, Bruce, "Seepage From Freewater Above Impermeable Tailings," *Journal of the Geotechnical Engineering Division,* ASCE, Vol. 107, No. GT11, **Proc. Paper 16652,** November, 1981, pp. 1563-1577

U.S. Customary-SI Conversion Factors

In accordance with the October, 1970 action of the ASCE Board of Direction, which stated that all publications of the Society should list all measurements in both U.S. Customary and SI (International System) units, the following list contains conversion factors to enable readers to compute the SI unit values of measurements. A complete guide to the SI system and its use has been published by the American Society for Testing and Materials. Copies of this publication (ASTM E-380) can be purchased from ASCE at a price of $3.00 each; orders must be prepaid.

All authors of *Journal* papers are being asked to prepare their papers in this dual-unit format. To provide preliminary assistance to authors, the following list of conversion factors and guides are recommended by the ASCE Committee on Metrication.

To convert	To	Multiply by
inches (in.)	millimeters (mm)	25.4
feet (ft)	meters (m)	0.305
yards (yd)	meters (m)	0.914
miles (miles)	kilometers (km)	1.61
square inches (sq in.)	square millimeters (mm^2)	645
square feet (sq ft)	square meters (m^2)	0.093
square yards (sq yd)	square meters (m^2)	0.836
square miles (sq miles)	square kilometers (km^2)	2.59
acres (acre)	hectares (ha)	0.405
cubic inches (cu in.)	cubic millimeters (mm^3)	16,400
cubic feet (cu ft)	cubic meters (m^3)	0.028
cubic yards (cu yd)	cubic meters (m^3)	0.765
pounds (lb) mass	kilograms (kg)	0.453
tons (ton) mass	kilograms (kg)	907
pound force (lbf)	newtons (N)	4.45
kilogram force (kgf)	newtons (N)	9.81
pounds per square foot (psf)	pascals (Pa)	47.9
pounds per square inch (psi)	kilopascals (kPa)	6.89
U.S. gallons (gal)	liters (L)	3.79
acre-feet (acre-ft)	cubic meters (m^3)	1,233

NONLINEAR LATERAL DYNAMIC STIFFNESS OF PILES

By Demosthenes C. Angelides,[1] A. M. ASCE and José M. Roësset,[2] M. ASCE

INTRODUCTION

Several procedures have been developed in recent years to determine the dynamic response of piles subjected to horizontal or vertical loads of relatively small amplitude, and where the soil can be assumed to behave as a linear elastic material. Most of these theories yield very similar results indicating that the key features of the problem are now well understood.

It has been long recognized, however, that nonlinear effects, such as nonlinear soil behavior, slippage, and eventual gapping, play a fundamental role in the response of piles to cyclic loads of moderate to large amplitude. These characteristics have been implicitly incorporated in models of piles as beams on elastic foundation where the Winkler type springs are given by the *p-y* or *t-z* curves.

The concept of the *p-y* curves was introduced initially by McClelland and Focht (12) as the first significant attempt to model nonlinear behavior in the resistance of soil to lateral deflection of piles. Matlock and Reese (10) extended this approach using a finite difference formulation to discretize the pile and the nonlinear foundation. Matlock (11) presented *p-y* curves and their analytical expressions for soft clays, and Reese, et. al., (15,16) established similar curves for stiff clays. A distinction was made by Matlock (11) between static (implying monotonic) and cyclic loading. The cyclic loading *p-y* curves deviate from the static ones when the deflection at the mudline reaches a limiting value due to cyclic degradation of the soil. It should be noted that these cyclic *p-y* curves represent an envelope of the cyclic behavior, and do not describe explicitly the reduction of stiffness of the soil as a function of the magnitude of the force for a transient excitation, nor as a function of the number of cycles for harmonic loading.

More recently, Stevens and Audibert (18), by analyzing previous experimental information from several sources, suggested modification of the *p-y* curves given by Matlock (11). They recommended a different relation between the characteristic

[1]Sr. Consulting Struct. Engr., Research and Development Div., McDermott Inc., P.O. Box 60035, New Orleans, La. 70160.

[2]Prof. of Civ. Engrg., The Univ. of Texas at Austin, Austin, Tex. 78712.

Note.—Discussion open until April 1, 1982. To extend the closing date one month, a written request must be filed with the Manager of Technical and Professional Publications, ASCE. Manuscript was submitted for review for possible publication on February 25, 1981. This paper is part of the Journal of the Geotechnical Engineering Division, Proceedings of the American Society of Civil Engineers, ©ASCE, Vol. 107, No. GT11, November, 1981. ISSN 0093-6405/81/0011-1443/$01.00.

soil deflection, y_c, i.e., the deflection at one half the ultimate soil resistance, and the pile diameter, and a modification of the ultimate lateral soil resistance coefficient, N_p.

Methods of dynamic pile analysis based on *p-y* curves can treat nonlinearities quite realistically; they cannot directly handle, however, soil inertia or radiation damping effects.

In this paper an attempt is made to explore the effect of nonlinear soil behavior (without slippage or gapping) on the dynamic response of piles subjected to lateral loads, using a finite element model for the soil region adjoining the pile, a consistent boundary matrix at some distance to reproduce radiation effects, and an interative equivalent linearization technique to estimate the variation of soil properties with level of strain. Results obtained with this procedure are compared with those derived from application of the *p-y* curves and the differences are examined.

Description of Model

The main model used in this study is an extension of the formulation presented by Blaney, et. al, (4) for the linear elastic case. A cylindrical region of soil surrounding the pile (Fig. 1) is discretized using toroidal finite elements. The consistent boundary matrix derived by Kausel (7) for problems in cylindrical coordinates is placed at the edge of the core region. The pile is modeled as a series of beam segments attached through rigid links to the finite element nodes.

An iterative equivalent linearization is applied to the elements of the core region, following the same general method used by Seed and Idriss (17) for seismic studies of soil deposits (one-dimensional pure shear condition), and implemented in such well known programs as LUSH (8) and FLUSH (9) for two-dimensional or pseudo-three-dimensional conditions. In each cycle of analysis, soil properties are assumed to be constant, with a shear modulus, G, and a hysteretic damping ratio, D_s, consistent with the amplitude of the shear strain, $\gamma_{r\theta}$, obtained as a result of the previous cycle. The selection of this strain is clearly arbitrary. Moreover, the value of this strain changes in the circumferential direction with the sine of the angle θ, but the model assumed a single set of values of G and D_s for each toroidal element, making them, therefore, independent of θ and equal to the values that would occur at $\theta = \pm 90°$.

In addition to the finite element model, special purpose computer programs were developed discretizing the pile with linear members and replacing the soil with lumped springs at the nodes. The spring characteristics were derived from Matlock's and Stevens and Audibert's *p-y* curves. For both models, hollow, steel piles with aspect ratio (length, L, over diameter, d) equal to 45, diameters of 4 ft, 2 ft and 1 ft, and thicknesses of 2.5 in., 1.25 in., and 0.625 in., respectively, were considered. These result in a value of $K_r = E_p I / E_s L^4$ of 1.82×10^{-5} for all cases, with E_p the pile modulus of elasticity, E_s the soil modulus of elasticity, L the length of pile, and I its moment of inertia.

Since the objective of this study was to observe trends in behavior, no attempt was made to simulate any particular soil profile. Even so, it was desirable to have soil properties reasonably typical of soft clays. One of the problems encountered in comparing results of analytical or numerical formulations based

on the theory of elasticity with those of *p-y* curves is to select consistent values of soil parameters. For the finite element solution, the soil behavior is characterized by the shear modulus, and its variation with shear strain; a second elastic constant, such as the bulk modulus and the total unit weight, is required to compute the shear wave velocity. The *p-y* curves, on the other hand, are normally developed from the undrained shear strength, the effective (submerged) unit weight of the soil, and a characteristics strain, ϵ_{50}, which is equal to the strain at one-half the maximum deviator stress in an undrained laboratory triaxial test. The relationship between shear modulus and undrained shear strength is not easily established. It was decided, therefore, to use a soil for which

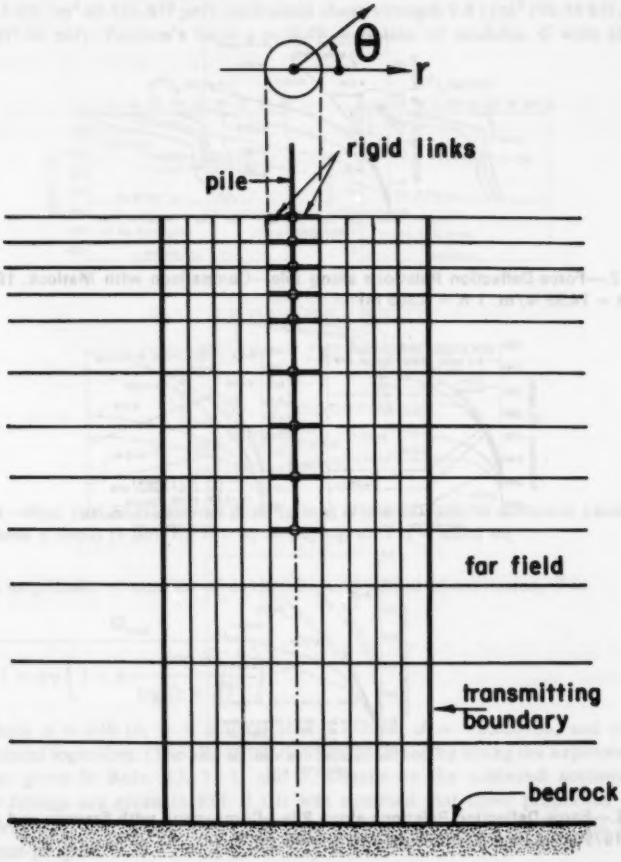

FIG. 1.—Geometry of Problem

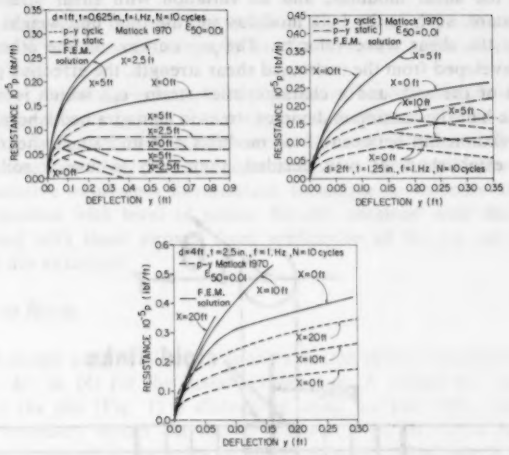

FIG. 2.—Force-Deflection Relations along Pile—Comparison with Matlock, 1970 (1 lbf/ft = 14.59 N/m; 1 ft = 0.305 m)

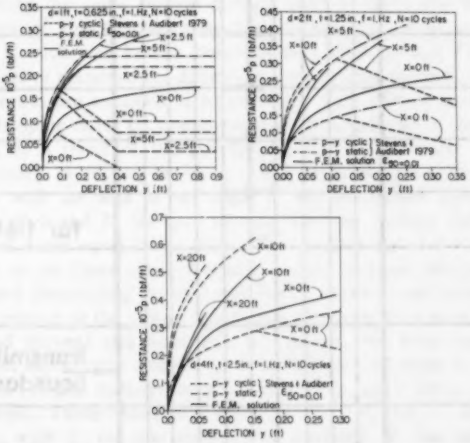

FIG. 3.—Force-Deflection Relations along Pile—Comparison with Stevens and Audibert, 1979 (1 lbf/ft = 14.59 N/m; 1 ft = 0.305 m)

experimental information was available. The desired data were the undrained shear strength, the dynamic shear modulus at small strains, and the variation of this modulus with shear strain amplitude, number of cycles, and frequency (or period) of the excitation. The soil selected is a plastic, overconsolidated clay with an overconsolidation ratio of 4, extensively studied by NGI (13) and Andersen (1,2). This experimental information provided the variation of shear modulus with number of cycles, N, and shear strain amplitude, γ. To account for the effect of frequency, data reported by Fisher, et. al, (5) for a plastic clay with the same overconsolidation ratio and very similar characteristics were used.

The soil properties used for the analysis were: modulus $G_{max} = 1{,}600\ t/m^2$ (15,734 kN/m^2 or 328,477 psf); undrained shear strength 9.8 t/m^2 (96.14 kN/m^2 or 2,007.06 psf); Poisson's ratio $\nu = 0.49$; variation of modulus G with shear

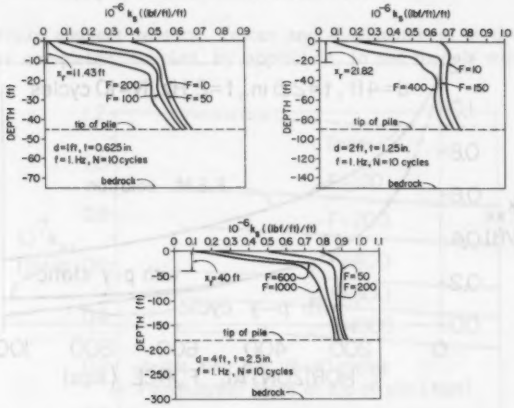

FIG. 4.—Real Part of Horizontal Soil Springs Versus Depth for Different Levels of Pile Force F (kips) [1 (lbf/ft)/ft = 47.84 (N/m)/m; 1 ft = 0.305 m]

strain amplitude, γ, number of cycles, N, and period of excitation, T is

$$G = \frac{G_{max}}{1 + a\gamma\left(1 + b\dfrac{\log N}{\log (c + dT)}\right)} \quad \ldots\ldots\ldots\ldots\ldots\ldots\ldots\ldots\ldots\ldots (1)$$

in which $a = 216.16$; $b = 0.1038$; $c = 2.777988$; $d = -0.059706$; and log = the natural logarithm. (The above relation was obtained by fitting the experimental curves given in Refs. 13, 2, 1, and 5. Details on the achieved accuracy in these fittings are given in Ref. 3.) It was assumed that these properties were uniform over the soil deposit, 300 ft deep. The value of γ used in the finite element program is that of γ_{re} previously explained.

Following Hardin and Drnevich (6), the relation between the hysteretic damping ratio, D_s, and the shear modulus was taken as

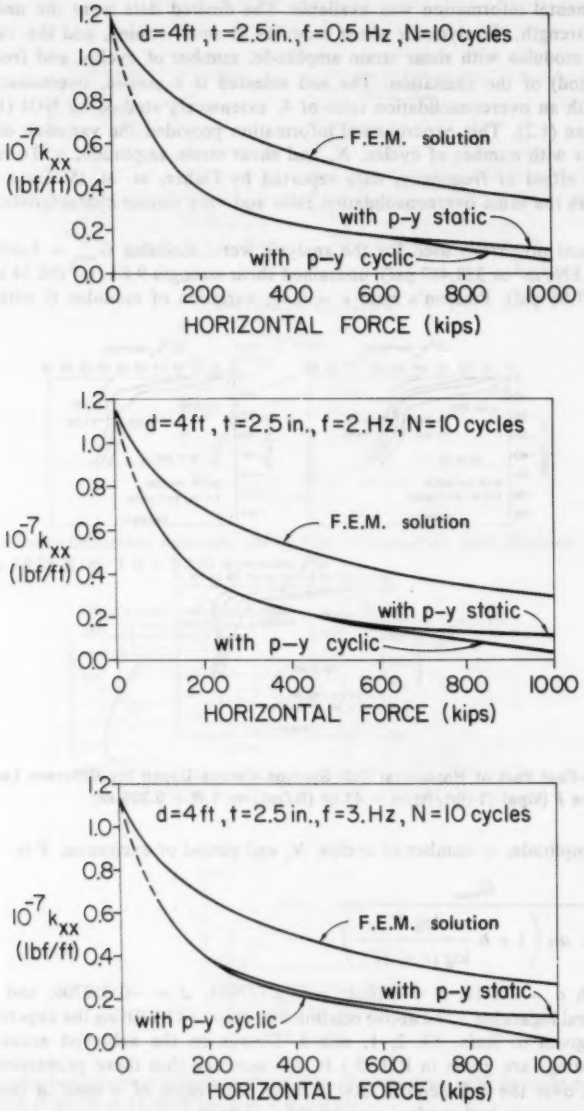

FIG. 5.—Variation of k_{xx} with Level of Force, for Different Frequencies (1 lbf/ft = 14.59 N/m; 1 kip = 4.45 kN; 1 ft = 0.305 m)

$$D_s = D_{max}\left(1 - \frac{G}{G_{max}}\right) \quad \ldots\ldots\ldots\ldots\ldots\ldots\ldots\ldots\ldots\ldots\ldots\ldots\ldots\ldots (2)$$

No information was available on the value of D_{max} for the soil selected. Hardin and Drnevich suggest for saturated cohesive soils an expression for D_{max} which is a function of the effective mean principal stress, $\bar{\sigma}_0$, the number of cycles, N, and the frequency of excitation, f:

$$D_{max} = 0.31 - (0.03 + 0.0003f)\bar{\sigma}_0^{1/2} + 0.015f^{1/2} - 0.0065 \log N \ldots\ldots\ldots (3)$$

in which $\bar{\sigma}_0 = kg/cm^2$. Since the modulus G_{max} had been considered constant over the depth of the soil layer, it was decided to take also a constant D_{max}, neglecting the effect of $\bar{\sigma}_0$.

Equivalent Soil Springs

In the finite element solution, forces and displacements in the soil along the pile are completely coupled, by opposition, to the models where Winkler

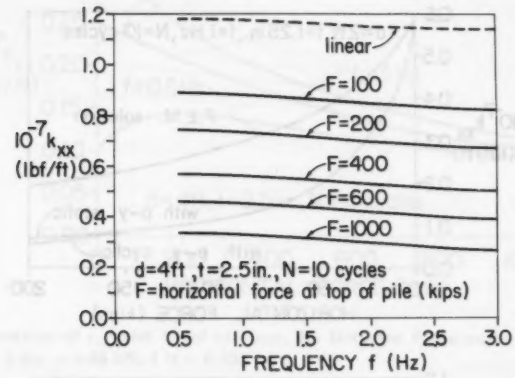

FIG. 6.—Variation of k_{xx} with Frequency, for Different Levels of Force (1 lbf/ft = 14.59 N/m; 1 kip = 4.45 kN; 1 ft = 0.305 m)

springs are lumped at a discrete number of nodes. To establish a comparison with the *p-y* curves, the stiffness matrix of the soil cavity, corresponding to a given level of forces at the head of the pile (computed with the final iterated soil properties), was multiplied by the nodal displacements along the pile to obtain equivalent soil forces. The resulting force deformation relations are then a function of the deformed shape and, therefore, of the relative stiffness of the pile with respect to the soil.

In Fig. 2, the force-deflection relations obtained with this procedure are presented and compared to the *p-y* curves, derived from Matlock's (11) rules, for three pile diameters and three locations along the piles. The forces resulting from the finite element model for a given deflection are 2–2.5 times larger

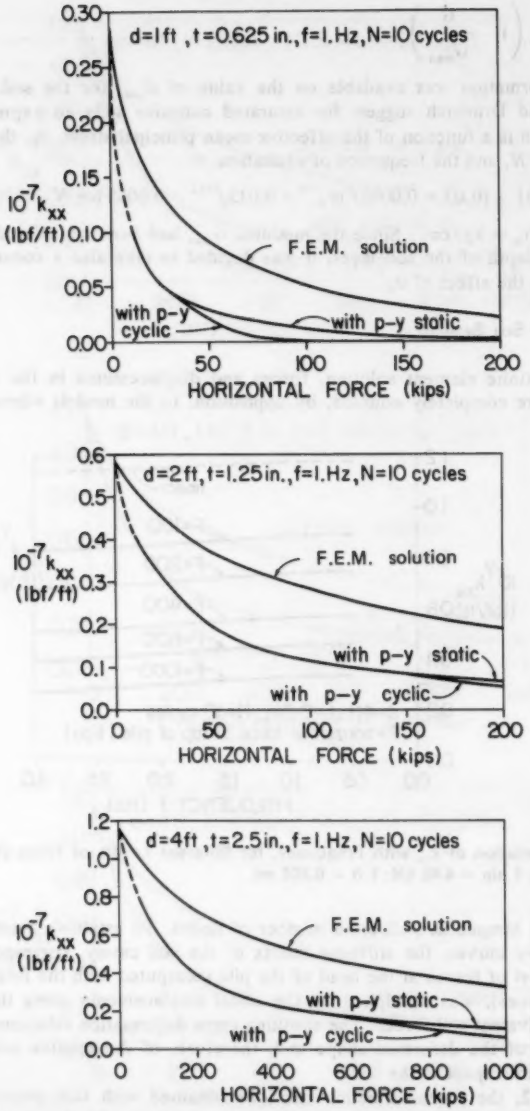

FIG. 7.—Variation of k_{xx} with Level of Force, for Different Pile Diameters (1 lbf/ft = 14.59 N/m; 1 kip = 4.45 kN; 1 ft = 0.305 m)

than those predicted by the static (monotonic) *p-y* curves. The discrepancy is even larger when cyclic degradation starts to take place. The limiting deflection at which cyclic degradation occurs, and the cyclic *p-y* curves deviate from the static ones, is not encountered for the 4-ft diam pile even under the largest force at the pile head (1,000 kips). It occurs, however, for lower magnitudes of forces as the pile diameter decreases.

Several reasons may cause the difference in results:

1. The iterative procedure is, by itself, only an approximation and an even cruder one when dealing, as in the present case, with a truly three-dimensional situation.

2. The assumed constitutive equations for the soil are only approximate, and the relation between stiffness (shear modulus) and strength is an additional source of uncertainty.

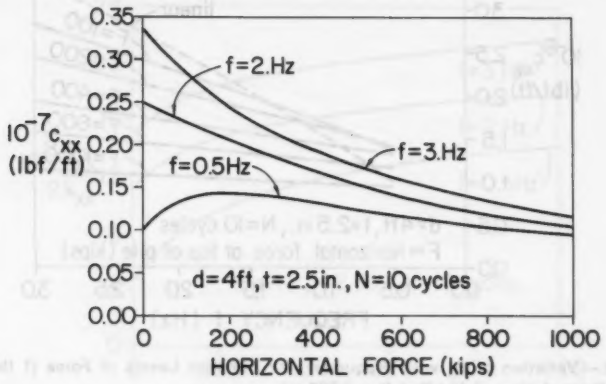

FIG. 8.—Variation of c_{xx} with Level of Force, for Different Frequencies (1 lbf/ft = 14.59 N/m; 1 kip = 4.45 kN; 1 ft = 0.305 m)

3. Results are based on 10 cycles of loading, but the *p-y* curves are supposed to represent a lower bound to the response after an unspecified number of cycles.

4. Slippage and flow of soil immediately adjacent to the pile are not considered. Studies with two-dimensional models by Yegian and Wright (20), including these effects, showed better agreement with the *p-y* curves, but still not a perfect match.

5. The fact that the soil cannot take tension near the surface and that gaps will open is also ignored. Studies by Thompson (19), with a two-dimensional model, showed that the soil forces could decrease by a factor of two when this effect was considered.

Fig. 3 shows, on the other hand, a comparison of the force-deflection relations for the soil, obtained from the finite element model, with the *p-y* curves suggested

by Stevens and Audibert (18). The agreement is now much better near the surface, but the forces corresponding to a given deflection from the *p-y* curves are larger than those predicted by the finite element solution at some depth. The finite element results seem to be between the *p-y* curves of Matlock and those of Stevens and Audibert.

The variation of the real part of the soil springs, k_s, with depth, is shown in Fig. 4 for different levels of horizontal force at the pile head and for pile diameters of 4 ft, 2 ft, and 1 ft. It should be noted that, while there is nonlinear soil behavior over the complete length of the pile, the reduction in soil stiffness is particularly large over a small depth. This depth seems to increase slightly with level of force, and is comparable to the depth of reduced resistance, x_r, indicated by Matlock (11). The values of x_r for each case are shown in the

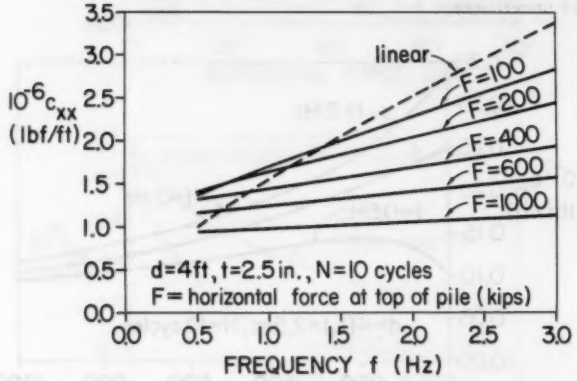

FIG. 9.—Variation of c_{xx} with Frequency, for Different Levels of Force (1 lbf/ft = 14.59 N/m; 1 kip = 4.45 kN; 1 ft = 0.305 m)

figure. It appears, thus, that some basic trends of behavior are well reproduced by the nonlinear model.

Horizontal Pile Stiffness

The finite element model, and the programs developed using the *p-y* curves, were then used to investigate trends in horizontal pile stiffness and damping characteristics. The lateral stiffness of the pile was obtained in both cases by applying a force at the pile head, which was free to rotate, computing the deflection through a series of iterations, and dividing the force by the top deflection. Clearly this represents only one particular form of excitation (horizontal force at the pile top, no moment or axial load). Some analyses were performed for more general conditions, such as fixed head piles with moments and axial forces, in addition to the lateral load; but no parametric studies were conducted for these cases, due to the large number of parameters involved. Results presented here are therefore limited to the case of a pile hinged at the top.

For the linear case, it is customary to express the stiffness in the form

$$K_{xx} = k_{xx} + ic_{xx} \quad \ldots \quad (4)$$

The real part, k_{xx}, represents the constant of an equivalent spring, which may vary with frequency. The imaginary part, c_{xx}, represents the loss of energy. The ratio $D = c_{xx}/2k_{xx}$ can then be considered as the effective damping ratio at each frequency. The D value independent of frequency represents a hysteretic type damping associated with nonlinear soil behavior; a D value, increasing linearly with frequency, represents a viscous type damping characteristic of a loss of energy by radiation.

The variations of k_{xx} with level of horizontal force at the pile head, predicted by the finite element solution, and by the model with lumped nonlinear springs based on Matlock's p-y curves, are shown in Fig. 5 for a pile diameter of

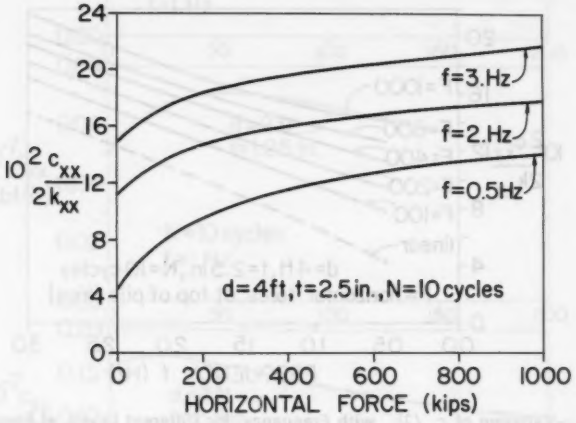

FIG. 10.—Variation of $c_{xx}/2k_{xx}$ with Level of Force, for Different Frequencies (1 kip = 4.45 kN; 1 ft = 0.305 m)

4 ft and three values of the excitation frequency (0.5, 2, and 3 Hz). The curves are very similar for the three frequencies, with a marked decrease of stiffness with increasing force. It should be noted, however, that the level of force needed to initiate cyclic degradation with the p-y curves decreases with increasing frequency. The stiffnesses predicted by the finite element solution are 2–2.5 times larger than those obtained with the p-y model, a result consistent with that obtained for the equivalent soil springs.

The variation of pile stiffness, k_{xx}, with frequency for various force amplitudes, is further shown in Fig. 6 for the same pile diameter and the finite element model. The slope of these curves is essentially invariant with the level of force, but the relative decrease of stiffness with frequency is larger as the force at the pile head increases.

The effect of the pile diameter is shown in Fig. 7. The variation of the pile stiffness, with level of force, is shown for three pile diameters (4 ft, 2 ft, and 1 ft), a frequency of 1 Hz and the two models (finite elements and lumped springs). Comparison of the results from the two formulations leads to the same observations made in relation to Fig. 5: the stiffness predicted by the finite element solution is 2–2.5 times larger than that obtained from the static (monotonic) *p-y* curves. The cyclic degradation, predicted by the *p-y* curves, takes place at much smaller force levels as the pile diameter decreases.

Effective Damping Under Horizontal Forces

The variation of the imaginary part, c_{xx}, of the lateral pile stiffness, with level of force at the pile head, is shown in Fig. 8 for a pile diameter of 4 ft and frequencies of 0.5 Hz, 2 Hz, and 3 Hz. For the smallest frequency

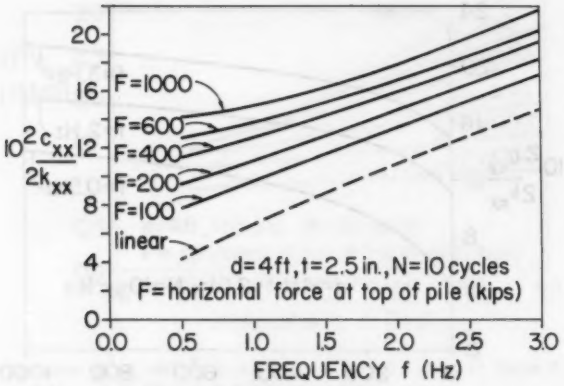

FIG. 11.—Variation of $c_{xx}/2k_{xx}$ with Frequency, for Different Levels of Force (1 kip = 4.45 kN; 1 ft = 0.305 m)

(0.5 Hz), the c_{xx} term increases initially with increasing force, reaches a maximum, then decreases. For the higher frequencies, it decreases monotonically. This behavior can be explained by considering that there is an increase in internal hysteretic type damping, due to soil nonlinearity, and a decrease in radiation damping, due to the softening of the core region with respect to the far field. For low frequencies, the increase in internal damping is larger than the decrease in radiation, up to a certain level of force. Beyond this level of force, the internal damping remains essentially constant or increases very slowly, while the radiation damping keeps decreasing. For larger frequencies, the c_{xx} term, due to radiation, becomes much more important than the contribution of the material damping, and therefore the total c_{xx} decreases monotonically with increasing level of force. These results correspond to the finite element solution where the pile was assumed to remain in contact with the surrounding soil at all times. Due to the appearance of gaps, one might expect a reduction

in the internal soil damping (smaller area of the hysteresis loops).

The variation of c_{xx}, with frequency, is shown in Fig. 9 for various levels of horizontal force at the pile head. For low frequencies, the lines cross each other. In fact, for frequencies smaller than the natural frequency of the soil deposit (about 0.25 Hz in this case), there would be no radiation, and the only term would be due to internal soil damping. Over the range of frequencies

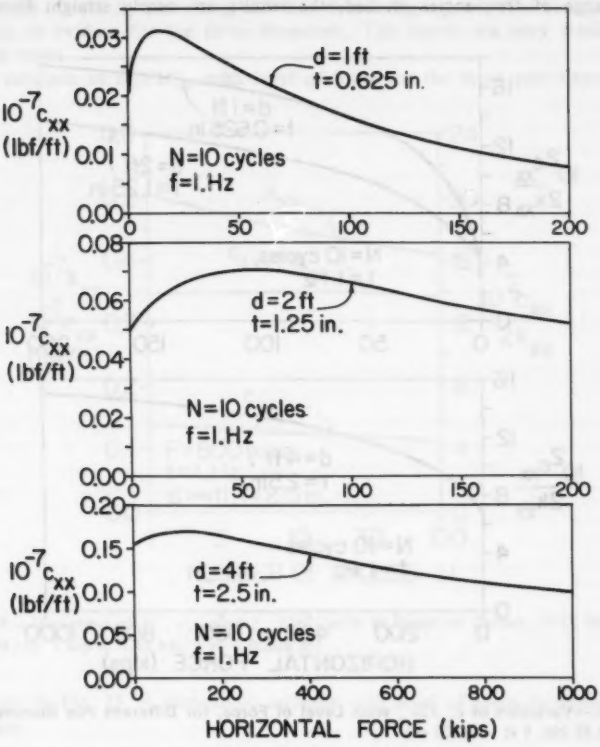

FIG. 12.—Variation of c_{xx} with Level of Force, for Different Pile Diameters (1 lbf/ft = 14.59 N/m; 1 kip = 4.45 kN; 1 ft = 0.305 m)

studied, the c_{xx} term varies almost linearly, with the slope decreasing as the level of force increases.

The above results are of interest if one intends to replace the pile by a spring with a stiffness, k_{xx}, and a viscous dashpot, c_{xx}/ω, both of which are functions of the frequency of excitation, $\omega(\omega = 2\pi f)$, and of the amplitude of the applied force. It is also interesting to consider the effective damping

ratio, $c_{xx}/2k_{xx}$, taking into account the variation of both terms. Fig. 10 shows the variation of this term with level of force for the 4-ft diam pile, and the three frequencies 0.5 Hz, 2 Hz, and 3 Hz. In all cases, the ratio increases with increasing level of force. This indicates that the reduction of the real stiffness, k_{xx}, more than compensates for the reduction in c_{xx}.

The variation of $c_{xx}/2k_{xx}$, versus frequency for the various force levels, is shown in Fig. 11. This ratio increases with increasing force. Note that over the range of frequencies studied, the results are nearly straight lines with

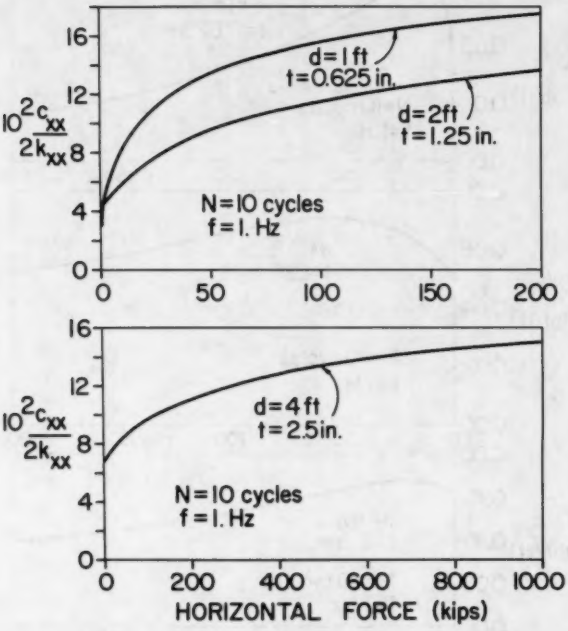

FIG. 13.—Variation of $c_{xx}/2k_{xx}$ with Level of Force, for Different Pile Diameters (1 kip = 4.45 kN; 1 ft = 0.305 m)

approximately the same slope. As the level of force increases, the curvature of the lines increases.

For the range of higher frequencies, which may be of interest for machine foundations or offshore structures under seismic excitation, it would appear that relatively simple formulae could be obtained from the results of this study. No attempt is made, however, to obtain such formulae, since the main purpose of this study is to investigate trends which may not be affected too much by the simplifying assumptions, rather than to obtain specific quantitative results which would be sensitive to the model.

In the low frequency range, the radiation damping would be very small and the only important contribution would come from the internal soil damping. This would be the range of interest for offshore structures under extreme wave loading.

The effect of the pile diameter in c_{xx} is shown in Fig. 12 for three diameters (d = 4 ft, 2 ft, and 1 ft), and for constant frequency 1 Hz. The variation of c_{xx} is plotted versus level of force. Typical behavior, associated with small frequencies of initially increasing and then decreasing c_{xx}, with increasing level of force, is evident for the three diameters. The trends are very similar in all three cases.

The variation of $c_{xx}/2k_{xx}$, with level of force for the three pile diameters,

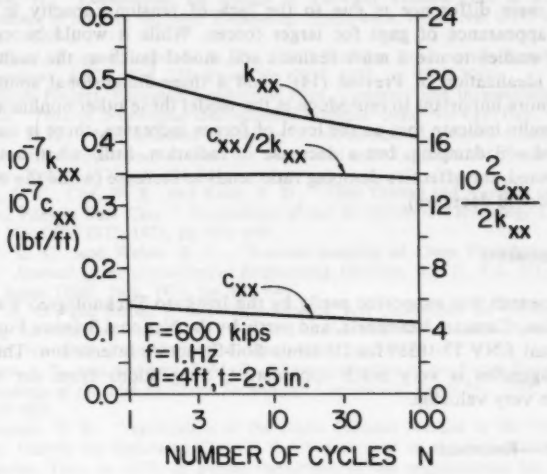

FIG. 14.—Variation of k_{xx}, c_{xx}, and $c_{xx}/2k_{xx}$ with Number of Cycles, N (1 lbf/ft = 14.59 N/m; 1 kip = 4.45 kN; 1 ft = 0.305 m)

is shown in Fig. 13. A monotonic increase with level of force is common to all cases.

Effect of Number of Cycles

All the results considered previously were obtained assuming 10 cycles of loading for the constitutive model described earlier. As was pointed out, the number of cycles will have some effect on the values obtained and the comparison with the p-y solution. To investigate the relative magnitude of this effect, the 4-ft diam pile is studied under a force of amplitude, 600 kips (2,670 kN), and a frequency of 1 Hz. Fig. 14 shows the variation of the pile stiffness, k_{xx}, the equivalent dashpot constant, c_{xx}, and the effective damping, $c_{xx}/2k_{xx}$, versus number of cycles, N, for this case.

Summary and Conclusions

An attempt has been made in this study to investigate the effect of nonlinear soil behavior on the dynamic stiffness of single piles, using a simplified nonlinear model and an iterative linearization procedure. Because of the crudeness of the soil model, and the fact that important effects such as slippage, separation, and gapping are not considered, care must be exercised in interpreting the results. One should not, in particular, attribute too much significance to the actual numerical values. It appears, however, that some important trends can be predicted well, even with this simple idealization.

Comparing the results of this analysis with those obtained using the p-y curves (perhaps the best solution available and with an experimental backup), it appears that the main difference is due to the lack of tension capacity in the soil, and the appearance of gaps for larger forces. While it would be convenient in future studies to use a more realistic soil model [such as the multiple-yield surfaces idealization of Prevost (14)], and a three-dimensional solution, it is perhaps more important to reproduce in the model these other nonlinear effects.

The results indicate that as the level of forces increases, there is an increase in internal soil damping, but a decrease in radiation. Still, when both effects are combined, the effective damping ratio tends to increase (while the equivalent dashpot would decrease).

Acknowledgments

This research was supported partly by the Instituto Technológico Venezolano del Petróleo, Caracas, Venezuela, and partly by the National Science Foundation, under Grant ENV 77-18339 for Dynamic Soil-Structure Interaction. The support of both agencies is very much appreciated. Suggestions from the reviewers have been very valuable.

Appendix I.—References

1. Andersen, K. H., "Behaviour of Clay Subjected to Undrained Cyclic Loading," *Proceedings of the First International Conference on the Behaviour of Offshore Structures*, BOSS '76, Vol. I, 1976, pp. 392–403.
2. Andersen, K. H., Hansteen, O. E., Høeg, K., and Prevost, J. H., "Soil Deformations Due to Cyclic Loads on Offshore Structures," *Report 52412-6*, Norwegian Geotechnical Institute, Mar., 1977.
3. Angelides, D. C., "Stochastic Response of Fixed Offshore Structures in Random Sea," thesis presented to the Massachusetts Institute of Technology, at Cambridge, Mass., in 1978, in partial fulfillment of the requirements for the degree of Doctor of Philosophy; also *Research Report R78-37*, Massachusetts Institute of Technology, Oct., 1978.
4. Blaney, G. W., Kausel, E., and Roësset, J. M., "Dynamic Stiffness of Piles," *Proceedings of the 2nd International Conference on Numerical Methods in Geomechanics*, V.P.I., ASCE, 1976, pp. 1001–1012.
5. Fischer, J. A., Koutsoftas, D. C., and Lu, T. D., "The Behaviour of Marine Soils Under Cyclic Loading," *Proceedings of the First International Conference on the Behaviour of Offshore Structures*, BOSS '76, Vol. II, 1976, pp. 407–417.
6. Hardin, B. O., and Drnevich, V. P., "Shear Modulus and Damping in Soils: Design Equations and Curves," *Journal of Soil Mechanics and Foundations Division*, ASCE, Vol. 98, SM7, Proc. Paper 9006, July, 1972, pp. 667–692.

7. Kausel, E., "Forced Vibrations of Circular Foundations on Layered Media," *Research Report R74-11,* Massachusetts Institute of Technology, Cambridge, Mass., Jan., 1974, pp. 240.
8. Lysmer, J., Udaka, T., Seed, H. B., and Hwang, R., "LUSH—A Computer Program for Complex Response Analysis of Soil-Structure Systems," *Report No. EERC74-4,* Earthquake Engineering Research Center, University of California, Berkeley, Calif., Apr., 1974.
9. Lysmer, J., Udaka, T., Tsai, C. F., and Seed, H. B., "FLUSH—A Computer Program for Approximate 3-D Analysis of Soil-Structure Interaction Problems," *Report No. EERC75-30,* Earthquake Engineering Research Center, University of California, Berkeley, Calif., Nov., 1975.
10. Matlock, H., and Reese, L. C., "Generalized Solutions for Laterally Loaded Piles," *Journal of Soil Mechanics and Foundations Division,* ASCE, Vol. 86, No. SM5, Proc. Paper 2626, Oct., 1960, pp. 63–91.
11. Matlock, H., "Correlations for Design of Laterally Loaded Piles in Soft Clay," *Proceedings of the 2nd Offshore Technology Conference,* Paper No. OTC 1204, 1970, pp. I-577–I-594.
12. McClelland, B., and Focht, J. A., Jr., "Soil Modulus for Laterally Loaded Piles," *Transactions,* ASCE, Vol. 123, Paper No. 2954, 1958, pp. 1049–1086.
13. "Research Project, Repeated Loading on Clay, Summary and Interpretation of Test Results," *74037-9,* Norwegian Geotechnical Institute, Oslo, Norway, Oct., 1975.
14. Prevost, J. H., "Mathematical Modelling of Monotonic and Cyclic Undrained Clay Behaviour," *International Journal for Numerical and Analytical Methods in Geomechanics,* Vol. 1, 1977, pp. 195–216.
15. Reese, L. C., Cox, W. R., and Koop, F. D., "Field Testing and Analysis of Laterally Loaded Piles in Stiff Clay," *Proceedings of the 7th Offshore Technology Conference,* Paper No. OTC 2312, 1975, pp. 671–690.
16. Reese, L. C., and Welch, R. C., "Lateral Loading of Deep Foundations in Stiff Clay," *Journal of the Geotechnical Engineering Division,* ASCE, Vol. 101, No. GT7, Proc. Paper 12862, July, 1975, pp. 633–649.
17. Seed, H. B., and Idriss, I. M., "Influence of Soil Conditions on Ground Motions During Earthquakes," *Journal of Soil Mechanics and Foundations Division,* ASCE, Vol. 95, No. SM1, Proc. Paper 6347, Jan., 1969, pp. 99–137.
18. Stevens, J. B., and Audibert, J. M. E., "Re-examination of p-y Curve Formulations," *Proceedings of the 11th Offshore Technology Conference,* Paper No. OTC 3402, 1979, pp. 397–403.
19. Thompson, G. R., "Application of the Finite Element Method to the Development of p-y Curves for Saturated Clays," thesis presented to the University of Texas, at Austin, Tex., in 1977, in partial fulfillment of the requirements for the degree of Master of Science.
20. Yegian, M., and Wright, S. G., "Lateral Soil Resistance-Displacement Relationships for Pile Foundations in Soft Clays," *Proceedings of the 5th Offshore Technology Conference,* Paper No. OTC 1893, 1973, pp. II-663–II-676.

Appendix II.—Notation

The following symbols are used in this paper:

c = shear wave velocity in soil;
c_{xx} = imaginary part of horizontal pile stiffness (equivalent dashpot constant for horizontal excitation);
c_{zz} = imaginary part of vertical pile stiffness (equivalent dashpot constant for vertical excitation);
D = $c_{xx}/2k_{xx}$ = effective damping ratio at each frequency;
D_s = hysteretic soil damping ratio;
d = pile diameter;

E_p = pile modulus of elasticity;
E_s = soil modulus of elasticity;
F = horizontal force at top of pile;
f = frequency;
G = dynamic shear modulus;
G_{max} = dynamic shear modulus at small strains;
I = pile moment of inertia;
i = imaginary number ($\sqrt{-1}$);
K_{xx} = horizontal complex pile stiffness;
k_s = real part of soil springs;
k_{xx} = real part of horizontal pile stiffness;
k_{zz} = real part of vertical pile stiffness;
L = length of pile;
log = natural logarithm;
N = number of cycles;
OCR = overconsolidation ratio;
p = soil resistance (force per unit length of pile);
r = polar radius;
T = period;
t = wall thickness of pile;
x = distance from mudline;
x_r = depth of gap zone;
y = deflection of each pile segment;
y_c = deflection at one-half ultimate soil resistance;
z = vertical axis;
γ = shear strain amplitude;
γ_{rz} = shear strain amplitude on vertical plane;
$\gamma_{r\theta}$ = shear strain amplitude on horizontal plane;
γ_t = total unit weight of soil;
ϵ_{50} = strain at one-half maximum principal stress difference in undrained test;
τ = cyclic total stress;
τ_{hf} = shear stress of failure for static loading;
ϕ = polar angle; and
ω = radian frequency.

COUPLED HEAT AND WATER FLOWS AROUND BURIED CABLES

By Omar N. Abdel-Hadi,[1] A. M. ASCE, and James K. Mitchell,[2] F. ASCE

INTRODUCTION

The phenomenon of water movement in soils due to thermal gradients is important in relation to several problems, including heat dissipation from buried power cables, underground storage of hot and cold materials, moisture movement and distribution in pavement bases and subgrades, and the soil as a medium for plant growth. Thermally-induced moisture movements can lead to changes in both the thermal and isothermal properties of the soil which can subsequently affect the functioning of the soil for its intended purpose.

Thermally induced soil water movement in unsaturated soils is a complex process. The various components of thermally-induced soil water movement and the physical laws governing them are presented in this paper. The relationships developed are illustrated by their use as a basis for predictions of transient and steady-state temperature and moisture distributions around buried electrical transmission cables.

Buried transmission cables generate heat, causing their sheath temperature to rise. The allowable current loading may be limited by the maximum permissible cable sheath temperatures. Temperatures higher than 50° C–60° C may lead to cable failure and thermal instability of the soil around the cable, caused by the fact that the soil water migrates away from the cable under thermal gradient, leading to a marked decrease in thermal conductivity of the cable environment. The result of this is that the ability of the backfill to dissipate heat is decreased.

BACKGROUND

The problem of moisture movement in unsaturated soils is less understood than moisture movement in saturated soil. This is due to the simpler transport mechanism and mathematical description associated with saturated flow as opposed to unsaturated flow. In saturated soils moisture movement occurs in

[1]Geotechnical Engr., Geotechnical Consultants, Inc., San Francisco, Calif.
[2]Prof. and Chmn., Dept. of Civ. Engrg., Univ. of California, Berkeley, Calif. 94720.

Note.—Discussion open until April 1, 1982. To extend the closing data one month, a written request must be filed with the Manager of Technical and Professional Publications, ASCE. Manuscript was submitted for review for possible publication on September 12, 1979. This paper is part of the Journal of the Geotechnical Engineering Division, Proceedings of the American Society of Civil Engineers, ©ASCE, Vol. 107, No. GT11, November, 1981. ISSN 0093-6405/81/0011-1461/$01.00.

the liquid phase only. In unsaturated soils the flow takes place in both the vapor and liquid phases.

A comprehensive review of the literature on water migration under thermal gradients showed that several theories now exist. To predict the rate of water migration, many researchers have used Fick's law modified to take into account both the reduction of diffusion cross section by the solid matrix and the liquid water and the tortuosity of the diffusion path through the medium. Thus, they implicitly assume that the transport takes place in the vapor phase. It is observed, however, that this theory underestimates the quantity of water vapor transport under temperature gradients by a factor of 3 to 10 (6,15,19).

Taylor and Cary (18) used the general theory of irreversible thermodynamics to account for the simultaneous flow of water and heat in porous media under the influence of thermal gradients and other secondary energy gradients. Philip and DeVries (13) considered moisture flow in vapor and liquid phases, and the interaction of liquid and vapor phases. Laboratory experiments, Casset, et al. (2), showed close correlation with the Philip and DeVries theory, while Taylor and Cary's approach underestimated the flow rate by a factor of 10 to 40. The theory of Philip and DeVries was modified and used for the analysis of moisture flow in base courses under pavements by Raudkivi and U'u (14). The theory of Philip and DeVries appears to provide the most comprehensive basis for development of a model for prediction of transient flow of water in unsaturated soils under thermal gradients. Accordingly, it was adapted for the studies described herein.

Scope

In this paper, a summary of the Philip and DeVries theory is presented. Evaluation of the soil parameters needed, according to the theory, is described along with examples. The relative importance of the properties affecting the rate and amount of water migration under thermal gradients is illustrated. Finally, a field test program is described which provides a basis for comparison between predicted and actual values of moisture and temperature distributions.

Philip and De Vries Theory

In an analysis of moisture movement in unsaturated soils under a thermal gradient, the following must be considered: (1) Vapor phase transport; (2) liquid phase transport; and (3) interrelationship of the vapor and liquid phases.

Vapor Phase Transport.—The following equation was obtained by Philip and DeVries (13) for the vapor flux density. It is the vapor diffusion equation, modified so as to apply to porous media, and extended to separate the isothermal and thermal components of vapor transfer and to take into account the effect of relative humidity on the transfer:

$$\frac{q_{vap}}{\rho_w} = -D_{T_v} \nabla T - D_{\theta_v} \nabla \theta \qquad (1)$$

in which: q_{vap} = vapor flux density, in grams per square millimeter per second; ρ_w = density of water, in grams per cubic millimeters; and D_{T_v} = thermal

vapor diffusivity, in square millimeters per second per degrees Celsius, which is also equal to

$$D_{T_v} = \frac{D_0}{\rho_w} \nu \alpha a h \frac{d\rho_0}{dT} \quad \ldots\ldots\ldots\ldots\ldots\ldots\ldots\ldots\ldots\ldots\ldots\ldots\ldots\ldots (2)$$

in which D_0 = molecular diffusivity of water vapor in air, in square millimeters per second; ν = "mass flow factor" introduced to allow for the mass flow of vapor arising from the difference in boundary conditions governing the air and vapor components of the diffusion system. It is equal to $P/(P - p)$; in which P = the total gas pressure; and p = the partial vapor pressure in the pore space; α = tortuosity factor allowing for extra path length; a = volumetric air content of the soil, in cubic millimeters of air per cubic millimeters; h = relative humidity; ρ_0 = density of saturated water vapor, in grams per cubic millimeters; T = temperature, in degrees Kelvin; ∇ = partial derivative with respect to distance; and D_{θ_v} = isothermal vapor diffusivity, in in square millimeters per second which is also equal to

$$D_{\theta_v} = \frac{D_0}{\rho_w} \nu \alpha a \frac{\rho_0 g h}{RT} \frac{\partial \psi}{\partial \theta} \quad \ldots\ldots\ldots\ldots\ldots\ldots\ldots\ldots\ldots\ldots\ldots\ldots\ldots\ldots (3)$$

in which g = acceleration due to gravity, in millimeters per second square; R = gas content, in ergs per grams per degrees Celsius; ψ = suction head, in millimeters, in thermodynamic equilibrium with the water in the medium; θ = volumetric water content, in cubic millimeters of water per cubic millimeter of soil volume = $\omega \rho_d / \rho_w$; ω = weight of water / weight of dry soil, as a percentage; and ρ_d = soil dry density, in grams per cubic millimeter.

Liquid Phase Transport.—Philip and DeVries obtained the following equation for the liquid flux density. This equation is based on Darcy's law for liquid transfer in unsaturated media and extended to separate the isothermal and thermal components of liquid transfer:

$$\frac{q_{liq}}{\rho_w} = -D_{T_l} \nabla T - D_{\theta_l} \nabla \theta - k_\theta i \quad \ldots\ldots\ldots\ldots\ldots\ldots\ldots\ldots\ldots\ldots\ldots\ldots\ldots\ldots (4)$$

in which q_{liq} = liquid flux density, in grams per square millimeters per second; D_{T_l} = thermal liquid diffusivity, in square millimeters per second per degrees Celsius which is also equal to

$$D_{T_l} = k_\theta \frac{\psi}{\sigma} \frac{d\sigma}{dT} \quad \ldots\ldots\ldots\ldots\ldots\ldots\ldots\ldots\ldots\ldots\ldots\ldots\ldots\ldots\ldots\ldots (5)$$

in which k_θ = unsaturated hydraulic conductivity, in millimeters per second; σ = surface tension of water, in dynes per millimeter; D_{θ_l} = isothermal liquid diffusivity, in square millimeters per second, which is also equal to

$$D_{\theta_l} = k_\theta \frac{\partial \psi}{\partial \theta} \quad \ldots\ldots\ldots\ldots\ldots\ldots\ldots\ldots\ldots\ldots\ldots\ldots\ldots\ldots\ldots\ldots (6)$$

in which i = unit vector in the positive z direction.

Interaction of Vapor and Liquid Phases.—Philip and DeVries (13) modified the equation for the thermal vapor diffusivity D_{T_v} given by the simple vapor

transport theory (Eq. 2), because it underestimates the water vapor transport by a factor of 3 to 10, as mentioned earlier in this paper. Their modified equation accounts for the interaction between vapor and liquid phases, and the difference between average temperature gradient in the air-filled pores and in the soil as a whole. They found the modified equation to predict order of magnitude and general behavior in satisfactory agreement with experimental observations. The modified equation is as follows:

$$D_{T_v} = \frac{D_0}{\rho_w} v\,(a + f(a) \cdot \theta)\, hb \frac{d\rho_0}{dT},$$

in square millimeters per second per degrees Celsius . . . . (7)

in which $f(a) = a/a_k$ for $0 < a < a_k = 1$ for $a \geq a_k$; in which a_k = the value of a (volumetric air content) at which liquid continuity in pores no longer exists; or a_k = the value of a at which $\theta = \theta_k$; in which θ_k = the moisture content at which k (hydraulic conductivity) falls to some small arbitrary fraction of its saturated value, and b = the ratio of the average temperature gradient in the air-filled pores to the overall temperature gradient.

Comprehensive Theory.—The total water movement in an unsaturated soil due to a temperature gradient and its resulting water content gradient is equal to the sum of the flows occurring in the two phases; vapor and liquid. Thus:

$$\frac{q}{\rho_w} = \frac{q_{vap}}{\rho_w} + \frac{q_{liq}}{\rho_w} \qquad (8)$$

in which q = the total water flow, in grams per square millimeter per second. Substituting the expressions for q_{vap}/ρ_w, Eq. 1, and q_{liq}/ρ_w, Eq. 4, in Eq. 8 yields:

$$\frac{q}{\rho_w} = -(D_{T_v} + D_{T_\ell})\nabla T - (D_{\theta_v} + D_{\theta_\ell})\nabla\theta - k_\theta i = -D_T \nabla T - D_\theta \nabla_\theta - k_\theta i \qquad (9)$$

in which $D_T = D_{T_v} + D_{T_\ell}$ = Thermal water diffusivity . . . . (10)

$D_\theta = D_{\theta_v} + D_{\theta_\ell}$ = Isothermal water diffusivity . . . . (11)

Eq. 9 is the governing expression for moisture movement under a thermal gradient in unsaturated soils as proposed by Philip and DeVries. Differentiation of (9) and application of the continuity requirement gives the general differential equation:

$$\frac{\partial\theta}{\partial t} = \nabla(D_T \nabla T) + \nabla(D_\theta \nabla\theta) + \frac{\partial k_\theta}{\partial z} \qquad (12)$$

The heat conduction equation for the soil is:

$$C\frac{\partial T}{\partial t} = \nabla(\lambda \nabla T); \quad \frac{\partial T}{\partial t} = \nabla\left(\frac{\lambda}{C}\nabla T\right); \quad \text{and} \quad \frac{\partial T}{\partial t} = \nabla(\chi \nabla T) \qquad (13)$$

in which C = volumetric heat capacity of the soil, in calories per cubic millimeter per degrees Celsius; λ = thermal conductivity, in calories per millimeter per second per degrees Celsius; and χ = thermal diffusivity, in square millimeters

per second. Eqs. 12 and 13 are the simultaneous equations describing coupled heat and moisture transfer in partially saturated soils.

Evaluation of Soil Parameters

From Eqs. 12 and 13 it is clear that the variation of four soil parameters with the water content (or with degree of saturation) is needed in order to predict the moisture transfer. These parameters are: (1) k_θ (hydraulic conductivity); (2) D_θ (isothermal water diffusivity); (3) D_T (thermal water diffusivity); and (4) χ (thermal diffusivity). These four parameters have been evaluated for several soils (9) as well as for the soils of the field test described later. Crushed limestone, referred to as PG and E limestone screenings, were used in the field test, and the soil parameters obtained for this soil are presented here

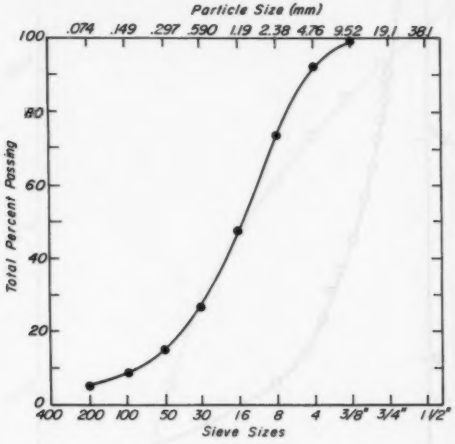

FIG. 1.—Particle Size Distribution for PG & E Crushed Limestone Screenings

as examples. The gradation curve for this material is shown in Fig. 1. The temperature range used in the evaluation of the soil parameters was 10° C–60° C. The methods for evaluation of the soil parameters are given in the following section.

Hydraulic Conductivity, k_θ.—Marshall (8) derived the following equation for the relation between the hydraulic conductivity and the size distribution of the pores in an isotropic material

$$k = \epsilon^2 n^{-2} \frac{[r_1^2 + 3r_2^2 + 5r_3^2 + \ldots + (2n-1)r_n^2]}{8} \quad \ldots\ldots\ldots\ldots\ldots\ldots \quad (14)$$

in which k = specific hydraulic conductivity, in square millimeters; ϵ = porosity, in cubic millimeters per cubic millimeters; n = total number of pore classes; and r_i = mean radius of the pores in the pore class i, in millimeters. Eq.

14 makes it possible to calculate the hydraulic conductivity of porous material from the size distribution of its pores. Pore size measurements can be made by measuring the water withdrawn when the suction on the soil is progressively increased. The radius of the largest water-filled pore under a suction of ψ millimeters is given by:

$$r = \frac{2\sigma}{\rho_w g \psi} \quad \ldots \quad (15)$$

in which σ = surface tension of water, in dynes per millimeter; ρ_w = density

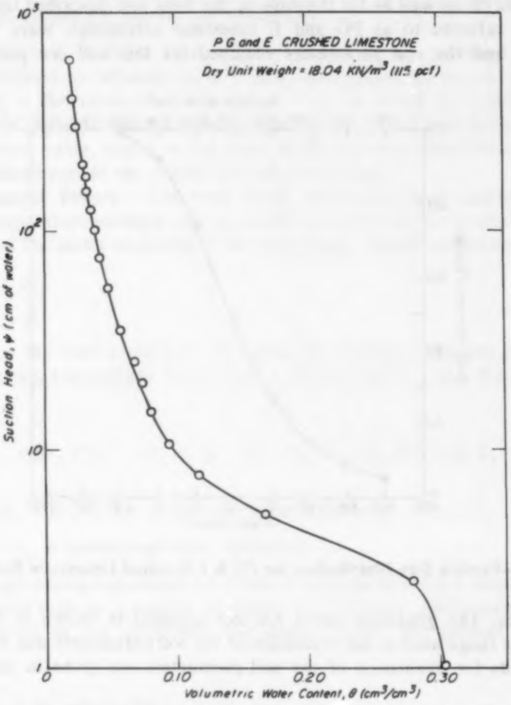

FIG. 2.—Relationship Between Suction Head and Volumetric Water Content for PG & E Crushed Limestone

of water, in grams per cubic millimeter; g = acceleration due to gravity, in millimeters per square second. In applying Eq. 14, it is often more convenient to use the suction in place of the pore radius. Therefore, Eq. 14 becomes

$$k = \frac{\sigma^2}{2\rho_w^2 g^2} \epsilon^2 n^{-2} \left[\psi_1^{-2} + 3\psi_2^{-2} + 5\psi_3^{-2} + \ldots + (2n-1)\psi_n^{-2}\right] \quad \ldots \quad (16)$$

The units of the hydraulic conductivity can be converted to millimeters per second by multiplying the specific hydraulic conductivity by $\rho_w g/\eta$ in which η grams per millimeter per second = the viscosity of water. Thus, we obtain:

$$k\left(\frac{\text{millimeters}}{\text{second}}\right) = \frac{\sigma^2}{2\rho_w g \eta}\epsilon^2 n^{-2}[\psi_1^{-2} + 3\psi_2^{-2} + 5\psi_3^{-2} + \ldots + (2n-1)\psi_n^{-2}] \quad (17)$$

In the derivation of this equation by Marshall, ϵ was used as the water-filled

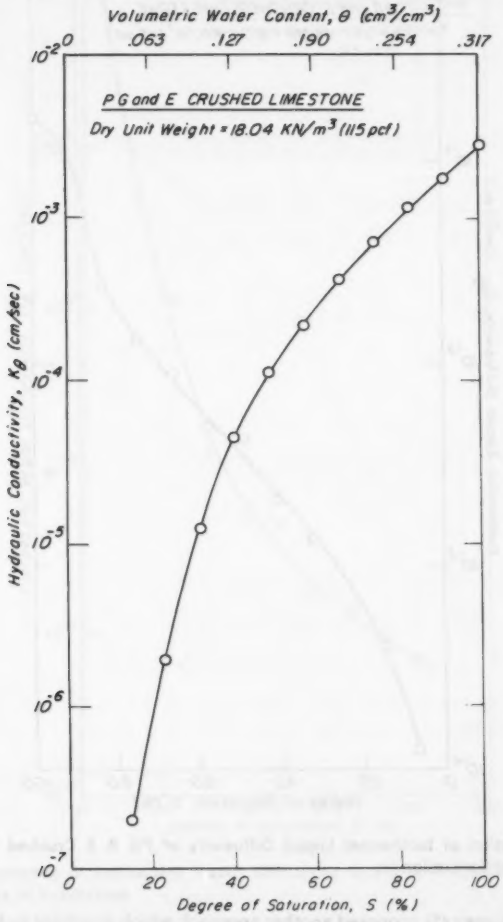

FIG. 3.—Variation of Hydraulic Conductivity of PG & E Crushed Limestone with Degree of Saturation

porosity at each water content θ_i for which the hydraulic conductivity (k) is calculated, and n was the number of pore classes in the water content interval from zero to θ_i. Thus both ϵ and n decrease as the water content decreases.

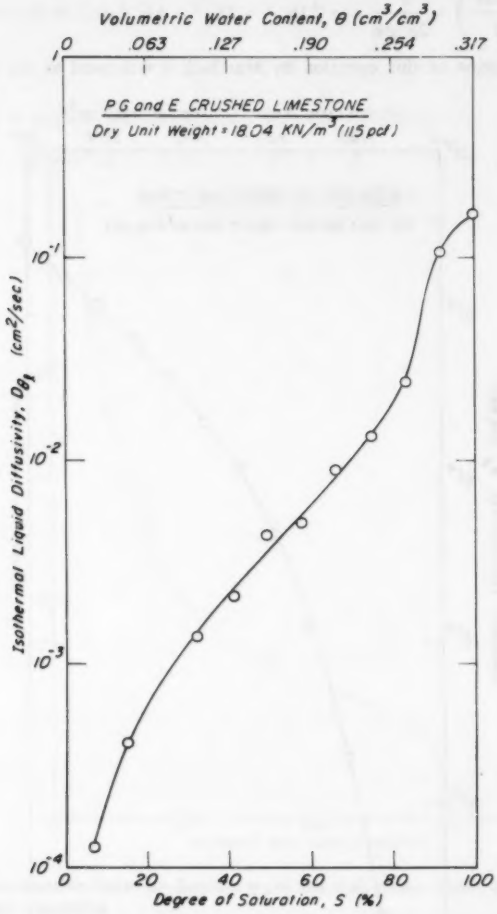

FIG. 4.—Variation of Isothermal Liquid Diffusivity of PG & E Crushed Limestone with Degree of Saturation

Green and Corey (5) proposed another approach which is similar to Marshall's and leads to the same results. They assumed ϵ to be the water-saturated porosity, θ_s, and n to be the total number of pore classes at $\epsilon = \theta_s$. In this approach

ϵ and n remain constant when the hydraulic conductivity (k) is calculated for different values of water content (θ). This approach was used in calculating the hydraulic conductivity of the soils in this investigation.

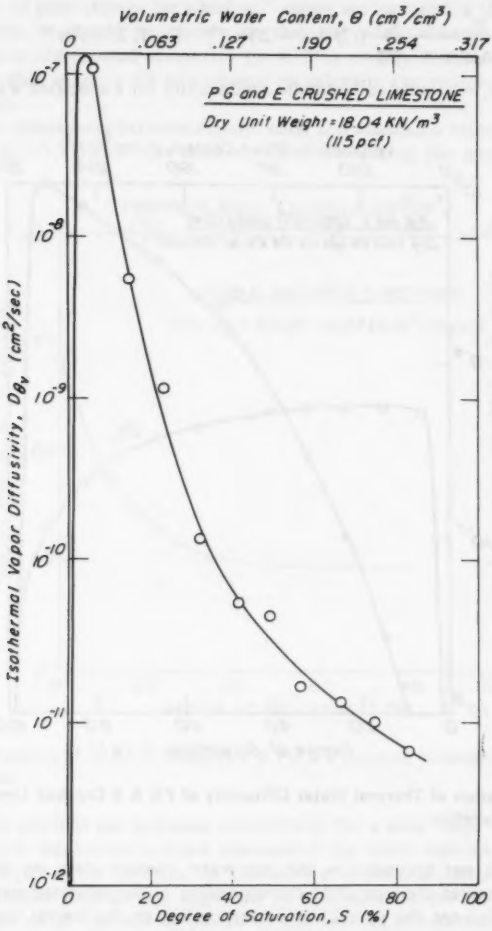

FIG. 5.—Variation of Isothermal Vapor Diffusivity of PG & E Crushed Limestone with Degree of Saturation

A matching factor is usually introduced into Eq. 17 to equate the calculated and measured hydraulic conductivities. Elzeftawy and Marshall (4) stated that

matching at water saturation has a distinct advantage over matching at desaturation water contents mainly because it is simpler and more accurate to measure saturated hydraulic conductivity. Rewriting Eq. 17 in the following form and introducing a matching factor, we obtain:

$$k(\theta)_i = \frac{k_s}{k_{sc}} \frac{\sigma^2}{2\rho_w g \eta} \frac{\epsilon^2}{n^2} \sum_{j=i}^{m} [(2j + 1 - 2i)\psi_j^{-2}] \quad i = 1, 2, \ldots, m \quad \ldots\ldots\ldots (18)$$

in which $k(\theta)_i$ = calculated hydraulic conductivity for a specified water content,

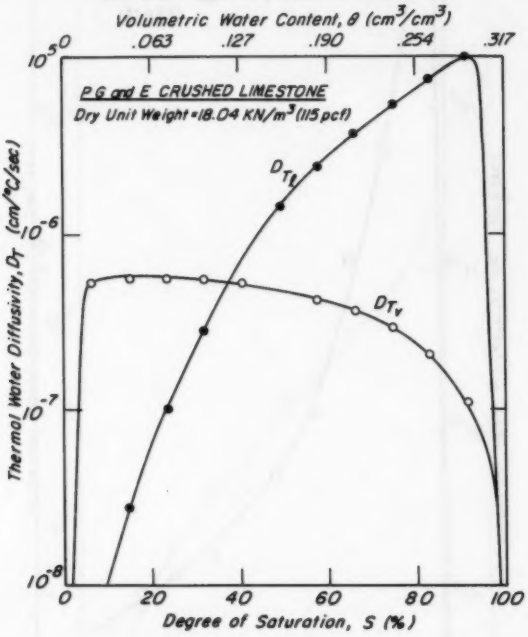

FIG. 6.—Variation of Thermal Water Diffusivity of PG & E Crushed Limestone with Degree of Saturation

in millimeters per second; i = the last water content class on the wet end, e.g., $i = 1$ denotes the pore class corresponding to the saturated water content, and $i = m$ denotes the pore class corresponding to the lowest water content for which hydraulic conductivity is calculated; (k_s/k_{sc}) = matching factor (measured saturated hydraulic conductivity/calculated saturated hydraulic conductivity; and m = total number of pore classes (pore class is a pore size range corresponding to a water content increment) between $\theta = \theta_L$ and θ_S, in which θ_L = the lowest water content on the experimental moisture content-suction head curve. Thus:

$$n = m\left[\frac{\theta_S}{\theta_S - \theta_L}\right]$$

Constant value for m is used at all water contents, and the value of m establishes the number of pore classes for which ψ_j^{-2} terms are included in the calculation at saturation. m should be chosen so that the water content-suction head relationship is represented accurately ($m \geq 10$ is usually suitable for most soil types). A value of $m = 12$ was chosen to calculate the results given in this investigation.

From the comparison between experimental and calculated values, it has been concluded (3,5,7,11) that this method, after introducing the matching factor,

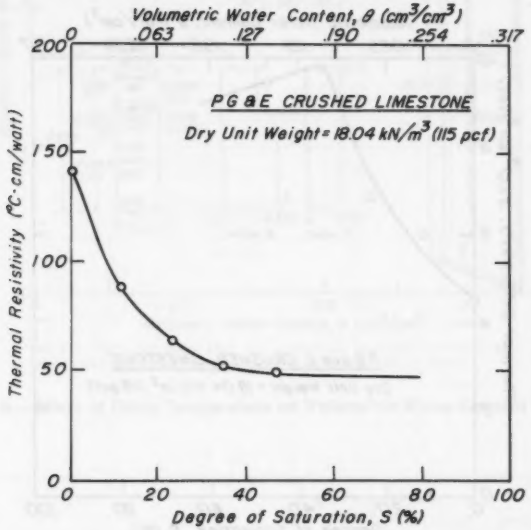

FIG. 7.—Variation of Thermal Resistivity of PG & E Crushed Limestone with Degree of Saturation

successfully predicts the hydraulic conductivity for a wide range of soils.

The suction head-water content relationship for sandy soils can be obtained using "Tempe" pressure cells. In this device cylindrical samples approx 50 mm in diameter and 20 mm high can be subjected to pressures up to one atmosphere. After the soil is placed in the cell, it is saturated with water. The soil is allowed to drain following sequential subjection to increasing air pressure. Volumetric water content is determined from the value of the withdrawn water after equilibrium is reached at each pressure and the water content of the sample at the end of the test. The suction head-water content relationship for PG and E crushed limestone is shown in Fig. 2. The suction head-water content relationship is a hysteretic function; i.e., θ depends upon whether the

soil is drying or wetting. The data in Fig. 2 is for drying.

The suction head-water content curves are strongly affected by the soil gradation and the soil fines content (silt and clay). For silty and clayey soils, the suction range of interest extends to much higher values than can be measured by the "tempe" cell. Therefore, for finer soils suction-water content measurements were made using a pressure plate apparatus which can accommodate suctions as high as 15 atmospheres (1).

The saturated hydraulic conductivity for various void ratios (dry densities) was measured for the sandy soils in the laboratory using falling head permeability test equipment. Eq. 18 was used to calculate the hydraulic conductivity using a short computer program written for this purpose. The hydraulic conductivity

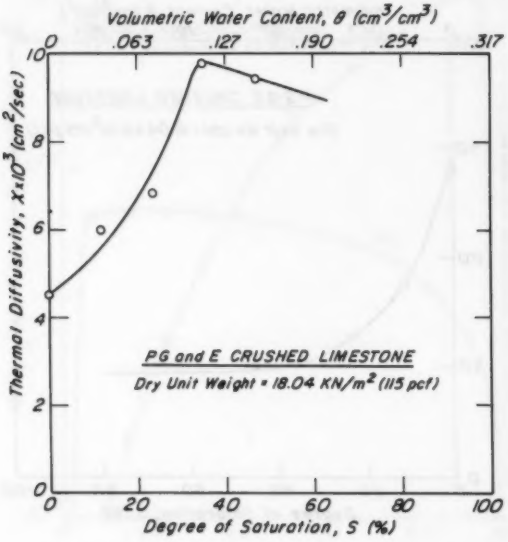

FIG. 8.—Variation of Thermal Diffusivity of PG & E Crushed Limestone with Degree of Saturation

of PG and E crushed limestone is shown in Fig. 3 as a function of both water content and degree of saturation.

Isothermal Water Diffusivity, D_θ

Isothermal Liquid Diffusivity, D_{θ_l}.—Eq. 6 was used to calculate D_{θ_l}. Since the soil water content suction head relationship is hysteretic, it follows that D_{θ_l} is also an hysteretic function. Then, in calculating D_{θ_l} from k_θ data (Fig. 3), it is necessary to consider whether the soil is wetting or drying. The values of D_{θ_l}, for drying, versus degree of saturation of PG and E crushed limestone is shown in Fig. 4.

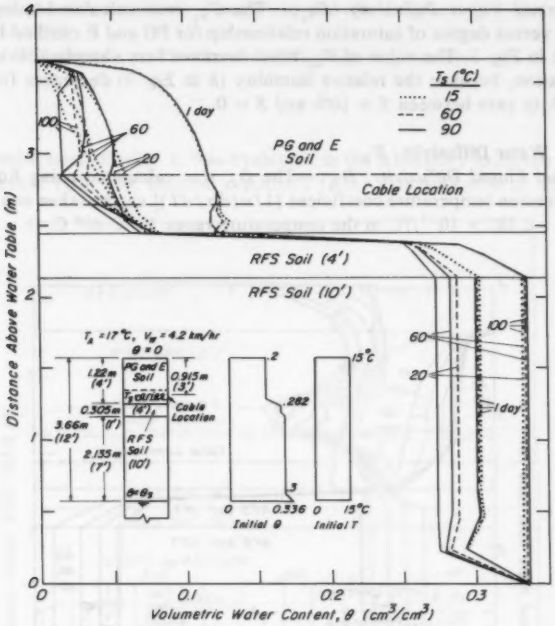

*RFS Soil (x') indicates that the properties used for this soil are those obtained from Richmond Field Station soil at x' depth

FIG. 9.—Effect of Cable Temperature on Volumetric Water Content Profile

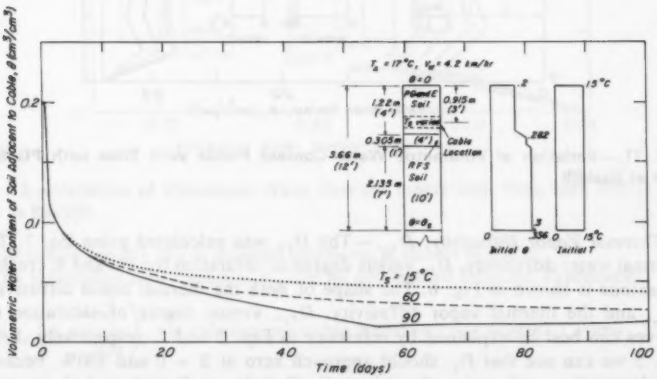

FIG. 10.—Effect of Cable Temperature on Volumetric Water Content of Soil Adjacent to Cable

Isothermal Vapor Diffusivity, D_{θ_v}.—The D_{θ_v} was calculated using Eq. 3. The D_{θ_v} versus degree of saturation relationship for PG and E crushed limestone is shown in Fig. 5. The value of D_{θ_v} must decrease very sharply at low degrees of saturation, because the relative humidity (h in Eq. 3) decreases from more than 50% to zero between $S = 10\%$ and $S = 0$.

Thermal Water Diffusivity, D_T

Thermal Liquid Diffusivity, D_{T_ℓ}.—The D_{T_ℓ} was calculated using Eq. 5. The surface tension temperature coefficient $[1/\sigma(d\sigma/dT)]$ can be taken as a constant value of -2.285×10^{-3}/°C in the temperature range 10° C–60° C.

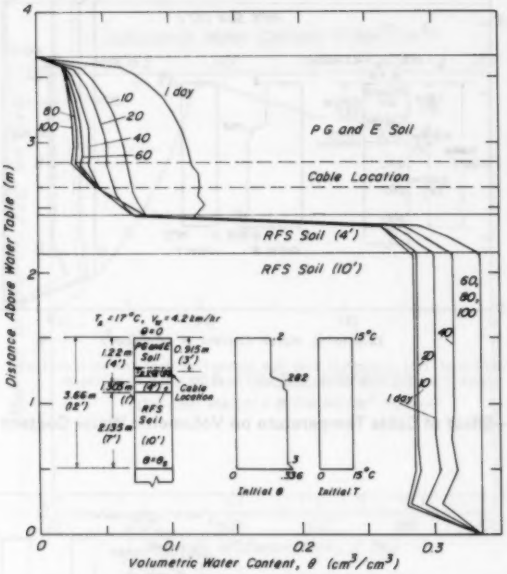

FIG. 11.—Variation of Volumetric Water Content Profile with Time with PG & E Soil as Backfill

Thermal Vapor Diffusivity, D_{T_v}.—The D_{T_v} was calculated using Eq. 7. The thermal water diffusivity, D_T, versus degree of saturation for PG and E crushed limestone is shown in Fig. 6. The shape of both the thermal liquid diffusivity, D_{T_ℓ}, and the thermal vapor diffusivity, D_{T_v}, versus degree of saturation (S) curves can best be explained by reference to Eqs. 5 and 7, respectively. From Eq. 5 we can see that D_{T_ℓ} should approach zero at $S = 0$ and 100%, because the hydraulic conductivity, k_θ, is practically zero at $S = 0$, and the suction head ψ is zero at $S = 100\%$. From Eq. 7 it is clear that D_{T_v} approaches zero at $S = 0$ and 100% because the relative humidity, h, decreases to zero at

S = 0, and the volumetric air content (a) and the function $f(a)$ are equal to zero at S = 100%.

Thermal Diffusivity, χ.—The thermal diffusivity is given by:

$$\chi = \frac{\lambda}{C} \quad \text{(19)}$$

The thermal conductivity, λ, was evaluated in the laboratory using the thermal needle method (10). The thermal resistivity ($1/\lambda$) versus degree of saturation

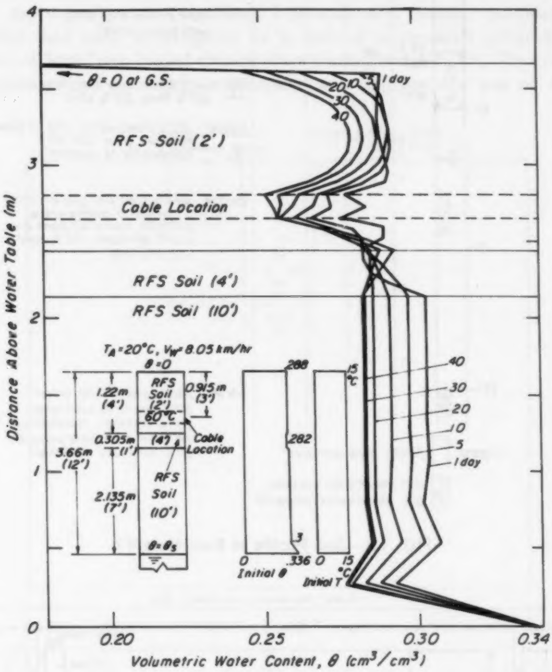

FIG. 12.—Variation of Volumetric Water Content Profile with Time with RFS (2 ft) Soil as Backfill

relationships for PG and E crushed limestone is shown in Fig. 7.

The volumetric heat capacity, C, can be determined from the expression:

$$C = \gamma_d \left(c + \frac{w}{100} \right), \quad \text{in calories per cubic millimeter per degrees Celsius}$$

in which c = specific heat of dry soil, in calories per gram; γ_d = unit dry weight, in grams per cubic millimeter; and w = water content, percent dry weight.

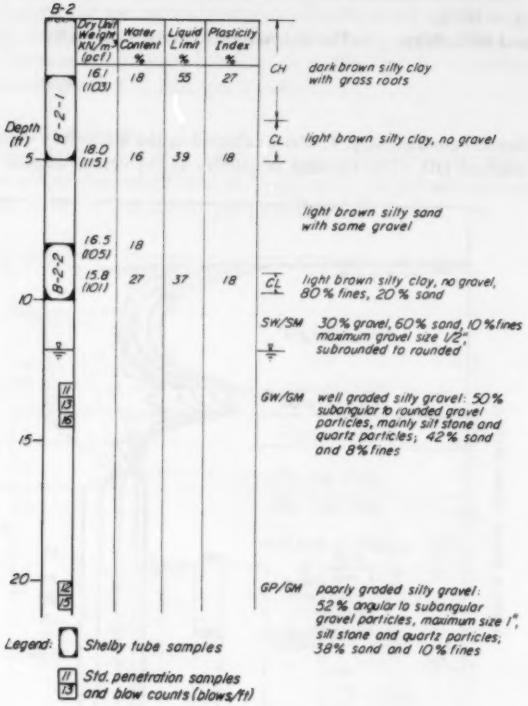

FIG. 13.—Soil Profile at Bore Hole #2

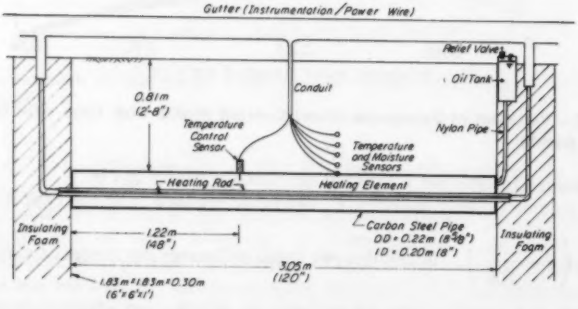

FIG. 14.—Test Section Arrangement

The thermal diffusivity versus degree of saturation relationship for PG and E crushed limestone is shown in Fig. 8. The shape of the thermal diffusivity (χ)-degree of saturation (S) curve reflects the changes in the ratio λ/C with increasing saturation. The values of λ increase rapidly at low degrees of saturation (less than about 30%), while the rate of increase of λ decreases appreciably at higher saturations. On the other hand, C increases steadily with the increase in the degree of saturation. Therefore, the values of λ/C increase at low degrees of saturation, until a limit is reached at which the ratio λ/C starts to decrease.

The preceding relationships and properties make possible the prediction of moisture movements under combined hydraulic and thermal gradients. Their applicability has been investigated as a part of a research program on the dissipation of heat from buried electrical transmission cables (9). The complexity of the relationships and their interdependence requires the use of computer

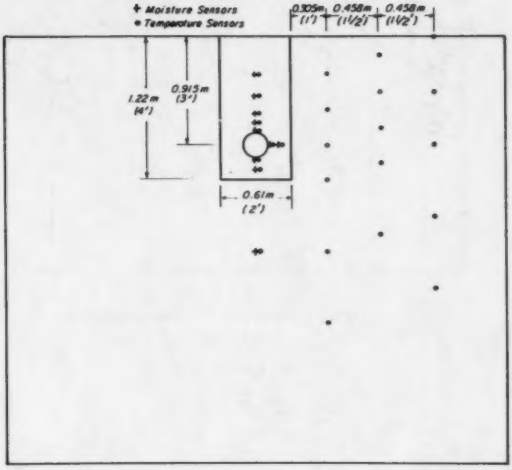

FIG. 15.—Design Locations of Moisture and Temperature Sensors in Field Trench

solutions. An explicit finite difference computer program was developed for analysis of flows in one dimension (1). Although a two-dimensional program would better represent the actual conditions, its greater complexity prohibited its development at this stage of the research.

Parameter Study

The properties obtained for three soils which have been widely used as cable backfill materials (PG and E crushed limestone, Round-Robin sand, and Fire Valley thermal sand) were used to analyze the relative importance of different parameters on the amount and rate of water movement under thermal gradients in a trench, cable, and backfill system using the one-dimensional coupled flow

computer program referred to in the foregoing. The native soil conditions, into which the cable and backfill are placed, were taken as 4 ft of highly plastic silty clay overlying a 1-ft thick layer of low plasticity silty clay underlain by silty sand and gravel. This profile is essentially that at the field test site to be described later, and it is referred to as the RFS soil profile.

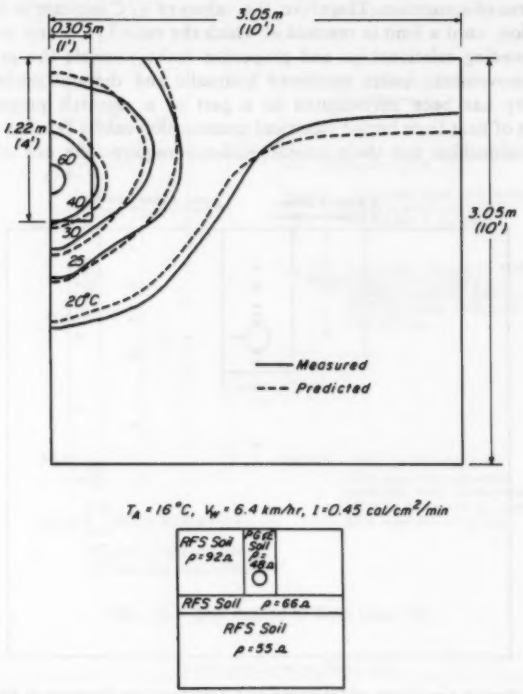

FIG. 16.—Measured and Predicted Temperature Distribution 5 Days After Heating Cable

The following parameters were studied:

1. Cable temperature.
2. Backfill soil type.
3. Open or closed system at ground surface.
4. Depth of water table.
5. Cable depth.
6. Values and distribution of initial soil water content.
7. Values and distributions of initial soil temperature.
8. Trench depth.

9. Weather variables: (1) Air temperature; (2) wind velocity; and (3) solar radiation.

Only the effects of cable temperature and backfill soil type are presented here to illustrate the type of results obtained. The ground surface was assumed to be at constant temperature and open to free evaporation. It was assumed also that the cable sheath temperature was increased instantaneously to a constant value.

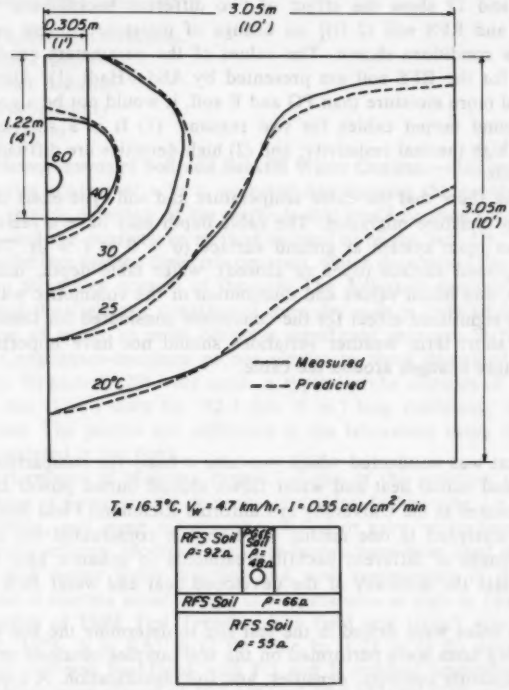

FIG. 17.—Measured and Predicted Temperature Distribution 20 Days After Heating Cable

Fig. 9 shows the predicted change of volumetric water content distribution with time for different cable temperatures and for the conditions shown on the sketch drawn beside the results, and Fig. 10 shows the change in moisture content of the soil adjacent to the cable with time for the same conditions. From Fig. 9 it is clear that the moisture content of both RFS soil layers do not change significantly either with time or with temperature. It is also clear from Figs. 9 and 10 that the moisture content of PG and E limestone decreases

appreciably from its initial as-compacted value with time for all cable temperatures. This is mainly due to gravitational flow, because the soil cannot hold more moisture than its field capacity (maximum amount of moisture that can be held against the force of gravity). From Fig. 10 it can be seen that after 100 days of operation, the moisture contents of soil adjacent to the 60° C and 90° C cables decrease to about 62% and 40% of that around the 15° C cable, respectively. Such moisture losses could be important if they are accompanied by decreases in thermal conductivity. In that case the ability of a cable backfill system to dissipate heat could be impaired.

Figs. 11 and 12 show the effect of two different backfill soil types [PG and E soil and RFS soil (2 ft)] on change of moisture content profile with time for the conditions shown. The values of the parameters needed for the predictions for the RFS soil are presented by Abdel-Hadi (1). Although RFS soil can hold more moisture than PG and E soil, it would not be a good backfill material around buried cables for two reasons: (1) It is a silty clay having a relatively high thermal resistivity; and (2) high densities are difficult to obtain with clay soils.

The results show that the cable temperature and soil type exert the greatest influence on moisture migration. The cable depth may have a relatively large effect for an open system at ground surface ($\theta = 0$ at $t > 0$). The type of system at ground surface (open or closed), water table depth, initial ground temperature, and initial values and distribution of the volumetric water content do not have significant effect for the conditions considered for these analyses. In general, short term weather variations should not have important effects on the moisture changes around the cable.

Field Test

A field test was conducted which provides a basis for comparison between theoretical and actual heat and water flows around buried power cables. The test site is located at the University of California Richmond Field Station (RFS). The trench analyzed is one among ten trenches constructed for analysis of the effectiveness of different backfill treatments to enhance heat dissipation and to evaluate the accuracy of the developed heat and water flow predictive methods (9).

Five bore holes were drilled in the test site to determine the soil conditions, and laboratory tests were performed on the soil samples obtained to determine the in-situ moisture contents, densities, and soil classification. A typical boring log is shown in Fig. 13. The soil at the test site consists generally of a stiff dark brown, highly plastic silty clay (CH) overlying a slightly inclined layer of light brown low plasticity silty clay (CL) about 1 ft thick at a depth of about 4 ft. Below this layer is a layer of silty sand and silty gravel with some silty clay seams. Free ground water was encountered at a depth of about 12 ft.

Thermal and hydraulic properties of the three main layers of the test site were evaluated in exactly the same way as described earlier for the PG and E crushed limestone and are reported by Abdel-Hadi (1).

Conduit and Heating System.—An 11-ft long, 8-in. I.D., carbon steel standard pipe was used as the casing of a simulated electrical transmission cable. A

heating rod was used as a heating element inside the pipe to generate the heat that could be expected in a real buried cable system. The space between the heating element and the pipe was filled with oil. Fig. 14 shows a schematic drawing of this heating system. The system is capable of producing 200 watts/ft under full load. A controller was designed to maintain constant temperature on the pipe, supply constant heat input, or supply programmed heat input.

To avoid the build-up of high pressure due to thermal expansion of the oil, an oil tank with a relief valve (+10 psi) was installed near the ground surface.

Weather Parameter Measurements.—The following weather parameters were measured during the field test:

1. Wind speed and direction.
2. Air temperature.
3. Net solar radiation.
4. Relative humidity.
5. Precipitation.

In-situ Measurements of Soil and Backfill Water Content.—Accurate measurement of water content of soils is essential for studying the problem of water movement in-situ. A review of the methods that could be used for this purpose was made, and the capacitance method seemed to be the best (1). This method is based on the fact that the dielectric constant, which determines the capacitance, depends on the water content of the soil. The dielectric constant of water is about 80 and the dielectric constant of oven-dry soils is only about 2.6. Thus, the addition of water to soils causes a significant increase in the dielectric constant. Capacitance-moisture probes similar to those described in Selig, et al. (16) and Wobschell (20) were used. A typical probe consists of a cylindrical case 25.4 mm (1 in.) diam by 152.4 mm (6 in.) long containing an electronic circuit inside. The probes are calibrated in the laboratory using the same soil to be encountered in the field.

Field Performance of Moisture Probes.—Some of the moisture probes failed due to leakage of water into the electronic circuit inside the probe; i.e., insufficient water proofing, and some other probes failed or gave misleading results due to temperature effects. Modified moisture probes have been used in subsequent trenches, with better water proofing and with components in the electronic circuit rated to operate satisfactorily at temperatures as high as 120° C.

Construction of Field Test Trench.—The field test trench was constructed on May 2, 1978. It is 0.61 m (2 ft) wide by 1.22 m (4 ft) deep by 3.05 m (10 ft) long and was backfilled with PG and E crushed limestone screenings. The screenings were placed at 18.1 kN/m^3–18.8 kN/m^3 (115 pcf–120 pcf) dry density and about 13% water content. The instrumentation around the cable consisted of 25 temperature sensors and 10 moisture probes arranged as shown in Fig. 15. Measurements of the soil and weather data were initiated immediately after the construction of the trench. Measurements under isothermal conditions continued for 20 days. Then the pipe was heated to a sheath temperature of 60° C, and this temperature was held constant.

Comparison of Measured and Predicted Temperature Distribution

The purposes of the field test program included evaluation of theoretical methods for predicting temperature distributions as a function of time and position

as well as moisture content distributions.

Temperature predictions were made using a finite element computer program "HEAT" (17). This program solves both transient and steady-state linear heat conduction problems in two dimensions with time dependent boundary conditions. The governing equations in the program are the heat balance and heat flow. The effects of conduction, convection, and solar radiation at the ground surface can be accounted for. Predictions were made for the time required for the pipe sheath to reach 60° C and for the temperature distribution around the pipe

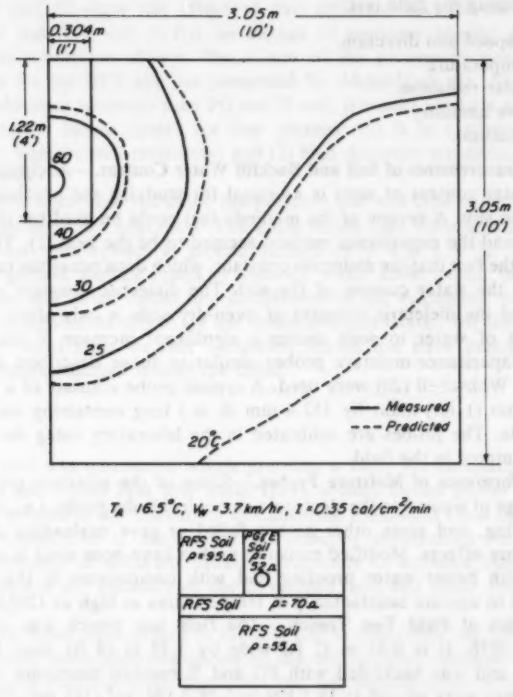

FIG. 18.—Measured and Predicted Temperature Distribution 40 Days After Heating Cable

at different times after pipe heating was initiated. Measured weather data and initial moisture and temperature conditions in the field were used in the predictions. The predicted time required for the cable sheath temperature to reach 60° C due to a heat input rate of 200 watts/ft was about 11 hr, while the actual time was about 12 hr.

Figs. 16–19 show comparisons between measured and predicted temperature distributions at 5 days, 20 days, 40 days, and 80 days after heating the pipe,

respectively. Also shown on each figure are the weather conditions (T_A = air temperature, V_W = wind velocity, I = solar radiation) and soil thermal resistivities, ρ, used for the calculations.

From these figures the following can be observed:

1. For times less than 40 days after heating the cable the agreement is excellent between the measured and predicted temperature contours.
2. For times greater than 40 days after heating the cable, the agreement is reasonably good, but the gap between the measured and predicted contours increases with time. This is mainly because of the accumulating error resulting from using the temperatures obtained theoretically at any time as the initial value for prediction of the temperatures at the following time.

In general, the predictions of the temperature distributions around the cable using program HEAT are good. The temperature profiles generated by the one-dimensional computer program for the conditions presented in Figs. 16–19 match fairly well with the measured field temperature profiles above the cable. However, the program underestimates the temperature gradients measured in the trench immediately below the cable. This is believed to be due to the two-dimensional nature of the problem.

Comparison of Measured and Predicted Moisture Content Distributions

Before construction of the field test trench, a theoretical prediction for the drying of the backfill soil was made using laboratory measured properties of the soil expected to be used as backfill. After the heating of the field trench, the results obtained from the moisture probes indicated that the drying of the backfill soil due to both gravity and temperature gradient was at a slower rate than predicted. Several possible reasons for this difference in drying rate were investigated.

The saturated hydraulic conductivity of a sample obtained from the actual backfill soil, Sample 2, was found to be 1×10^{-4} mm/s compared to 2.7×10^{-4} mm/s for the sample of the soil tested previously in the laboratory, Sample 1. Also, Sample 2 had slightly more fines passing #200 sieve (about 8%) than Sample 1 tested previously (about 5%), although the two samples had essentially the same gradation curve. These differences are very important, because the predicted values of water content are very sensitive to the hydraulic conductivity of the soil. Using the new value and a new measured relationship between the suction head and water content for Sample 2, the coupled flow parameters were recalculated and used to predict new values for the water content around the cable with time.

Because of the failure of some of the moisture probes due to both insufficient waterproofing and temperature effects, and because of some suspicious water content values obtained from some other moisture probes, a borehole was made every 20 days to obtain actual water contents from soil samples.

Fig. 20 shows the measured values obtained from the bore hole samples and the predicted values using properties obtained from Samples 1 and 2. The following can be observed from these results:

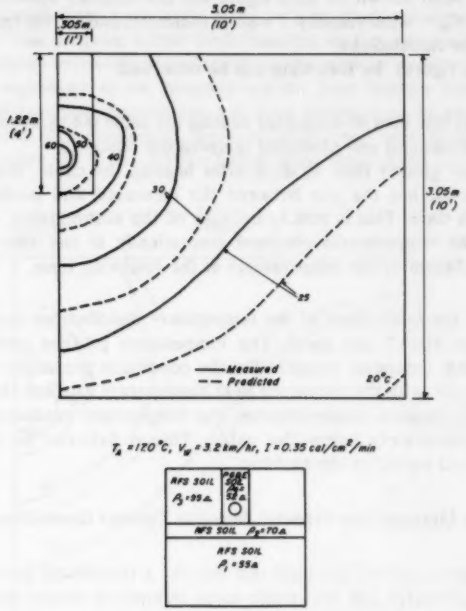

FIG. 19.—Measured and Predicted Temperature Distribution 80 Days After Heating Cable

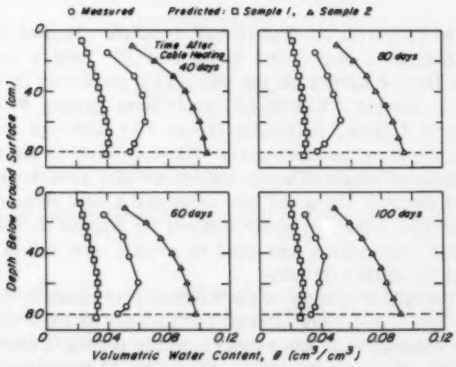

FIG. 20.—Comparison of Measured and Predicted Moisture Content of Backfill Soil Above Cable

1. Neither of the predicted water content profiles, using properties of Samples 1 and 2, agrees well with the measured profile from bore hole samples. However, the measured profile lies inside a wide band formed by the two predicted profiles.
2. Neither of the predicted water content profiles shows the drop in water content just above the cable (water migration under thermal gradient) which is seen in the measured profile.
3. A relatively small change in the soil gradation and density may have great effect on the predicted water contents. This fact raises questions about the ability to predict accurately the amount of water content changes under thermal gradients for materials of the type studied herein, especially considering the uncertainties involved in both measuring the properties of truly representative samples and the field handling and placement of soils. Further research on this question is in progress.

One Dimensional Versus Two Dimensional Model

The geometry of the trench-cable system allows the flow of water and heat away from the cable in all radial directions. Nonetheless, it had been thought, since the cable is confined in a trench surrounded by relatively impervious soil, that some insight into the moisture migration problem and some estimate of water content profiles in the test trenches might be obtainable from a one-dimensional model. Additionally, a one-dimensional formulation was used first because of the greater difficulty associated with the two-dimensional numerical analysis. Final conclusions about the adequacy of the one-dimensional model cannot yet be drawn from the analysis of this single trench.

Development of a two-dimensional model would provide the following advantages as compared with the presently available one-dimensional solution:

1. Actual geometry could be simulated.
2. More representative boundary conditions could be used.
3. Comparison between measured and predicted water content and temperature contours could be made.

Summary and Conclusions

The theory of Philip and DeVries (13) was used for prediction of thermally induced moisture movement in unsaturated soils. Theoretical analysis of moisture movement and the parameters affecting it in a typical trench, buried electrical cable, and backfill system indicated that the most important parameters affecting the rate and amount of moisture migration away from the cable should be cable temperature and soil type. Gravitational flow, surface evaporation, and isothermal diffusion have great effect on the moisture changes in the backfill and are mainly responsible for early changes of the moisture content in the trench backfill.

A field test simulating an actual buried cable system was conducted to evaluate predictive methods for time-dependent temperature and moisture distributions. Capacitance-probes for moisture content measurements did not perform well because of insufficient waterproofing and temperature effects. Actual moisture content values of the trench backfill were obtained from borehole soil samples.

The water content profiles predicted for the field trench using soil properties obtained from two backfill samples, differing slightly in gradation and density, matched poorly with the measured profile. However, the measured profile fell within the band formed by the two predicted profiles. The predicted water content values were found to be very sensitive to small changes in the soil gradation and density.

The finite element computer program "HEAT" was used to predict the temperature distribution around the cable at different times after initiation of cable heating. The results showed that there is excellent agreement between the measured and predicted temperature contours up to 40 days and good agreement between the contours from 40 days–100 days.

Acknowledgment

The studies described in this paper were sponsored by the Electric Power Research Institute, Palo Alto, California, under the agreement No. RP 7841-1, Backfill Materials for Underground Power Cables. John C. McMillan a graduate research assistant at the University of California, at Berkeley, California, reviewed carefully the work presented in this paper. K. N. Akay of the Pacific Gas and Electric Company provided valuable technical input.

Appendix.—References

1. Abdel-Hadi, O. N., "Flow of Heat and Water Around Underground Power Cables," thesis presented to the University of California, at Berkeley, Calif., in 1978, in partial fulfillment of the requirements for the degree of Doctor of Philosophy.
2. Cassel, D. K., Nielsen, D. R., and Biggar, J. W., "Soil Water Movement in Response to Imposed Temperature Gradients," *Soil Science Society of America*, Proc. 33, 1969, pp. 493–500.
3. Elzeftawy, A., and Dempsey, B. J., "Prediction Model for Hydraulic Conductivity and Moisture Diffusivity of Highway Soils," presented at the January, 1977, 56th Annual Meeting of the Transportation Research Board.
4. Elzeftawy, A., and Mansell, R. S., "Hydraulic Conductivity Calculations for Unsaturated Steady-State and Transient-State Flow in Sand," *Soil Science Society of America*, Proc. 39, 1975, pp. 599–605.
5. Green, R. E., and Corey, J. C., "Calculation of Hydraulic Conductivity: A Further Evaluation of Some Predictive Methods," *Soil Science Society of America*, Proc. 35, 1971, pp. 3–8.
6. Gurr, C. G., Marshall, T. J., and Hutton, J. T., "Movement of Water in Soil Due to a Temperature Gradient," *Soil Science*, Vol. 74, 1952, pp. 335–345.
7. Kunze, R. J., Vehera, G., and Graham, K., "Factors Important in the Calculation of Hydraulic Conductivity," *Soil Science Society of America*, Proc. 32, 1968, pp. 760–765.
8. Marshall, T. J., "A Relation Between Permeability and Size Distribution of Pores," *Journal Soil Science*, Vol. 9, 1958.
9. Mitchell, J. K., Kao, T-C., and Abdel-Hadi, O. N., "Backfill Materials for Underground Power Cables," Phase I, Thermal Resistivity Measurement Methods, Backfill Treatments, Heat and Moisture Flow Analysis, Report prepared for the Electric Power Research Institute, June, 1977.
10. Mitchell, J. K., and Kao, T-C., "Measurement of Soil Thermal Resistivity," *Journal of the Geotechnical Engineering Division*, ASCE, Vol. 104, No. GT10, Proc. Paper 14080, Oct., 1978, pp. 1307–1320.
11. Nielsen, D. R., Kirkham, D., and Perrier, E. R., "Soil Capillary Conductivity: Comparison of Measured and Calculated Values," *Soil Science Society of America*, Proc. 24, 1960, pp. 157–160.

12. Penman, H. L., "Gas and Vapor Movement in Soil," *International Journal Agricultural Science*, Vol. 30, 1940, pp. 437–462.
13. Philip, J. R., and DeVries, D. A., "Moisture Movement in Porous Materials Under Temperature Gradients," *Transactions*, American Geophysical Union, Vol. 38, The American Geographical Union of the Academy of Sciences, National Research Council, Washington, D.C., 1957, p. 222.
14. Raudkivi, A. J., and U'u, N. V., "Soil Moisture Movement by Temperature Gradient," *Journal of the Geotechnical Engineering Division*, ASCE, Vol. 102, No. GT12, Proc. Paper 12645, Dec., 1976, pp. 1225–1244.
15. Rollins, R. L., Spangler, M. G., and Kirkham, D., "Movement of Soil Moisture Under a Thermal Gradient," *Highway Research Board Proceedings*, 33, 1954, pp. 492–508.
16. Selig, E. T., Wobschall, D. C., Mansukhani, S., and Motiwala, A., "Capacitance Sensor for Soil Moisture Measurement," *Transportation Research Record 532*, 1975, pp. 64–76.
17. Taylor, R. L., "HEAT, A Finite Element Computer Program for Heat-Conduction Analysis," *Report 75-1*, prepared for Civil Eng. Lab., Naval Construction Battalion Center, Port Hueneme, California, Department of Civil Engineering, University of California, Berkeley, Calif., May, 1975.
18. Taylor, S. A., and Cary, J. W., "Linear Equations for the Simultaneous Flow of Matter and Energy in a Continuous Soil System," *Soil Science Society of America*, Proc. 28, 1964, pp. 167–172.
19. Taylor, S. A., and Cavazza, L., "The Movement of Soil Moisture in Response to Temperature Gradients," *Soil Science Society of America*, Proc. 18, 1954, pp. 351–358.
20. Wobschall, D., "A Frequency Shift Dielectric Soil Moisture Sensor," *IEEE Transactions on Geoscience Electronics*, Vol. 16, Apr., 1978.

TOLERABLE SETTLEMENT OF BUILDINGS[a]

By Harvey E. Wahls,[1] F. ASCE

INTRODUCTION

Settlement analyses are a critical part of the selection and design of building foundations. The anticipated settlement must be predicted, and, then, the tolerance of the structure to the predicted settlement must be evaluated. The purpose of this paper is to review current concepts and practices for establishing tolerable settlements for buildings. Procedures for prediction of settlement are not considered.

Previous reviews (3,4) have indicated many of the difficulties of establishing allowable settlements for buildings. Clearly, settlement that affects the safety or function of a structure is unacceptable. Such considerations may be the governing factors for warehouses and industrial mill buildings. However, appearance also is of concern for many types of buildings, and significant cracking of architectural elements usually will be unacceptable to most owners of residential, office, and commercial buildings.

The determination of the settlement that will cause significant cracking of structural members or architectural elements, or both, is a complex indeterminate analytical problem. It is affected by many factors, including the type and size of the structure, the properties of the structural materials and the subsurface soils, and the rate and uniformity of settlement. Because of these complexities, critical settlements have not been determined analytically. Instead, almost all criteria for tolerable settlement have been established empirically on the basis of observations of settlement and damage in existing buildings. Usually, a qualitative assessment of the level of damage is correlated with some measure of differential settlement. Then, an attempt is made to relate the differential settlement to the maximum absolute settlement.

Several inherent limitations to this empirical approach to tolerable settlements should be recognized. The primary problem is the scarcity of complete and reliable case studies. The assessment of the type and degree of damage usually is qualitative. Often, detailed descriptions of the structures and soil conditions

[a]Presented at the October 27–31, 1980, ASCE Annual Convention and Exposition, held at Hollywood, Fla.

[1]Prof. of Civ. Engrg., North Carolina State Univ., Raleigh, N.C.

Note.—Discussion open until April 1, 1982. To extend the closing date one month, a written request must be filed with the Manager of Technical and Professional Publications, ASCE. Manuscript was submitted for review for possible publication on March 12, 1981. This paper is part of the Journal of the Geotechnical Engineering Division, Proceedings of the American Society of Civil Engineers, ©ASCE, Vol. 107, No. GT11, November, 1981. ISSN 0093-6405/81/0011-1489/$01.00.

are not available. Sometimes erroneous assumptions are made regarding the relation of damage to settlement. Not all cracking is due to settlement, and, conversely, the absence of cracking does not necessarily mean there has been no settlement. Relatively few settlement records are reported for undamaged buildings, and, consequently, the available case studies are biased toward situations in which damage has been observed.

With the preceding limitations in mind, the currently accepted settlement criteria will be reviewed and the basis for these criteria will be discussed. Some simple conceptual ideas will be used to illustrate the effects of various factors and to aid the interpretation of observed data.

Definitions

Settlement refers to the vertical displacement of the foundation. Because

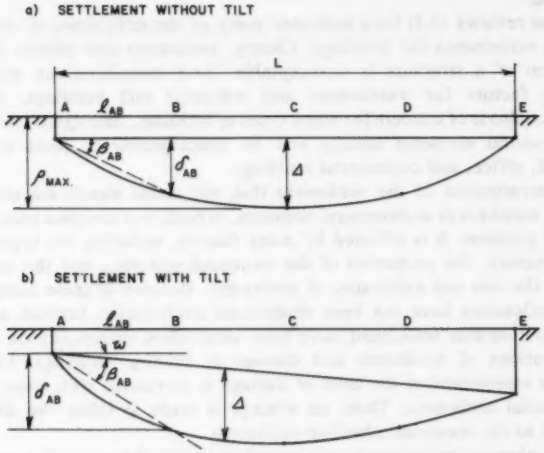

FIG. 1.—Definitions of Settlement Terminology

damage commonly is related to variations in the settlement at different locations in the building, the differential settlement is usually of more interest than absolute settlement. Common terminology for describing absolute and differential settlement is defined for cases without and with a component of rigid body rotation or tilting in Fig. 1(*a*) and 1(*b*), respectively. The following terms are defined ρ_i = vertical displacement at i; δ_{ij} = differential settlement between i and j; Δ = relative deflection = maximum displacement from a straight line connecting two reference points; ω = tilt = rigid body rotation; $\beta_{ij} = \delta_{ij}/l_{ij} - \omega$ = angular distortion; and Δ/L = deflection ratio, which is an approximate measure of the curvature of the settlement curve.

Early Experience

In 1948, Peck (7) presented an excellent history of foundation engineering practices in Chicago. The period between 1880 and 1900 is of particular interest because of the common use of isolated spread footings and the recognition of settlement as a major design consideration. Peck identifies 60 buildings of nine or more stories, which were constructed on spread footings during the period 1883–1895. Three major structures (the Auditorium, the Board of Trade, and the Polk Street Station) quickly suffered major damage because of large differential settlements between heavily loaded tower sections and adjacent lower sections. As a result of the experiences with these structures, engineers subsequently attempted to design structures with loads more evenly distributed so as to produce relatively uniform settlement. Then, the foundations were constructed above the desired final grade to provide an allowance for settlement. For several buildings, including the well-known 16-story Monadnock Building and the 21-story Masonic Temple, allowance was made for 8–9 in. (200–300 mm) of anticipated settlement.

Peck summarizes that as a result of their experiences, "By 1895 most engineers and architects in Chicago felt themselves masters of their foundation problems. They accepted the idea that a certain amount of distortion of building frames due to differential settlement was inevitable, and, if anticipated, was not harmful."

Time ultimately has provided the opportunity to judge the relative success of these early foundation engineers and their treatment of potential settlement. Peck cites several cases in which the observed settlements exceeded 12 in. (300 mm). For the Monadnock Building, the maximum settlement eventually exceeded 21 in. (530 mm), and differential settlements in excess of 4 in. (100 mm) were observed. Thus, the settlements clearly must have been seriously underestimated in the original designs. However, Peck reports that aside from the three structures with towers, which have been mentioned previously, no serious structural damage was reported for 56 of the remaining 57 structures listed in his study, and 38 were still in service in 1940. Many subsequently have been replaced by much larger high rise office buildings, but several of these early structures, including the Monadnock Building, remain in use today.

Several basic points are illustrated by the Chicago experiences. First, buildings should be expected to settle. Second, differential settlement is more critical than total settlement. Third, structures and their foundations can be designed to minimize differential settlement. Finally, significant settlements can be tolerated without impairing the safety and function of many structures.

Development of Current Criteria for Differential Settlement

Almost all current tolerable settlement criteria for buildings are based on the classic studies by Skempton and MacDonald (9) and by Polshin and Tokar (8). Skempton and MacDonald (9) reported observations of settlement and damage for 98 buildings, including both steel and reinforced concrete frame structures and structures with load-bearing walls. Buildings supported on spread footings, mats, and piles were included in the study. Damages to panel walls, interior partitions, floors, or primary structural members were reported for 40 structures.

Because most of the damage appeared to be related to distortional deformations,

"angular distortion" was selected as the critical index of settlement. They concluded that cracking of load-bearing walls or panel walls in frame structures is likely when δ/l exceeds $1/300$ and that structural damage is probable when δ/l exceeds $1/150$. Finally, Skempton and MacDonald suggested $\delta/l = 1/500$ as a design criterion that provides some factor of safety against any cracking.

The Skempton-MacDonald criteria subsequently were incorporated into recommended limiting values of angular distortion proposed by Bjerrum (1). See Table 1. A more recent study by Grant, Christian, and Vanmarcke (5) reviewed settlement and damage data for an additional 95 buildings, of which 56 reportedly had suffered some damage. This study supports the Skempton-MacDonald conclusion that cracking should be anticipated when δ/l exceeds $1/300$.

Both Skempton and MacDonald and Grant, et al. assume that tilting is rigid body rotation which does not contribute to the distortion of the structure, and, thus, both have removed the differential settlement due to tilting from the computed values of angular distortion. Leonards (6) questions the validity of

TABLE 1.—Limiting Angular Distortion[a]

Category of potential damage (1)	$\beta = \delta/\ell$ (2)
Danger to machinery sensitive to settlement	1/750
Danger to frames with diagonals	1/600
Safe limit for no cracking of buildings[b]	1/500
First cracking of panel walls	1/300
Difficulties with overhead cranes	1/300
Tilting of high rigid buildings becomes visible	1/250
Considerable cracking of panel and brick walls	1/150
Danger of structural damage to general buildings	1/150
Safe limit for flexible brick walls, $L/H > 4$[b]	1/150

[a]From Bjerrum (1).
[b]Safe limits include a factor of safety.

this assumption for a framed structure supported on isolated spread footings. For this case, he correctly notes that tilting contributes to the stress and strain in the frame unless each individual footing tilts or rotates through the same angle as the overall structure. Because this is unlikely to occur, he suggests that the effects of tilt should be included in the differential settlement criteria, particularly for framed structures on isolated footings.

It is interesting to note that Terzaghi and Peck (12) suggested that "Most ordinary structures, such as office buildings, apartment houses or factories can withstand a differential settlement between adjacent columns of 3/4 in." This is approximately equivalent to an angular distortion of $1/300$ if one assumes a typical column spacing of 20 ft (6 m).

Polshin and Tokar (8) presented Soviet experiences and included allowable settlement criteria from the 1955 USSR Building Code. These criteria, which were based on more than 25 yr of settlement observations, are summarized in Tables 2 and 3.

There are several notable differences between the Soviet criteria and the work of Skempton and MacDonald. Frame structures and load-bearing walls

are treated separately. For frames, the allowable settlement is expressed in terms of the slope, or the differential settlement between adjacent columns;

TABLE 2.—Allowable Settlement Criteria: 1955 U.S.S.R. Building Code[a]

Type of structure (1)	Sand and hard clay (2)	Plastic clay (3)
(*a*) $\beta = \delta/\ell$		
Civil- and Industrial-Building Column Foundations:		
For steel and reinforced concrete structures	0.002	0.002
For end rows of columns with brick cladding	0.007	0.001
For structures where auxiliary strain does not arise during nonuniform settlement of foundations	0.005	0.005
Tilt of smokestacks, towers, silos, etc.	0.004	0.004
Craneways	0.003	0.003
(*b*) Δ/L		
Plain brick walls:		
For multistory dwellings and civil buildings		
at $L/H \leq 3$	0.0003	0.0004
at $L/H \geq 5$	0.0005	0.0007
For one-story mills	0.0010	0.0010

[a]From Polshin and Tokar (8).

TABLE 3.—Allowable Average Settlement for Different Building Types[a]

Kind of building (1)	Allowable average settlement, in inches (millimeters) (2)
Building with plain brick walls	
$L/H \geq 2.5$	3 (80)
$L/H \leq 1.5$	4 (100)
Building with brick walls, reinforced with reinforced concrete or reinforced brick	6 (150)
Framed building	4 (100)
Solid reinforced concrete foundations of smokestacks, silos, towers, etc.	12 (300)

[a]From Polshin and Tokar (8).

which is very similar to the angular distortion criterion of Skempton and MacDonald without correction for tilt. The limiting values in the Soviet code

range from 1/500–1/200 and are approximately the same as the Skempton-MacDonald limits.

Polshin and Tokar's treatment of load-bearing walls introduced several significant concepts. First, instead of slope, the allowable settlement is defined in terms of deflection ratio, Δ/L. Then, the maximum allowable deflection ratio is assumed to be related to the development of a critical level of tensile strain in the wall. For brick walls, the critical tensile strain is assumed to be 0.05%. Using these concepts, the deflection ratio at which cracking occurred in brick walls is related theoretically to the length to height ratio, L/H, of the wall. The theoretical relation agrees with observations of damaged and undamaged buildings. Finally, for multistory brick buildings, a larger deflection ratio is allowed for structures supported on plastic clay than for structures founded on sand or hard clay. Presumably, the slower rate of settlement for plastic clays allows time for creep of the structure and increases the level of tensile

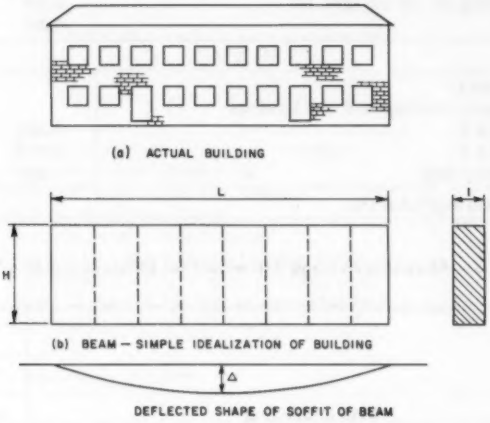

FIG. 2.—Rectangular Beam Analogy for Building (2)

strain, and, therefore, the deflection ratio at which cracking begins.

In summary, the Polshin and Tokar paper generally supports the Skempton-MacDonald criteria for framed structures but imposes more stringent limits on differential settlement of load-bearing brick walls. Polshin and Tokar also introduce the important roles of critical tensile strain, (L/H) as a measure of structural flexibility and the rate of settlement. The concepts of Skempton and MacDonald and Polshin and Tokar can be found in most current settlement criteria. Essentially, similar criteria are used in the USA (10), the USSR (8) and many other countries (9,11).

The state-of-the-art report by Burland and Wroth (2), presented at the 1974 Conference on Settlement of Structures at Cambridge University, has contributed significantly to the understanding of factors that influence the allowable settlement of structures. Using the concept that visible cracking begins when a critical value of tensile strain is reached, Burland and Wroth proposed that a building

RECTANGULAR BEAM

Points of Critical Tensile Strain

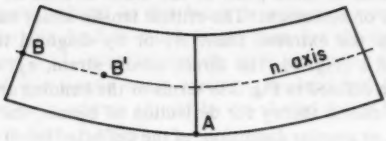

Direct Tension (A)—(extreme fiber)

ε_b = direct tensile strain

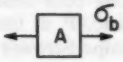

$$\varepsilon_b = \frac{\sigma_b}{E} = \frac{Mc}{EI} \qquad \sigma_b = \frac{Mc}{I}$$

Diagonal Tension (B)—(neutral axis)

ε_d = diagonal tensile strain

$$\varepsilon_d = \frac{\gamma}{2} = \frac{\tau}{2G} = \frac{3V}{4AG} \qquad \tau = \frac{3V}{2A}$$

FIG. 3.—Definition of Critical Tensile Strain

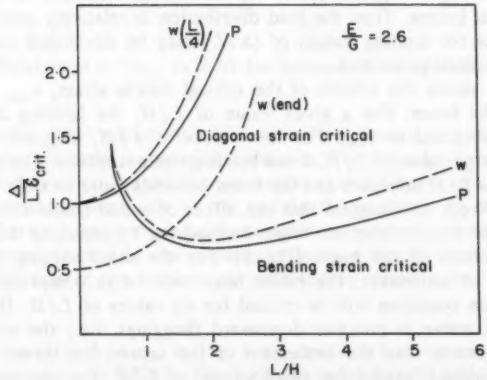

FIG. 4.—Relation of $\Delta / L\epsilon_{crit}$ to L/H for Isotropic Beam—Neutral Axis at Mid-Depth (2)

may be represented approximately by a simple rectangular beam (Fig. 2). This model then is used to show the factors that affect the settlement at which cracking begins.

In this idealization, the deflection ratio, Δ/L, at which the critical tensile strain, ϵ_{crit}, is reached at some point in the beam is used as the criterion for allowable deflection or settlement. The critical tensile strain may develop either by direct tension in the extreme fiber, A, or by diagonal tension along the neutral axis, B or B', (Fig. 3). The direct tensile strain, ϵ_b, and the diagonal tensile strain, ϵ_d, are defined in Fig. 3 in terms of the bending and shear stresses, respectively. Using elastic theory for deflection of beams, the deflection ratio, Δ/L, and the slope, or angular distortion, of the deflected beam can be expressed in terms of the elastic properties of the beam and either of the critical tensile strains, ϵ_b or ϵ_d. Burland and Wroth considered the deflections of a simple beam, including both bending and shear effects, for two loading conditions: (1) A point load, P, at the mid-span; and (b) a uniformly distributed load, w. The relationships between Δ/L and critical tensile strain for these cases are presented in Appendix I.

The role of various factors on the establishment of the allowable (Δ/L) may be observed by plotting the relation of $\Delta/L\epsilon_{crit}$ to L/H. Fig. 4 shows these relations for the case of an isotropic beam with the neutral axis at the mid-depth and Poisson's ratio equal to 0.3, for which the ratio of Young's modulus to the shear modulus, $E/G = 2.6$. Curves are plotted for the central point load and the uniformly distributed load assuming either bending strain or diagonal strain may be critical. When bending strain is assumed critical, the curves are relatively insensitive to the assumed load distribution. When diagonal strain is assumed critical, the curves for the two loading conditions are again similar if shear stress at the quarter-point of the span is considered. However, if shear at the end of the beam is considered, the results are quite different for the two loading conditions. Burland and Wroth suggest that the theoretical shear stress conditions at the quarter-point are more representative of practical conditions in real beams. Then the load distribution is relatively unimportant, and the concepts for limiting values of (Δ/L) may be developed using only the case of the central point load.

Fig. 4 clearly shows the effects of the critical tensile strain, ϵ_{crit}, and the L/H ratio of the beam. For a given value of L/H, the limiting Δ/L will be directly proportional to ϵ_{crit}. For low values of L/H, diagonal strain is critical, and for large values of L/H, direct bending strain is critical. The allowable Δ/L increases as L/H increases and the beam becomes more flexible.

Burland and Wroth also suggest that the effect of a mat foundation, which is very stiff in the lateral direction, might be modeled by assuming the neutral axis is at the bottom of the beam (Fig. 5). For the usual sagging (concave upward) pattern of settlement, the entire beam will be in compression, and the diagonal strain condition will be critical for all values of L/H. However, if the settlement curve is concave downward (hogging), i.e., the settlement of the ends is greater than the settlement of the center, the direct bending strains become critical, except for small values of L/H. For this condition, the allowable deformations will be significantly smaller than for the case with the neutral axis at the middle. This result suggests that the allowable differential settlement should be smaller for cases in which the settlement curve is concave

downward, e.g. in the case of subsidence of ends due to adjacent excavations or differential heave due to swelling soils.

Burland and Wroth also note that many structures are more flexible in shear than in direct tension. They suggest that this condition may be modeled by varying the ratio E/G of the rectangular beam. The results show that diagonal strain becomes more critical as the beam is assumed more flexible in shear (Fig. 6). The allowable Δ/L is much larger than for the cases with the lower values of E/G, and Δ/L increases rapidly with increasing L/H.

On the basis of this simple beam analogy, Burland and Wroth propose that limiting deflection ratio criteria should be developed for at least three different cases, illustrated in Figs. 6 and 7:

1. Diagonal strain will be critical for framed structures, which typically are relatively flexible in shear, and reinforced load-bearing walls, which are relatively stiff in direct tension. This case may be approximated by the behavior of the rectangular beam with a high equivalent E/G, as shown by curve 3 in Fig. 6 and curve 1 in Fig. 7.

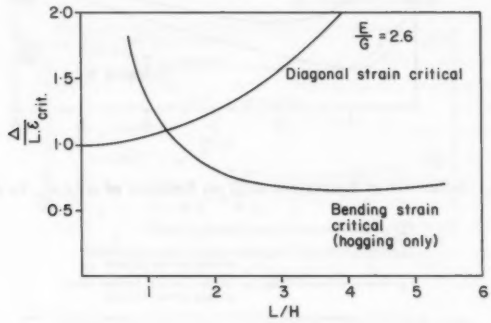

FIG. 5.—Relation of $\Delta/L\epsilon_{crit}$ to L/H for Isotropic Beam—Neutral Axis at Bottom (2)

2. *Bending strain* will be critical for unreinforced masonry walls and structures, which have relatively low tensile resistance. For the *sagging mode* (settlement curve concave upward), the behavior may be modeled by the isotropic rectangular beam with the neutral axis at the mid-depth, as shown by curve 2 in Figs. 6 and 7. For the *hogging mode* (settlement curve concave downward), the behavior may be approximated by the rectangular beam with low equivalent, E/G, and the neutral axis at the bottom, as indicated by curve 4 in Fig. 6 and curve 3 in Fig. 7.

The curves for $\Delta/L\epsilon_{crit}$ in Fig. 6 are converted to curves of Δ/L in Fig. 7 by assuming $\epsilon_{crit} = 0.075\%$. Fig. 7 also includes Polshin and Tokar's criterion for cracking of unreinforced load-bearing walls, which assumes $\epsilon_{crit} = 0.05\%$, and the Skempton-MacDonald criteria of 1/500 and 1/300 for angular distortion. In order to relate angular distortion to deflection ratio, Burland and Wroth

(2) assume that the maximum angular distortion of the beam equals the slope at the end supports.

The curves in Fig. 7 are compared with observed settlements and damage of real structures in Fig. 8. For frame buildings with L/H less than 3, the

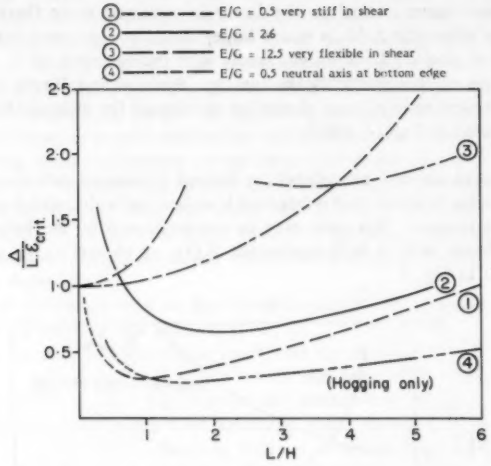

FIG. 6.—Influence of Equivalent E/G on Relation of $\Delta/L\epsilon_{crit}$ to L/H (2)

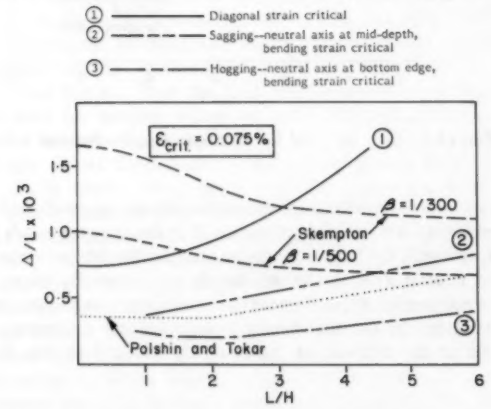

FIG. 7.—Proposed Criteria for Limiting Values of Δ/L

Burland-Wroth curve 1 and the Skempton-MacDonald criterion both appear to provide reasonable and satisfactory limits for the deflection ratio. For L/H greater than 3, the Skempton-MacDonald criterion is the more conservative

of the two. However, no field observations were available for comparison. For load-bearing walls in the sagging mode [Fig. 8(*b*)], the Skempton-MacDonald criterion appears to be unconservative while Polshin and Tokar's limit and curve

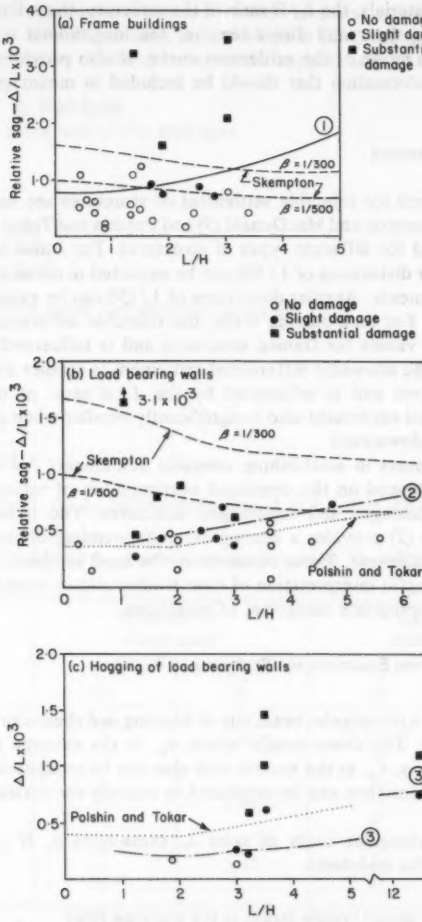

FIG. 8.—Comparisons of Observed Settlement and Damage with Proposed Criteria for Δ / L (2)

2 both appear to provide reasonable limits. Finally, Fig. 8(*c*) shows that load-bearing walls in the hogging mode may crack at deflection ratios that are much smaller than the Polshin-Tokar limits. However, curve 3 appears to provide

a reasonable limit for this case, but relatively few data are available.

In summary, the Burland-Wroth beam analogy provides a conceptual mechanism for understanding the factors that may influence tolerable settlements. The model can be used to demonstrate the effects of the critical tensile strain of the structural materials, the L/H ratio of the structure, the relative stiffnesses of the structure in shear and direct tension, the longitudinal stiffness of the foundation and the mode of the settlement curve. It also provides some insight into the type of information that should be included in meaningful settlement case histories.

Summary and Conclusions

The current criteria for tolerable settlement of structures are based primarily on the works of Skempton and MacDonald (9) and Polshin and Tokar (8). Different criteria are required for different types of structures. For frame buildings with panel walls, angular distortions of 1/300 can be expected to cause some cracking of architectural elements. Angular distortions of 1/150 can be expected to cause structural damage. For load-bearing walls, the tolerable differential settlement is smaller than the values for framed structures and is influenced by the L/H ratio of the wall. The allowable differential settlement is smaller than the values for framed structures and is influenced by the L/H ratio of the wall. The allowable differential settlement also is significantly smaller when the settlement pattern is concave downward.

Future improvements in establishing tolerable settlements for various types of structures will depend on the continued accumulation of reliable settlement records for both damaged and undamaged structures. The beam analogy of Burland and Wroth (2) provides a conceptual understanding of the factors that control tolerable settlement. These concepts can be used to identify information required for meaningful interpretation of case studies and to separate data from case studies into appropriate categories of structures.

Appendix I.—Deflection Equations for Rectangular Beams

The deflection of a rectangular beam due to bending and shear can be computed from elastic theory. The direct tensile strain, ϵ_b, in the extreme fiber and the diagonal tensile strain, ϵ_d, at the neutral axis also can be computed from elastic theory. These relations then can be combined to express the deflection in terms of either ϵ_b or ϵ_d.

For a simple rectangular beam of span L, cross-section, $H \times 1$, and with the neutral axis at the mid-depth

$$\epsilon_b = \frac{Mc}{EI} = \frac{6M}{EH^2} = \text{direct tensile strain at the extreme fiber} \quad \ldots\ldots\ldots (1)$$

and $$\epsilon_d = \frac{3V}{4GA} = \frac{3V}{4GH} = \text{diagonal tensile strain at the neutral axis} \quad \ldots\ldots (2)$$

in which M = bending moment; V = shear force; H = depth of beam; L = length of beam; E = Young's modulus; G = shear modulus; $A = H \times 1$ = cross-sec-

tional area of beam; $I = H^3/12$ = moment of inertia about the neutral axis; and $c = H/2$ = distance from neutral axis to extreme fiber.

A relation between deflection ratio, Δ/L, and angular distortion $\delta/\ell = \beta$ may be established by assuming that β can be represented by the slope of some portion of the beam. Three definitions of β are considered: β_0 = slope at the support = maximum slope; $\beta_{L/4}$ = slope at $L/4$, the quarter-point of the span; and β_{avg} = slope of chord between the support and $L/4$.

Point Load, P, at Mid-Span

For a single point load at the mid-span

$$M_{max} = \frac{PL}{4} \quad \ldots\ldots (3)$$

and $$\epsilon_{bmax} = \frac{3PL}{2EH^2} \quad \ldots\ldots (4)$$

The corresponding shear and diagonal strain are

$$V = \frac{P}{2} \quad \ldots\ldots (5)$$

and $$\epsilon_d = \frac{3P}{8GH} \quad \ldots\ldots (6)$$

Deflection ratio, Δ/L. Substituting Eqs. 3 and 5 into the expression for the

TABLE 4.—Coefficients for Equations 10 and 20

Definition of β (1)	Equation 10 Point Load		Equation 20 Uniform Load	
	C_1 (2)	C_2 (3)	C_3 (4)	C_4 (5)
β_0	$\frac{1}{3}$	2.60	$\frac{5}{16}$	3.90
$\beta_{L/4}$	$\frac{4}{11}$	2.84	$\frac{20}{57}$	3.28
β_{avg}	$\frac{4}{9}$	3.47	$\frac{5}{11}$	2.84

maximum deflection of a rectangular beam

$$\frac{\Delta}{L} = \frac{PL^2}{48EI} + \frac{3P}{8GH} = \left[\frac{2}{3}\left(\frac{L}{H}\right)^2\left(\frac{G}{E}\right) + 1\right]\frac{3P}{8GH} \quad \ldots\ldots (7)$$

In terms of ϵ_b

$$\frac{\Delta}{L} = \left[\frac{1}{6}\left(\frac{L}{H}\right) + \frac{1}{4}\left(\frac{H}{L}\right)\left(\frac{E}{G}\right)\right]\epsilon_b \quad \ldots\ldots\ldots\ldots\ldots\ldots\ldots\ldots (8)$$

In terms of ϵ_d

$$\frac{\Delta}{L} = \left[\frac{2}{3}\left(\frac{L}{H}\right)^2\left(\frac{G}{E}\right) + 1\right]\epsilon_d \quad \ldots\ldots\ldots\ldots\ldots\ldots\ldots\ldots (9)$$

Relation of Δ/L to $\delta/\lambda = \beta$

$$\frac{\Delta}{L} = C_1\beta\left[\frac{1 + 3.9\left(\frac{H}{L}\right)^2}{1 + C_2\left(\frac{H}{L}\right)^2}\right] \quad \ldots\ldots\ldots\ldots\ldots\ldots\ldots\ldots (10)$$

in which C_1 and C_2 are coefficients that depend on the definition of β. Values of C_1 and C_2 are given in Table 4.

Uniformly Distributed Load, w

For a uniformly distributed load over the entire span length

$$M_{max} = \frac{wL^2}{8} \quad \ldots\ldots\ldots\ldots\ldots\ldots\ldots\ldots\ldots\ldots\ldots\ldots (11)$$

and $$\epsilon_{bmax} = \frac{3w}{4E}\left(\frac{L}{H}\right)^2 \quad \ldots\ldots\ldots\ldots\ldots\ldots\ldots\ldots\ldots\ldots (12)$$

For this case, the shear and the diagonal strain vary linearly along the span length. At the support

$$V = \frac{wL}{2} \quad \ldots\ldots\ldots\ldots\ldots\ldots\ldots\ldots\ldots\ldots\ldots\ldots (13)$$

and $$\epsilon_d = \frac{3wL}{8GH} \quad \ldots\ldots\ldots\ldots\ldots\ldots\ldots\ldots\ldots\ldots\ldots (14)$$

At $L/4$ $$V = \frac{wL}{4} \quad \ldots\ldots\ldots\ldots\ldots\ldots\ldots\ldots\ldots\ldots\ldots (15)$$

and $$\epsilon_d = \frac{3wL}{16GH} \quad \ldots\ldots\ldots\ldots\ldots\ldots\ldots\ldots\ldots\ldots\ldots (16)$$

Deflection ratio (Δ/L). Using Equations 11 and 15

$$\frac{\Delta}{L} = \frac{5}{384}\frac{wL^3}{EI} + \frac{3wL}{16HG} = \frac{3wL}{16HG}\left[\frac{5}{6}\left(\frac{L}{H}\right)^2\left(\frac{G}{E}\right) + 1\right] \quad \ldots\ldots\ldots\ldots (17)$$

In terms of ϵ_b

$$\frac{\Delta}{L} = \left[\frac{5}{24}\left(\frac{L}{H}\right) + \frac{1}{4}\left(\frac{H}{L}\right)\left(\frac{E}{G}\right)\right]\epsilon_b \quad \ldots\ldots\ldots\ldots\ldots\ldots\ldots\ldots (18)$$

In terms of ϵ_d at $L/4$

$$\frac{\Delta}{L} = \left[\frac{5}{6}\left(\frac{L}{H}\right)^2\left(\frac{G}{E}\right) + 1\right]\epsilon_d \quad \ldots\ldots\ldots\ldots\ldots\ldots\ldots\ldots\ldots\ldots\ldots\ldots (19)$$

Relation of (Δ/L) to $(\delta/l) = \beta$

$$\frac{\Delta}{L} = C_3\beta\left[\frac{1 + 3.12\left(\frac{H}{L}\right)^2}{1 + C_4\left(\frac{H}{L}\right)^2}\right] \quad \ldots\ldots\ldots\ldots\ldots\ldots\ldots\ldots\ldots\ldots\ldots\ldots (20)$$

in which C_3 and C_4 are coefficients that depend on the definition of β. Values are given in Table 4.

Appendix II.—References

1. Bjerrum, L., "Allowable Settlement of Structures," *Proceedings European Conference on Soil Mechanics and Foundation Engineering*, Weisbaden, Germany, Vol. III, 1963, pp. 135–137.
2. Burland, J. B., and Wroth, C. P., "Allowable and Differential Settlement of Structures, Including Damage and Soil-Structure Interaction" *Proceedings*, Conference on Settlement of Structures, Cambridge University, Cambridge, England, 1974, pp. 611–654.
3. Feld, J., "Tolerance of Structures to Settlement," *Proceedings*, Specialty Conference on Design of Foundations for Control of Settlement, ASCE, Northwestern University, Evanston, Illinois, 1964, pp. 555–569.
4. Golder, H. Q., "The Allowable Settlement of Structures," *Proceedings*, 4th Pan-American Conference on Soil Mechanics and Foundation Engineering, Puerto Rico, Vol. I, 1971, pp. 171–187.
5. Grant, R., Christian, J. T., and Vanmarcke, E. H., "Differential Settlement of Buildings," *Journal of the Geotechnical Engineering Division*, ASCE, Vol. 100, No. GT9, Proc. Paper 10802, Sept., 1974, pp. 973–991.
6. Leonards, G. A., discussion of "Differential Settlement of Buildings," by Grant, R., Christian, J. T., and Vanmarcke, E. H., *Journal of Geotechnical Engineering Division*, ASCE, Vol. 101, No. GT7, July, 1975, pp. 700–702.
7. Peck, R. B., "History of Building Foundations in Chicago," Engineering Experimental Station Bulletin No. 373, University of Illinois, 1948.
8. Polshin, D. E., and Tokar, R. A., "Maximum Allowable Nonuniform Settlement of Structures," *Proceedings*, 4th Int. Conference on Soil Mechanics and Foundation Engineering, Vol. I, London, 1957, pp. 402–406.
9. Skempton, A. W., and MacDonald, D. H., "Allowable Settlement of Buildings," *Proceedings*, Institute of Civil Engineers, Part III, Vol. 5, 1956, pp. 727–768.
10. Sowers, G. B., and Sowers, G. F., *Introductory Soil Mechanics and Foundation Engineering*, 3rd ed., The Macmillan Co., New York, N.Y., 1970.
11. Starzewski, K., "Discussion of Allowable Settlement of Structures," *Proceedings*, Conference on Settlement of Structures, Cambridge University, 1974, pp. 808–810.
12. Terzaghi, K., and Peck, R. B., *Soil Mechanics in Engineering Practice*, 1st ed., John Wiley & Sons, Inc., New York, N.Y., 1948.

Appendix III.—Notation

The following symbols are used in this paper:

A = cross-sectional area of a rectangular beam;
c = distance from neutral axis to extreme fiber;

E = Young's modulus;
G = shear modulus;
H = depth of rectangular beam;
I = moment of inertia about neutral axis;
L = span length of beam;
M = bending moment;
P = point load;
V = vertical shear;
w = uniformly distributed load;
β = angular distortion;
Δ = relative deflection;
δ = differential settlement;
ϵ = tensile strain;
γ = shear strain;
ρ = vertical displacement;
σ = tensile stress;
τ = shear stress; and
ω = tilt or rigid body rotation.

Subscripts

b = direct tension;
crit = critical value;
d = diagonal tension;
i = arbitrary point along span length; and
j = arbitrary point along span length.

INSTABILITY OF AMUAY CLIFFSIDE

By T. William Lambe,[1] F. ASCE, Francisco Silva,[2] M. ASCE, and W. Allen Marr,[3] M. ASCE

INTRODUCTION

LAGOVEN's Amuay Refinery lies on the west coast of the *Peninsula de Paraguaná* by the *Golfo de Venezuela*. The peninsula lies between Caracas and Maracaibo, about 200 km east of Maracaibo.

Along the Amuay coast exists a cliffside having a typical height of 20 m–25 m. LAGOVEN (and its predecessor, Creole Petroleum Corp.) constructed earth embankments to enclose indentations in the cliffside, termed *quebradas*, for the storage of fuel oil. The Amuay Refinery has three of these oil storage reservoirs, FORS-1, FORS-2, and FORS-3. Lambe (1956 and 1963) has described these open reservoirs for storing fuel oil.

From industrial and domestic activities, perched water has developed above a stratum of weak clay, brown fat clay. The development of this perched water has triggered landslides along the Amuay cliffside. Much of the cliffside at Amuay exists in an unstable condition. Landslides have occurred at a dozen locations; surface tension cracks indicate incipient slides at many other locations. Landslide means "downward motion of a natural slope due to gravity." This paper uses the term *landslide* to describe a shear slide along the cliff even though water aids gravity in actuating slope movement and some of the Amuay cliffside has received alterations, smoothing, slope protection, etc.)

The consequences of a landslide along the Amuay cliffside can and do vary considerably. A slide in a relatively remote location merely causes inconvenience and the effort required to dress the failed cliffside. At the other extreme, a slide near a critical refinery facility could have catastrophic consequences. For example, a landslide which breached an oil storage reservoir could spill more than 10,000,000 barrels of oil into the sea, resulting in a loss of several hundred millions of dollars worth of stored oil, monumental political problems both national and international, and large environmental damage.

For nearly 30 yr LAGOVEN (South America) has supported and helped execute

[1]Prof., Dept. of Civ. Engrg., Massachusetts Inst. of Tech., Cambridge, Mass. 02139.
[2]Consulting Geotechnical Engr., 12 Baskin Rd., Lexington, Mass. 02173.
[3]Prof., Dept. of Civ. Engrg., Massachusetts Inst. of Tech., Cambridge, Mass. 02139.

Note.—Discussion open until April 1, 1982. To extend the closing date one month, a written request must be filed with the Manager of Technical and Professional Publications, ASCE. Manuscript was submitted for review for possible publication on January 7, 1981. This paper is part of the Journal of the Geotechnical Engineering Division, Proceedings of the American Society of Civil Engineers, ©ASCE, Vol. 107, No. GT11, November, 1981. ISSN 0093-6405/81/0011-1505/$01.00.

a geotechnical safety program aimed at preventing unacceptable performance—in particular, a landslide near an important facility. During this time, we have performed tests, both in the laboratory and in the field; made stability and flow analyses; taken field measurements (especially measurements of pore pressure and movement); and carried out preventive and remedial projects.

This paper describes the instability problem in Amuay and presents a method of analysis that can explain the landslides which have occurred. Another

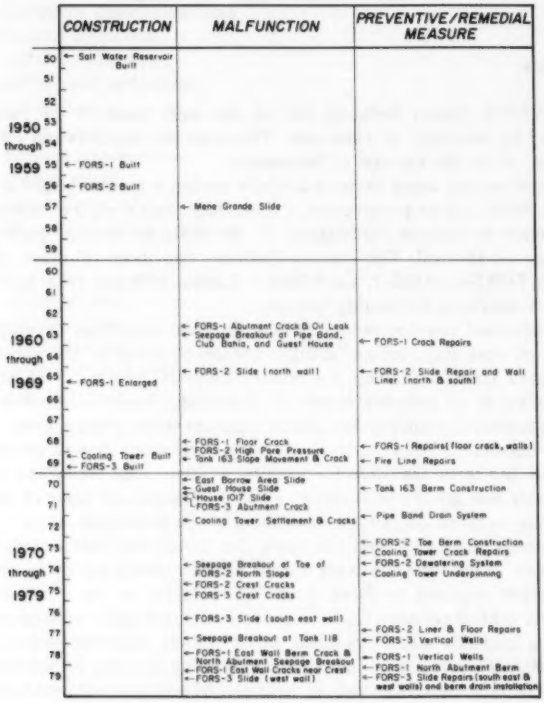

FIG. 1.—Geotechnical Events at Amuay

publication describes the geotechnical safety program. This program rests on predicting instability and then taking appropriate preventive-remedial measures.

Geotechnical Events at Amuay

Fig. 1 chronicles significant geotechnical events at Amuay, focusing particularly on the industrial area of the refinery. Creole built the first oil storage reservoir (FORS-1) in 1955. Creole built FORS-2 in 1956 and FORS-3 in 1969. The reservoirs

have performed very well. Essentially no problems have developed with the man-made embankments of compacted soil. Difficulties, however, have occurred at many locations along the cliffside, including the natural earth slopes enclosed within the oil storage reservoirs. The stability problems exist only along the natural cliffside and result from factors other than the presence of oil stored

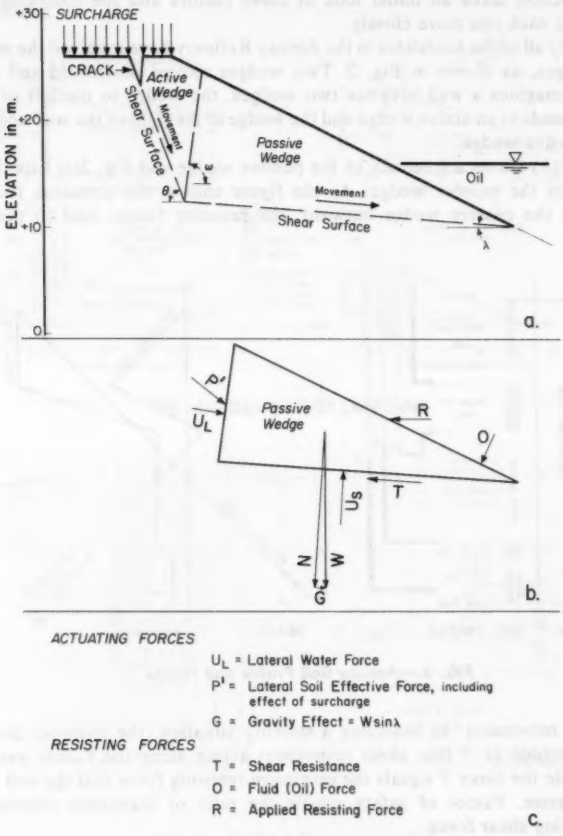

FIG. 2.—Landslide Forces

in the reservoirs. In fact, oil stored in a reservoir applies a force which helps resist a slide of the inside slope of the reservoir.

Fig. 1 also chronicles geotechnical malfunctions, measures taken to prevent landslides and measures taken to repair landslides. Fig. 1 indicates that the instability situation at Amuay has progressively worsened during the last 25 yr.

Slide Mechanism

This section examines the mechanism of a landslide at Amuay. The following three factors have overriding importance: (1) Geometry of the moving land mass; (2) strength of the soil in the failure zone; and (3) pore water pressure. This section takes an initial look at these factors and the following sections examine each one more closely.

Nearly all of the landslides in the Amuay Refinery have involved the movement of wedges, as shown in Fig. 2. Two wedges moved downward and outward. If one imagines a wall between two wedges, the wedge to the left of the wall corresponds to an active wedge and the wedge to the right of the wall corresponds to a passive wedge.

Fig. 2(*b*) shows a freebody of the passive wedge and Fig. 2(*c*) lists the forces acting on the passive wedge. As the figure shows, the actuating forces tend to push the passive wedge outward; the resisting forces tend to prevent the

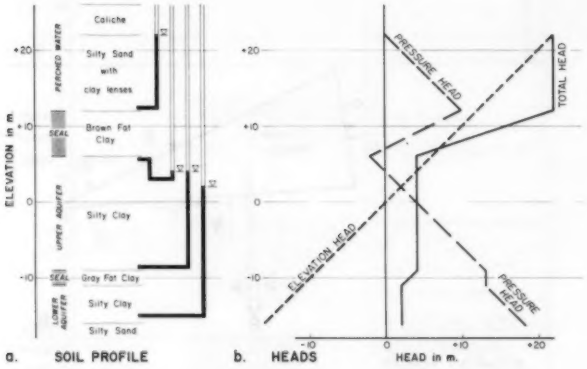

FIG. 3.—Amuay Soil Profile and Heads

outward movement. In analyzing a stability situation, the engineer determines the magnitude of T (the shear resistance) acting along the failure surface. In a landslide the force T equals the maximum resisting force that the soil strength can generate. Factor of safety equals the ratio of maximum resisting force to actuating shear force.

Fig. 3 shows the soil profile at Amuay and presents the heads existing in the ground water. The stratum of brown fat clay serves as a seal to entrap water entering from the ground surface. Fig. 3(*a*) indicates the readings in piezometers inserted at various locations in the profile. Fig. 3(*b*) portrays the heads existing in the ground water. As Fig. 3(*b*) shows, the development of perched water increases the pore pressure on the top of the brown fat clay. As later sections in this paper discuss, the buildup of pore pressure on top of the fat clay triggers the landslides along the Amuay cliff.

Geometry of Sliding Mass

An early step in analyzing a slide consists of determining the geometry of the earth mass which slid. Using visual observations and common surveying techniques, the engineer generally determines the exposed boundaries of the sliding mass. To delineate the below-surface portion of the slide proves much more difficult.

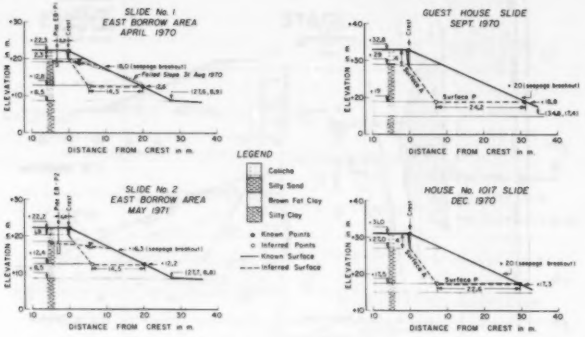

FIG. 4.—Geometry of Landslides

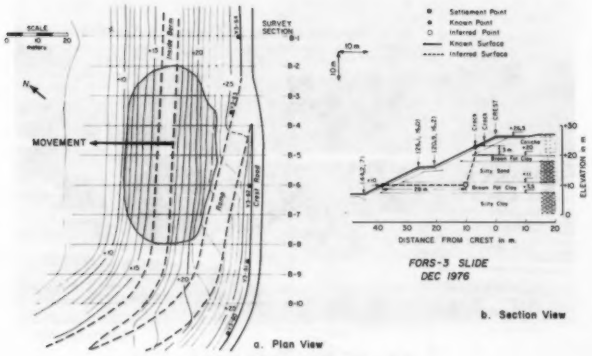

FIG. 5.—FORS-3 Slide, Dec., 1976

Aided by borings, excavations, surveys, probes, visual examinations, soil tests, etc., we have tried to define the geometry of 10 slides at Amuay. Figs. 4, 5, and 6 show the results of six of these attempts. Fig. 7 shows an actual slide at Amuay. On these geometries we have:

1. High confidence in: vertical crack; breakout of slides; and face of slope, before and after landslide.

2. Reasonable confidence in: location of the shear surface in clay; and angle of inclination of surface *A*.

3. Little confidence in: location of the surface between the active and passive wedges.

On two landslides we have located with good accuracy the shear surface

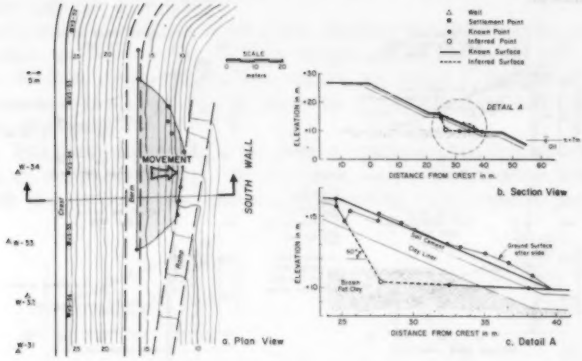

FIG. 6.—FORS-3 Slide, June, 1979

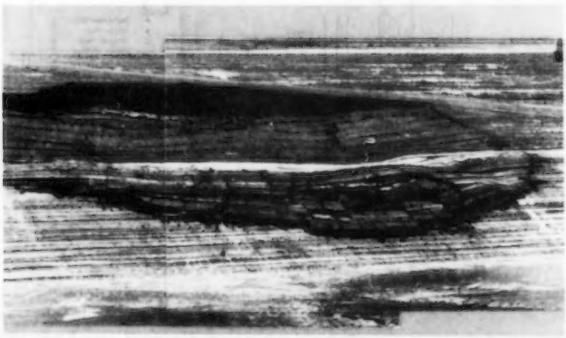

FIG. 7.—1976 FORS-3 Slide

in the fat clay. On one of these, rupture occurred in a very thin (5-mm thick) zone existing about 1 m below the top of the fat clay. On another slide we located two thin shear surfaces spaced about 300 mm apart in the stratum of fat clay.

We have not located on actual slides any surface acting like a retaining wall between the active and passive wedges. Further, we lack field data which would justify one to postulate some sort of progressive movement along the failure surface.

Trollope (1979, 1980) has made analyses and model tests which point to wedge failure geometry, not circular failure geometry, for subsoil conditions similar to those at Amuay.

Strength of Amuay Soils

Fig. 3 shows the typical profile of soils existing along the Amuay cliffside.

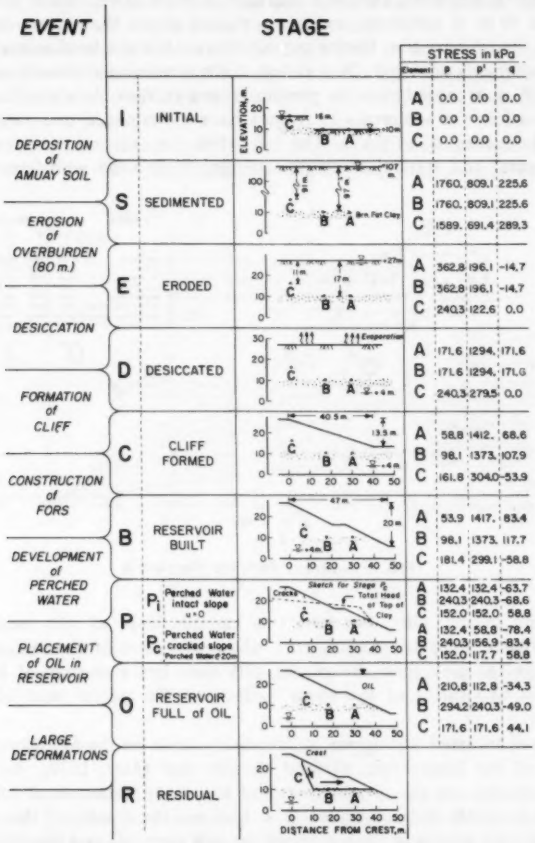

FIG. 8.—Geotechnical History of Amuay Cliff

A 2-m–5-m stratum of caliche, consisting of precipitants produced by the evaporation of ground water during recent geological times, caps the Amuay cliffside. While this cap furnishes protection from erosion, it cracks before landslides occur and furnishes little or no resistance to an incipient landslide.

The soils below the caliche consist of sediments deposited in shallow marine water during the Tertiary Period. Extensive and well-preserved malacological fauna indicate deposition during the Medium and Upper Miocene and Pliocene Epochs (Gonzalez de Juana, 1938; Feo-Codecido, 1971). Most sediments apparently came from the mountain range directly to the south of Amuay (Feo-Codecido, 1971). The maximum overburden on the present surface sediments occurred during the Pliocene Epoch; geologists have estimated that 100–200 m of additional sediments existed at that time. Results of oedometer tests suggest that about 80 m of additional sediments existed above the present-day ground surface at the refinery site. During periods when a low sea level existed, erosion of these sediments occurred. Desiccation of the remaining sediments could have extended 20 m or more below the present ground surface. As a result of erosion and desiccation, the sediments at Amuay have experienced overconsolidation, probably in excess of 1,470 kPa. The soil below the caliche varies considerably in both lateral and vertical directions, ranging from sand with lenses of clay

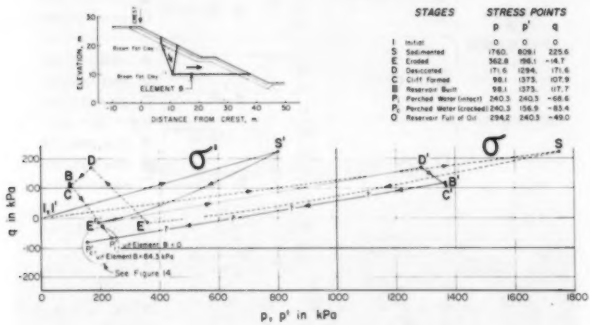

FIG. 9.—Stress Path for Element B

to silty sand to silty clay. We term this variable layer as silty sand. In the typical landslide along the Amuay cliff, about one third of the failure surface goes through the silty sand. Below the silty sand lies a stratum of brown fat clay. About two thirds of the shear surface of the typical landslide lies in the fat clay.

In 1977 we initiated a program of laboratory tests on the fat clay using the principles of the Stress Path Method (Lambe and Marr, 1979). As best we could, we traced out the stress history of three soil elements of interest on a potential landslide failure surface. Fig. 8 shows the results of this exercise. We studied eight events in the history of the soil elements and identified stages at the end of each event. For each of these stages we estimated stress values for the three elements under consideration. Fig. 8 tabulates the estimated stresses. Fig. 9 portrays the stress paths for element *B*, which approximates the average element for the shear surface through the clay.

Having the stress paths, we then conducted two series of tests. For one series we sedimented fat clay from a clay-water slurry. We then subjected

the sedimented clay to the stresses given in Figure 8 and sheared samples at certain of the stages.

In the other series of tests, we obtained undisturbed samples of fat clay from various locations in the refinery. From one location we obtained a sample at Stage C, from another a sample at Stage P_i, and another sample from Stage P_c. We ran drained tests and undrained tests on these samples.

We obtained values of residual strength two ways—one set of tests on an undisturbed sample from the shear surface of an actual landslide and another set of tests on samples subjected to large deformations.

Fig. 10 summarizes the results of laboratory tests on the undisturbed samples and the samples taken to residual strength. The residual strength depends upon the plasticity of the clay—the more plastic the clay, the lower the residual strength.

Fig. 10 shows that the strength of the fat clay depends considerably on the stress history of the clay and, further, that the test results do not give straight-line

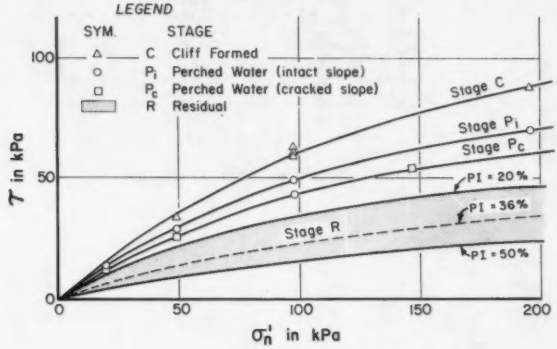

FIG. 10.—Strength of Brown Fat Clay

strength envelopes. The fat clay greatly loses strength with deformation. This strength loss contributes to slope failures—as described by Skempton (1964, 1977).

Pore Water Pressure

As Fig. 3 shows, perched water exists above the brown fat clay. The perched water causes positive pore pressures in the upper portion of the fat clay and silty sand overlying the clay. Fig. 3 indicates a pore pressure in the fat clay at elevation +12 m equal to 98 kPa. Without perched water, the water in the fat clay would exist at a negative pressure.

Fig. 11 presents contours of total head in the perched water at the top of the clay. These contours indicate that the perched water layer exists over most, if not all, of the refinery area. The contours further suggest that the source of water lies within the refinery. Field measurements dating back to the mid-60s

show that the total head has increased during the last decade.

The head described to this point comes from piezometers having sensors either above or below the fat clay. The heads represent values associated with seepage in the soil above and below the fat clay. Fig. 12 suggests the distribution of pore pressure in the fat clay near the southeast wall of FORS-3. The pore

FIG. 11.—Total Head Above Fat Clay

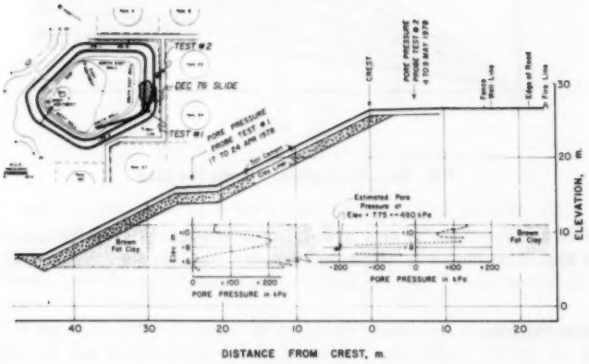

FIG. 12.—Pore Pressure in Brown Fat Clay, Southeast Wall, FORS-3

pressures plotted in Fig. 12 came from measurements made on a pore pressure probe advanced through the fat clay.

We have not yet explained some of the pore pressures shown in Fig. 12, especially the very high pore pressure (207.9 kPa, giving a total head of +30.2 m) occurring at elevation +9 in the fat clay. In making slide analyses and stability predictions, we have used values of pore pressure corresponding to

seepage existing above the fat clay. We reason that this pore pressure exists near the surface of the fat clay at the start of a landslide. What little evidence we have suggests that the shear zone in the fat clay has such a small thickness that drainage probably occurs during the early stages of a landslide. We suspect that the high pore pressures measured well within the fat clay result largely from excess pore pressures developed by deformations occurring during a landslide. We have low confidence in the correctness of this explanation. During the years ahead we shall focus attention on pore pressures within the fat clay in hopes of establishing the magnitude of pore pressure which will exist at the start of a landslide.

Slide Initiation

Sliding occurs when the sum of the forces actuating movement becomes equal to the sum of the maximum forces resisting movement. Referring to Fig. 2,

TABLE 1.—Stresses for Element B

Stage (1)		u, in kilopascals (2)	q, in kilopascals (3)	p', in kilopascals (4)	Strength line (5)	q_f, in kilopascals (6)	q_f/q (7)
B		−1,275.0	117.7	1,373.0	C	338.3	2.9
					P_t	250.1	2.1
					P_c	191.2	1.6
					R	112.8	0.9[6]
P	P_t	0	−68.6	240.3	C	98.1	1.4
					P_t	76.5	1.1
					P_c	65.7	0.9[6]
					R	25.5	0.3[7]
	P_c	84.3	−83.4	156.9	C	81.4	0.9[8]
					P_t	63.7	0.7[6]
					P_c	55.9	0.6[7]
					R	21.6	0.2[6]

we see that any one, or some combination, of the following can initiate a slide:

1. Increase P' (placement of surcharge).
2. Increase U_1 (build-up of perched water, development of excess pore pressure from shear).
3. Reduce O (drawdown of stored oil).
4. Increase U_s (buildup of perched water, development of excess pore pressure from shear).
5. Decrease c' or ϕ' (deformation of the clay, thereby lowering the strength parameters).
6. Alter W so as to increase G or decrease $W - U_s$, or both.

In the early 1970s we prepared Fig. 13 from analyses of actual slides and from laboratory tests on undisturbed samples of soil from the shear zone of

the east borrow slide area. We tried to relate ϕ' with age of slope. We reasoned that a decrease of ϕ' with age triggered landslides. This approach did not work well because:

1. We had trouble determining the age of a slope.
2. Time *per se* probably does not constitute the primary variable.
3. One cannot afford the flat slopes obtained from a design using a value of ϕ' equal to 8°.

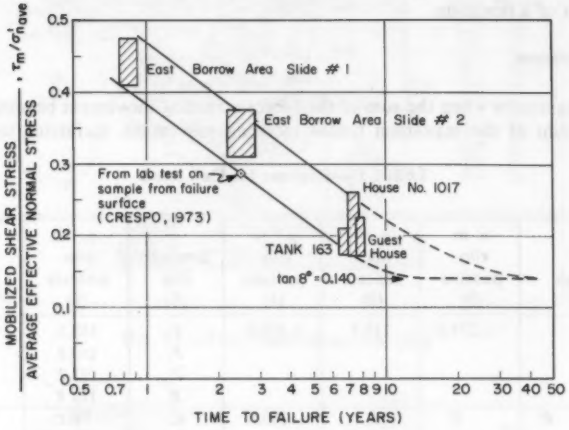

FIG. 13.—Clay Strength versus Age

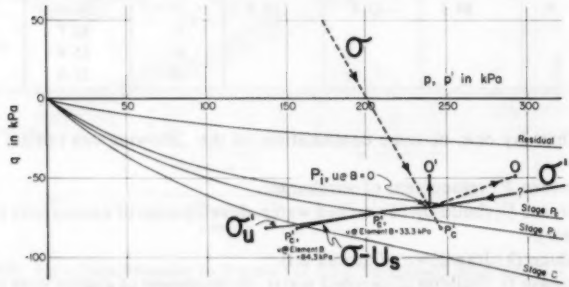

FIG. 14.—Strength and Stress Paths for Element B

Using the strength lines and stress paths for Element B shown in Fig. 14, we can show conceptually the factors causing a slide and can indicate the relative importance of each factor. Fig. 14 gives strength and stress paths for Element B, which approximates the average element for the shear surface of the passive wedge. Table 1 tabulates stresses for Element B for Stages B, P_i, and P_c.

We can see that going from Stage B to Stage P_c, for example, involves three significant changes:

1. An increase in applied shear stress (q goes from +117.7 kPa--83.4 kPa, a change of +201.1 kPa).
2. A decrease in effective stress (p' goes from +1,373 kPa to +157 kPa, a drop of +1,216 kPa.
3. A decrease in strength line (for any p' value, q_f loses about 3/4 in going from Stage C to residual, and drops about 1/3 in going from Stage C to Stage P_c).

The rise in perched water causes all of the increase in applied shear stress, all of the decrease in effective stress, and a major part of the drop in strength from Stage B to Stage P_c. The strength drop from P_c to R results from deformations caused partly by the increase in perched water and partly by other factors. Deformation in the clay, e.g., from the cyclic filling—emptying of the oil in the reservoir contributes to a decrease in strength.

Excess pore water pressures which develop from the undrained or partly drained, loading or unloading of the clay can contribute to the initiation of the landslide. As noted earlier in this paper, we have not yet sorted out the importance of excess pore pressures from shearing the clay.

In summary, the development and increase of perched water triggers slides by (listed in order of decreasing importance):

1. Decreasing effective stress, and thus strength.
2. Decreasing strength line.
3. Increasing shear stress.

Slide Analysis

We can place the tasks facing the geotechnical engineer solving stability problems into one of two categories, namely:

1. Slide analysis.
2. Stability prediction.

In slide analysis, a slide has occurred, i.e., the factor of safety equaled unity. The shear stress along the failure surface equaled the shear strength of the soil.

The geotechnical engineer does a slide analysis to gain insight and knowledge, and to explain an event which has occurred. Some engineers may attempt to use a slide analysis to validate a prediction method. A slide analysis constitutes an autopsy—i.e., a Type C Prediction according to Lambe (1973).

A stability prediction constitutes an assessment of stability—expressed as a factor of safety or the probability of failure—for an unfailed slope and a given set of conditions. This corresponds to a Type A Prediction. One may have any one of the following four situations:

1. Existing slope, existing conditions.
2. Existing slope, future conditions.

3. Future slope, existing conditions.
4. Future slope, future conditions.

In a stability prediction, the engineer must forecast what events can initiate sliding and usually he must forecast the strength and pore pressure that will exist at the future condition. Stability prediction usually presents the engineer with more complications and uncertainties than does slide analysis. This paper considers primarily slide analysis.

Fig. 15 shows an analysis of the FORS-3 Dec., 1976 slide.

We determined the geometry of the sliding mass as discussed in the section on geometry. We took ϕ' for the silty sand equal to 33° based on triaxial and direct shear tests results (the residual strength approximately equals the peak strength for the silty sand around FORS-3). We selected the strength of the clay from Fig. 10 using Stage P_c for the original landslide and residual strength for analyzing the situation after the landslide had occurred.

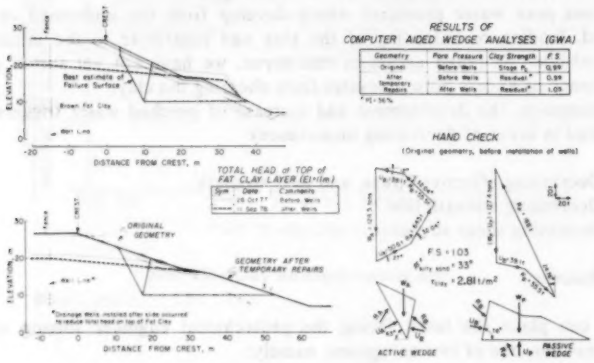

FIG. 15.—Analysis of Dec., 1976 Slide, FORS-3

Fig. 15 shows the distribution of total head on top of the fat clay used in the slide analyses.

The analyses shown in Fig. 15 prove that—knowing ahead the answer—we can calculate the correct factor of safety (unity) for a slide. This fact indicates either we used a correct procedure and correct parameters or a fortuitous cancellation of errors occurred in the analysis. We suspect the latter since we made several simplifications in the slide analysis including:

1. Using pore pressures from a steady-state flow net but measurements after a slide show much larger values.
2. Assuming the inclination of R_B.
3. Assuming deformations occur along two rigid wedges whereas the measured position of surface of slope suggest a more complex pattern of deformation.

Summary and Conclusions

This paper consists of a case study involving an unstable cliffside in Amuay, Venezuela. Since the late 1950s landslides have occurred. Without preventive measures, the instability conditions of the cliffside will continue to deteriorate.

The consequences of a landslide along the cliff depend upon the facilities near the landslide. A slide which breaches an oil storage reservoir could dump millions of barrels of fuel oil into the Caribbean Sea, an undesirable consequence of monumental proportions.

The instability exists in the natural cliffside. No stability problems have arisen in the man-made dams which enclose quebradas to form the oil storage reservoirs. The failure surfaces of the landslides lie mostly within a layer of weak plastic clay, termed fat clay. Most of the landslides involve wedge-type failure geometry.

This paper presents test data to show that the strength parameters of the fat clay decrease greatly with deformation.

Perched water arising from activities within the refinery has developed above the stratum of fat clay which acts as a seal. This perched water initiates the landslides. The rise in pore pressure from the perched water causes:

1. A drop in effective stress, and thus soil strength.
2. A drop in strength parameters, arising from deformations.
3. A rise in shear stress along a potential landslide shear surface.

A wedge-type slide analysis employing pore pressures inferred from readings on nearby piezometers and soil strength values obtained from laboratory tests yields a factor of safety of unity. The pore pressures used correspond to pressures existing prior to a landslide. The shear strength selected depends upon the stage of the clay just prior to the landslide.

The slide analysis illustrates that—knowing ahead the answer—we can calculate the correct factor of safety (unity) for a slide. This fact indicates either we used a correct procedure with correct parameters or a fortuitous cancellation of errors occurred in the analysis.

Acknowledgments

This paper employs laboratory and field measurements taken over a 25-year period. Many people contributed to the collection of these data. The writers have received support and encouragement from LAGOVEN engineers, especially Carlos Hernández and Mario Troconis. The writers appreciate the contributions they have received from others.

Appendix.—Bibliography

Dawson, "LEASE II—A Computerized System for the Analysis of Slope Stability," thesis presented to the Massachusetts Institute of Technology, at Cambridge, Mass., in January, 1972, in partial fulfillment of the requirements for the degree of Civil Engineer.

Feo-Codecido, G., "Geología y Recursos de la Península de Paraguaná," *Symposium on Investigations and Resources of the Caribbean Sea and Adjacent Regions*, UNESCO, Paris, France, 1971, pp. 231–240.

Gonzalez de Juana, Clemente, Contribución el estudio de la cuenca sedimentaria Zulia—Falcón, (A Contribution to the Study of the Zulia—Falcón Sedimentary Basin), Boletin de Geologia y Minería, Caracas, Venezuela, Dirección de Geología, tomo 2, No. 2–34, pp. 123–138, 1938, English edition, pp. 123–140.

Grismala, R. E., "Stability Analysis of Natural Slopes with Weak Strata," thesis presented to the Massachusetts Institute of Technology, at Cambridge, Mass., in 1978, in partial fulfillment of the requirements for the degree of Master of Science in Civil Engineering.

Lambe, T. W., and Marr, W. A., "Stress Path Method: Second Edition," *Journal of the Geotechnical Engineering Division*, ASCE, Vol. 105, No. GT6, Proc. Paper 14655, June, 1979, pp. 727–738.

Lambe, T. W., "Predictions in Soil Engineering," 13th Rankine Lecture, *Geotechnique*, Vol. 23, No. 2, June, 1973, London, England, pp. 149–202.

Lambe, T. W., "The Storage of Oil in an Earth Reservoir," *Journal*, Boston Society of Civil Engineers, Vol. XLIII, Number 3, July, 1956.

Lambe, T. W., "An Earth Dam for the Storage of Fuel Oil," *Proceedings of the Second Pan-American Conference on Soil Mechanics and Foundation Engineering*, July, 1973.

Lengster, M., "Stability of a Natural Slope," thesis presented to the Massachusetts Institute of Technology, at Cambridge, Mass., in 1977, in partial fulfillment of the requirements for the degree of Master of Science.

Platt, G. A., "Investigation of a Slope Instability at Amuay, Venezuela," thesis presented to the Massachusetts Institute of Technology, at Cambridge, Mass., in partial fulfillment of the requirements for the degree of Doctor of Philosophy.

Skempton, A. W., "Long-Term Stability of Clay Slopes," *Geotechnique*, Vol. 14, No. 2, June, 1964, London, England, pp. 77–101.

Skempton, A. W., "Slope Stability of Cutting in Brown London Clay," *Proceedings of the Ninth International Conference on Soil Mechanics and Foundation Engineering*, Vol. 3, 1977.

Tong, C. K., "Stability Control of a Natural Slope," thesis presented to the Massachusetts Institute of Technology, at Cambridge, Mass., in 1970, in partial fulfillment of the requirements for the degree of Master of Science.

Trollope, D. H., "The Collapse of Slopes," *Research Bulletin CS17*, Department of Civil and Systems Engineering, James Cook University of North Queensland, Australia, May, 1979.

Trollope, D. H., "Landslip Mechanisms," Lecture given at the Massachusetts Institute of Technology, Department of Civil Engineering, Cambridge, Massachusetts, October, 1980.

Voigt, B., "Correlation Between Atterberg Plasticity Limits and Residual Shear Strength of Natural Soils," *Geotechnique*, Vol. 23, No. 2, London, England, pp. 265–267.

FRICTION CAPACITY OF PILES DRIVEN INTO CLAY

By Leland M. Kraft, Jr.,[1] M. ASCE, John A. Focht, Jr.,[2] F. ASCE, and Srinath F. Amerasinghe,[3] M. ASCE

INTRODUCTION

A number of studies on axial pile capacity in clays have shown that the average frictional resistance, expressed as a fraction of the average undrained shear strength or average effective overburden pressure, decreases with increasing pile penetration. (15,19,24,32). The pile load test data that are the basis of the studies include: (1) Tests with variations in set-up time and stress history; (2) tests on piles redriven to deeper penetrations after earlier testing; and (3) tests on piles with oversized closure plates. These factors can combine to amplify the influence of pile length on axial capacity.

The influence of the length effect suggested by earlier studies has significant economic impact on offshore structures that are supported by large-diameter, open-end pipe piles driven to penetrations of 200 ft–500 ft (61 m–152 m). Consequently, controversy has continued about the applicability and validity of current capacity computation methods. In the past two or three years a modest amount of new load test data has become available, and several model and analytic studies have been completed. Therefore, to place the length effect into proper perspective, the writers reexamined the influence of pile length on frictional capacity in clays using current technology and philosophy. Some of the methods now being used to compute pile capacity and to study factors that affect pile capacity are summarized first to set the stage for this reevaluation.

DESIGN METHODS

Methods used to evaluate and compute unit shaft friction, f, for offshore piles in clay include the Lambda method, (32) the methods recommended by API RP 2A, (1) the β methods, (6,15,24,27) and the Janbu (19) method. The API methods may be referred to as the $f = s_u$ (s_u = undrained shear strength)

[1]Mgr., Special Projects Group, McClelland Engrs., Inc., Houston, Tex.
[2]Executive Vice Pres., McClelland Engrs., Inc., Houston, Tex.
[3]Geotechnical Engr., McClelland Engrs., Inc., Houston, Tex.

Note.—Discussion open until April 1, 1982. To extend the closing date one month, a written request must be filed with the Manager of Technical and Professional Publications, ASCE. Manuscript was submitted for review for possible publication on January 22, 1981. This paper is part of the Journal of the Geotechnical Engineering Division, Proceedings of the American Society of Civil Engineers, ©ASCE, Vol. 107, No. GT11, November, 1981. ISSN 0093-6405/81/0011-1521/$01.00.

approach for highly plastic clays or the α approach for stiff, overconsolidated clays of low plasticity. The β method and Janbu's method are effective stress approaches. Other effective stress approaches are being developed, but are not yet ready for design applications (14,21). The Lambda method, API methods, β methods, and Janbu's method are summarized in Table 1. A length effect

TABLE 1.—Design Methods

Method (1)	Formulation (2)
Vijayvergiya and Focht (1972)	$f = \lambda(\bar{\sigma}_{vm} + 2\,s_{um})$ λ = empirical coefficient = Func^{n}[c](L) s_{um} = mean undrained shear strength along pile $\bar{\sigma}_{vm}$ = mean $\bar{\sigma}_{vo}$ along pile $\bar{\sigma}_{vo}$ = effective overburden pressure L = pile penetration
API RP 2A (1980)	$f = \alpha\beta_1\bar{\sigma}_{vo}$; $\beta_1 = (s_u/\bar{\sigma}_{vo})$ s_u = undrained shear strength (i) Highly plastic clay NC:[a] $\alpha = 1$ OC:[b] $\alpha = 1$, but $f \not> $ the larger of 1 ksf or $(s_u)_{nc}$ (ii) Low to medium plasticity clay s_u, ksf: <0.5 → α: 1; 0.5–1.5 → 1–0.5 (lin. var^{n})[d]; >1.5 → 0.5
Beta	$f = \beta\bar{\sigma}_{vo}$
a. Burland (1973)	NC: $\beta = (1 - \sin\bar{\Phi})\tan\bar{\Phi}$ $\bar{\Phi}$ = effective angle of internal friction
b. Meyerhof (1976)	NC: β = Func$^{n}(L)$ OC: $\beta = 1.5\,(1 - \sin\bar{\Phi})\tan\bar{\Phi}\sqrt{OCR}$ OCR = Overconsolidation Ratio
c. Flaate and Selnes (1977)	$f = 0.4\sqrt{OCR}\;\mu_L\bar{\sigma}_{vo}$ $\mu_L = \dfrac{L + 65.6}{2L + 65.6}$; ($L$ in ft)
Janbu (1976)	$f = S_r(\bar{\sigma}_{vo} + a)$ $S_r = \tan\bar{\Phi}\,[\sqrt{1+\mu^2} + \mu\sqrt{1+r^2}]^{-2}$ in which $\mu = \tan\bar{\Phi}/\lvert r\rvert$; r = roughness number = Func^{n} (L); and a = attraction

[a] NC = Normally Consolidated.
[b] OC = Overconsolidated.
[c] Func^{n} (x) = Function of x; lin.
[d] lin. var^{n} = linear variation.

is implicitly included in the Lambda, Flaate and Selnes, and Janbu methods; Meyerhof incorporated a length effect into his chart for normally or slightly overconsolidated clays; and application of API Method 2 produces a length effect for normally consolidated clays.

Comparison of Methods.—Normally Consolidated Clays: Predicted β profiles

(ratio of average f to initial effective overburden pressure) for several of the pile capacity methods are compared in Fig. 1 to show the implied length effects. The β values from the λ method are obtained from $f = \lambda(1 + 2\beta_1)\bar{\sigma}_{vm}$, in which β_1 = the ratio of undrained shear strength to effective overburden pressure ($s_u / \bar{\sigma}_{vo}$); $\bar{\sigma}_{vm}$ = the mean effective overburden pressure over the pile penetration; and λ = an empirical coefficient. Because the λ method was not intended for short piles in normally consolidated clays (32) and overpredicts capacity for penetrations of less than about 50 ft, the band for λ is not plotted for the near-surface zone in Fig. 1. Pile capacities computed by the four methods

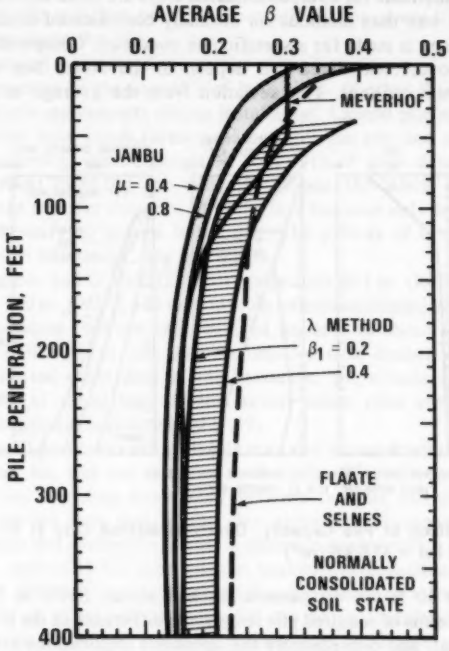

FIG. 1.—Comparison of β Values (1 ft = 0.305 m; 1 ksf = 47.9 kN/m^2)

differ by about ±25% relative to the median of the four methods.

The average β values implied by the API methods are not included in Fig. 1, but in normally consolidated clays, β ranges between 0.2–0.4 for all penetrations for Method 1 and for pile penetrations of less about 60 ft for Method 2. For Method 2 with pile penetrations of a few hundred feet in which $\alpha = 0.5$, the average β value is as low as 0.1 for a β_1 value of 0.2.

Measured and computed capacities were compared statistically for the Lambda and API methods by Drewry, Weidler, and Hwong (12). The means of the ratio of calculated to measured capacity were 1.13 for the λ method and 1.29

for the API methods, and the standard deviations were 0.31 for the λ method and 0.44 for the API methods. This suggests that the ±25% deviation between methods is no greater than the expected deviation between calculated and measured capacities for any particular method.

Overconsolidated Clays.—Drewry, Weidler, and Hwong (12) found that the ratio of calculated to measured capacity in overconsolidated soils was 0.83 for the API methods and 1.04 for the Lambda method. The standard deviations were nearly the same for both methods (0.18 for the Lambda method and 0.20 for the API methods).

Pile capacity methods for overconsolidated clays are more difficult to compare in a generalized way than methods for normally consolidated conditions. Therefore, a comparison is made for a specific site condition. Computed pile capacity curves for an overconsolidated soil deposit in the North Sea are compared in Fig. 2 for four methods. The deviation from the average of the curves is

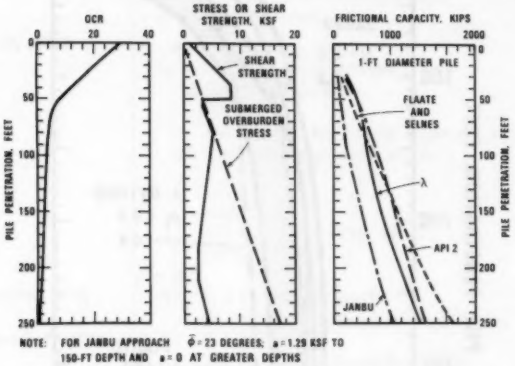

FIG. 2.—Comparison of Pile Capacity, Overconsolidated Clay (1 ft = 0.305 m; 1 kip = 4.45 kN; 1 ksf = 47.9 kN/m²)

about ±60% at 50 ft (15 m) penetration and about ±30% at 250 ft (76 m) penetration. In terms of required pile length, the difference in the pile penetration can be significant, and consequently the economic implications are great.

Pile Length Effect

Primary Causes.—Although a length effect does exist, it may be less pronounced than indicated by Fig. 1. Following are the four primary factors that are thought to contribute to a length effect:

1. Continued alterations to the soil fabric, and hence stress-strain and strength properties, with increasing pile length passing a soil element.
2. A strain or displacement softening response of the soil during pile loading. After reaching a peak shear stress, the stress transfer decreases with additional pile movement.

3. The influence of three-dimensional considerations (e.g. surface conditions, tip effects, lack of plane strain or plane stress conditions along pile length) on load transfer and distribution of stresses in the soil immediately surrounding the pile.
4. Variations in the soil properties along the pile length.

Once several feet of pile pass a point, further alteration to the soil fabric due to additional pile passing a point should be minimal. Additional changes in the soil fabric will occur during consolidation after driving which should have a consistent pattern along the pile length. After the consolidation, soil fabric along the pile will thus probably be relatively consistent if the soils were originally similar along the pile.

Three-dimensional considerations at the ground surface and at the pile tip may not be important to the capacity of long piles. Another three-dimensional effect is lateral pile movements during installation. Lateral pile movements can create an oversize hole which forms gaps between the pile and soil when piles are driven into strong, overconsolidated soils (31). If gaps develop, the load transfer is reduced. Even if a gap is not developed, the lateral movement can result in low load transfer for piles in stiff clays because only low lateral total stresses are necessary to keep a hole open. The effects of low load transfer appear to diminish with increasing pile length.

Aurora, Peterson, and O'Neill (2) report capacities of 1 in. (25.4 mm) diameter piles driven 38–100 in. (965–2,540 mm) into an overconsolidated compacted clay. These results indicate that the ratio of load transfer to shear strength is less in the upper 30–50% of the pile length compared with deeper sections. From our interpretation of other data in the literature, the effects are less severe in weak deposits (31) and may be less severe when piles are pushed rather than driven if alignment is maintained (7,29).

Variations in soil properties along the pile may also be important to the maximum shear stress that the soil can transfer to the pile. Piles driven into a profile of sand over clay can drag down sand between the pile and clay to provide shaft friction greater than that of the clay alone (31). Seasonal changes can result in shrinkage and swelling to further complicate interpretation of pile capacity measurements, especially for short piles in heavily overconsolidated clays.

Undoubtedly, the four primary factors that contribute to a length effect are interrelated, and all affect pile capacity, but the major contributors are thought to be the strain (displacement) softening phenomenon and lateral pile movements during installation.

Soil Softening.—The load transfer, as defined by shear stress-pile displacement (t-z) response, may exhibit a displacement softening behavior as shown in Fig. 3. If displacement softening occurs, the peak pile capacity corresponds to the capacity associated with the peak load transfer only when the pile is infinitely stiff and in a homogeneous soil. Short piles tend to have greater relative axial stiffnesses than do long piles. Thus, the displacement softening phenomenon is likely to be more pronounced in long piles than short piles. It may also be more pronounced for large diameter than small diameter piles for reasons presented subsequently. Fig. 4 shows the relative resistance that is developed at ultimate load for a less than infinitely stiff pile.

The effect of displacement softening on ultimate pile capacity has been long

recognized, and *t-z* analyses can be used to quantify the effect for a specific set of input conditions. The pile and soil properties that influence the development

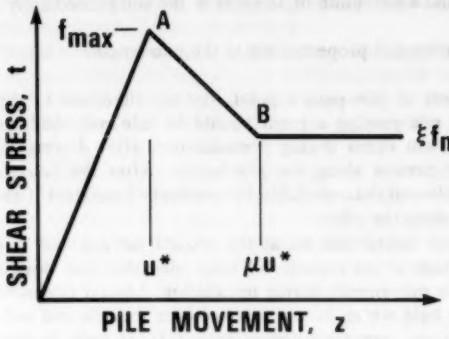

FIG. 3.—Idealized *t-z* Curve

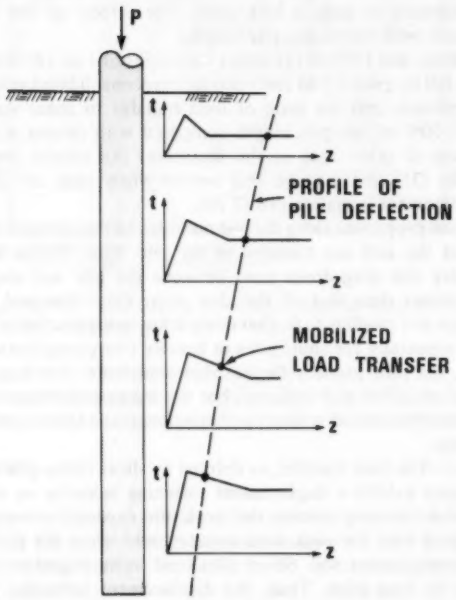

FIG. 4.—Load Transfer Along Pile

of ultimate pile resistance can be illustrated with an idealized *t-z* curve. Murff (26) used the *t-z* curve in Fig. 3 with $\mu = 1$ to compute the influence of relative

pile-soil stiffness on the ultimate pile capacity of a uniform pile in a homogeneous soil. The ratio of the ultimate capacity to the capacity if the peak transfer is mobilized simultaneously along the pile, is related to the amount of softening, ξ, and the pile-soil stiffness, π_3, defined by $\pi D f_{max} L^2/(AEu^*)$, in which D = the pile diameter; L = the pile length; A = the cross-sectional area of the pile; E = the pile modulus; f_{max} = the peak soil-pile friction; and u^* = the relative pile-soil movement at which f_{max} is developed. Murff's results are plotted in Fig. 5 as three solid line curves, in terms of a mobilized friction ratio f_{av}/f_{max}, and pile-soil stiffness ratio for three values of ξ.

Other analyses were performed as part of this study to evaluate the influence

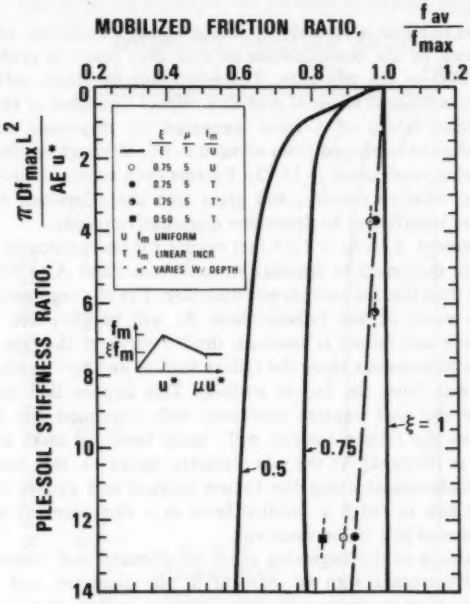

FIG. 5.—Mobilized Pile Capacity with Changes in Pile-Soil Stiffness

of the distribution of the peak shaft friction, f_{max}, along the pile, the degree of strain softening, and the variation of u^* with depth. These supplemental results are included in Fig. 5 as individual points and a dashed curve. The pile-soil stiffness ratio is defined in terms of the average f_{max} and u^* at the midpoint of the pile. For the case in which u^* varied with depth, u^* decreased in proportion to the reciprocal of the depth. The influence of the distribution of f_{max} and u^* on mobilized pile capacity is small. The ratio of ultimate pile capacity to the capacity if peak transfer is mobilized simultaneously, is influenced primarily by (1) Pile-soil stiffness; (2) amount of softening, ξ; and (3) rate of softening, μ. These results clearly demonstrate that it is unlikely that the average

friction for a pile can be reliably related to a single parameter obtained by combining all or eliminating some of these factors.

Critical Parameters.—Four key parameters (f_{max}, ξ, u^*, μ) are needed to define the idealized t-z curve shown in Fig. 3. The displacement, u^*, at maximum load transfer, can be determined with the procedure described by Kraft, Ray, and Kagawa (22). Effective stress concepts offer potential to predetermine the distribution of maximum load transfer, f_{max}, and the influence of lateral pile movements during installation on this transfer (21). The amount of softening, ξ, and the rate of softening, μ, are not a readily amenable to theoretical predictions. Some insight into the magnitude of ξ and μ can be gleaned from measured t-z responses and from laboratory tests designed to simulate load transfer between soil and a pile.

The soil next to a pile is severely remolded during installation, and the driving process followed by the consolidation process may result in preferred particle alignment parallel to the pile axis. The magnitude of strain softening of this remolded, reconsolidated material probably differs from that of the undistrubed material. Typical values of ξ from measured t-z responses and laboratory simulation studies have ranged from about 0.8–1.0, although smaller values may be encountered in some cases (8,11,23). Factors such as overconsolidation ratio, soil sensitivity, relative density, and grain size characteristics may affect ξ, but the data are insufficient to determine quantitative trends.

The displacement, $\delta_z = (\mu - 1)u^*$ that occurs for one particular pile diameter in moving from maximum to residual stress—from Point A to Point B in Fig. 3—is different than that for another pile diameter. The pile segment and adjoining soil up to the point of soil failure, Point A, will be governed by "elastic" conditions. Once soil failure is reached, the t-z curve of the pile segment will be governed by movements along the failure surface and by "elastic" conditions for the soil away from the failure surface. This implies that once failure is reached and if the load transfer decreases with continued pile displacement, the soil beyond the failure surface will "snap back" a small amount as its elastic energy is released. As the pile diameter increases, this action increases the relative displacement along the failure surface and causes the soil for a large diameter pile to reach a residual level at a displacement less than that for a small diameter pile in the same soil.

Pile displacement at the beginning point of ultimate load transfer, Point A, in a given soil increases with an increase in pile diameter, and the value of δ_z is nearly constant or decreases, due to "snap back", with an increase in pile diameter (22). Therefore, μ may decrease with an increase in pile diameter. These effects combine to result in pile length, or pile-soil stiffness, and have a greater impact on the capacity of larger diameter piles.

Typical values of μ that we have observed from load tests range from about 2–5. This range of μ values can be combined with the range in ξ values to determine the impact of the softening phenomenon on axial capacity. This effect is shown in Fig. 6 in terms of mobilized friction ratio and pile-soil stiffness for an ξ of 0.75 and three values of μ. These results show that the relative magnitude of reduction in the friction ratio decreases with an increase in pile-soil stiffness ratio. For π_3 greater than about 10, the additional friction ratio decrease is less than 15% if μ is less than about five. The above results show that π_3 and the shape of the t-z curve can explain at least part of the length effect.

Lateral Pile Movements.—Lateral pile movements during installation can also contribute to a length effect by affecting the magnitude of f_{max} along the pile length. The lateral vibrations result in low lateral stresses acting on the pile. The more pile that is driven, the greater the potential deterioration of the stresses, especially along the upper portion of the pile. The amount of lateral movement, the depth to which it extends, and the consequences are affected by the method and details of installation—driven, jacked, alignment control, free standing length, pilot hole, bending stiffness of the pile, soil strength, and soil stiffness. Any length effect due to lateral pile movements is not readily amenable to analysis, but the effective stress approach to pile capacity that uses cavity expansion to simulate pile installation has potential to make advances in this area.

Comment.—The foregoing concepts can be used to explain the effect of pile

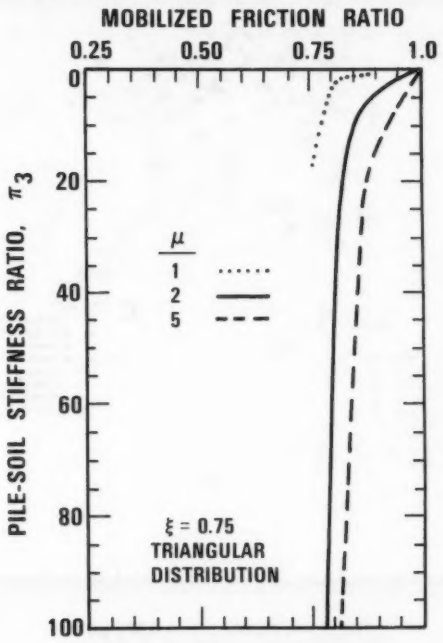

FIG. 6.—Range in Theoretical Length Effect

length on axial capacity, but unfortunately, data are unavailable to test the hypotheses. Thus, we must resort to empirical methods tempered with judgment until more detailed soils data combined with good quality load tests on long piles become available.

Empirical Correlations

Data Base.—Most procedures to compute the axial capacity of piles have

some degree of empiricism. In this study, the α, β, and λ approaches were correlated to both pile length, L, and pile-soil stiffness, π_3. Linear regression analyses were used to determine the most effective combination of dependent α, β, or λ and independent parameters L, ln (L), π_3, or ln π_3 for pile capacity predictions. The piles analyzed in this study were loaded to failure within a few hours after initiating the load test. They had diameters between about 6 in. (152 mm) and 30 in. (762 mm), lengths between 8 ft (2.4 m) and 333 ft (102 m), and included pipe piles, concrete piles, and timber piles. The available

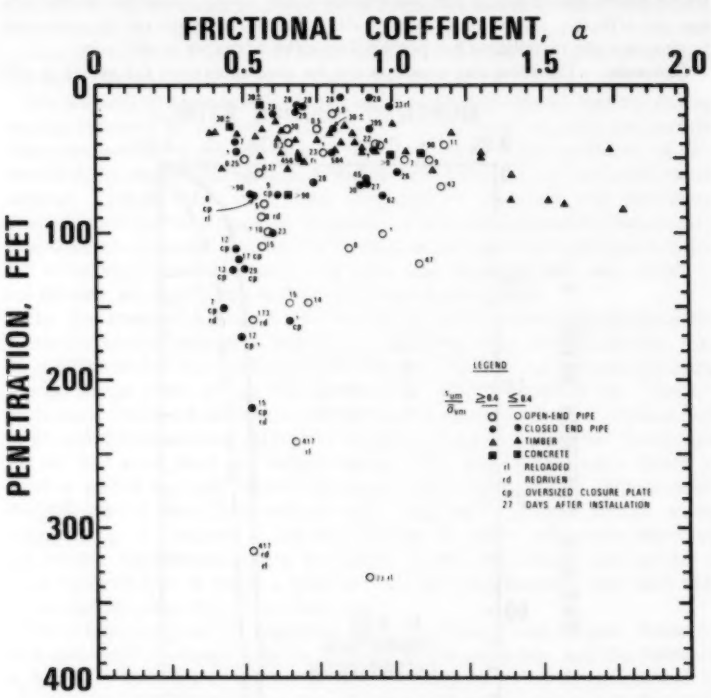

FIG. 7.—α Profile (1 ft = 0.305 m)

load test data include pipe pile data from Vijayvergiya and Focht (32), timber and concrete pile data from Flaate and Selnes (15), and data from Meyerhof and Murdock (25), Ito and Koizumi (18), Hutchinson and Jensen (17), Stermac, Selby, and Devata (30), Tomlinson (31), Danys (10), Brand, Muktanbhant, and Taechathummarak (5), Cooke, Price, and Tarr (7), Endley, Ulrich, and Gray (13), Rigden, Pettit, St. John, and Poskitt (28), and Kraft, Cox, and Verner (20). Although other well-documented, good quality test data may be available, the number of good quality load test data is relatively small compared with the number needed to evaluate in a statistically significant manner the effect

of the range in parameter variations on pile capacity. The acquisition of a modest number of additional data points will not statistically affect the regression analyses performed here.

The period between installation and testing for the pipe pile data was in excess of 30 days with the exception of the data from 44 of the 105 tests. It was less than 25 days for 30 of these 44 tests. Once a pile is tested to failure, its load carrying ability may decrease to a residual capacity with an increase in pile movement. Subsequent testing to failure in this case can result

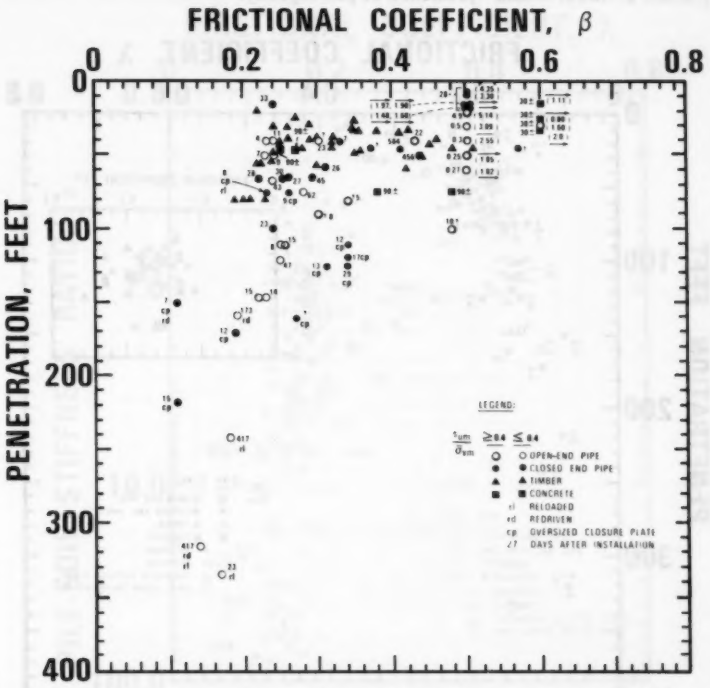

FIG. 8.—β Profile (1 ft = 0.305 m)

in peak loads less than the initial peak and closer to the residual capacity, as evidenced by data from Meyerhof and Murdock (25), Bergemann (3), and particularly Kraft, Cox, and Verner (20).

If a pile is redriven to a deeper penetration after long delays, the peak capacity may be less than could be developed if the pile were originally driven to the deeper penetration with minimal delays. Such behavior tends to occur when the soil exhibits a strain softening behavior and the pile is subjected to large movements. Therefore, piles loaded to failure and subsequently driven to deeper

penetrations for later testing may exhibit lower capacities for the deeper penetrations than would be developed if the piles were originally driven to the deeper penetration. If load test data are excluded for piles with less than full set-up, piles having oversized plates at the tip, and piles with sequential testing–redriving–retesting, the data base would not be sufficient to lend statistical significance to any empirical procedure. Therefore, the influences of set-up time, oversized closure plate, and loading history had to be neglected when performing regression analyses, in recognition of the fact that the results will provide a "lower bound" prediction of pile capacity.

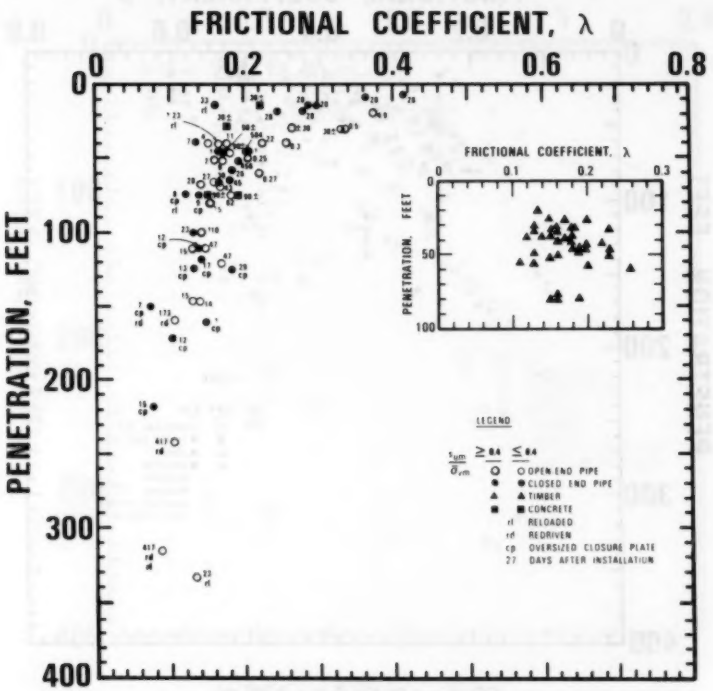

FIG. 9.—λ Profile (1 ft = 0.305 m)

Regression Analyses.—The load test data are presented in Figs. 7–9 in terms of depth profiles of average adhesion ratio (α = ratio of average adhesion, f_{av}, to average undrained shear strength, s_{um}); β values = $f/\bar{\sigma}_{vm}$; λ values, and in Fig. 10 as a profile of λ versus π_3, the pile-soil stiffness term. The amount of set-up time, piles with oversized closure plates, and piles redriven to deeper penetrations or reloaded, are identified for the data shown in Figs. 7–10. To compute π_3, we took f_{max} as the mean undrained shear strength and u^* as 0.1 in. (2.54 mm), as sufficient data were not available to determine

u^*. The value of 0.1 in. (2.54 mm) is consistent with the pile displacement at maximum load transfer used with empirical *t-z* curves (8,9). The elastic moduli of the piles were taken as 29,000,000 psi (200,000,000 kN/m^2) for steel, 2,600,000 psi (18,000,000 kN/m^2) for concrete, and 1,760,000 psi (12,000,000 kN/m^2) for timber. The wall thickness of some pipe piles was not known, thus π_3 could not be computed for all tests.

The data were separated according to pile type and soil stress history. No statistical difference in pile capacity factors (α, β, λ) was found between the

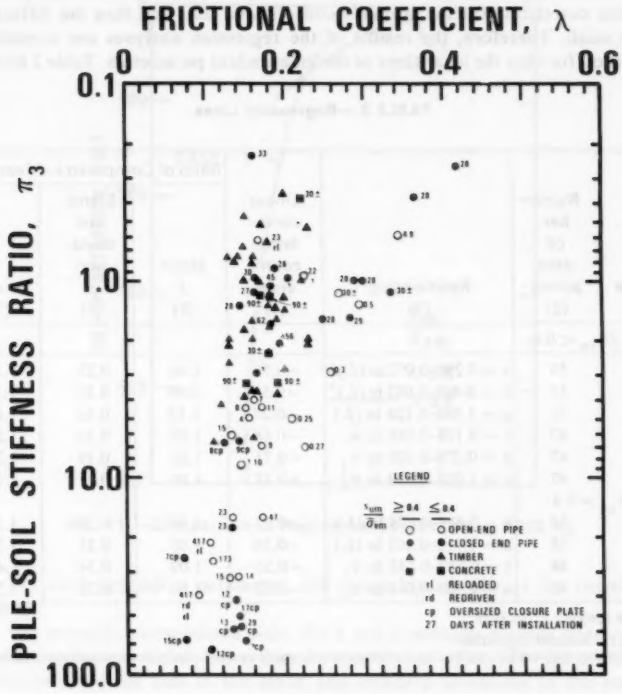

FIG. 10.—λ Profile

different pile types for the data used in this evaluation, although others have found timber piles to provide higher unit friction values than steel piles (4). A value of the average $s_{um}/\bar{\sigma}_{vm}$ of 0.4 was arbitrarily taken as the dividing line to approximately separate normally consolidated and overconsolidated soil deposits.

Regression analyses were made to relate α, β, and λ to pile penetration, ln of pile penetration, pile-soil stiffness, π_3, and ln of π_3. In each case, two regression analyses were made, one for piles in soils with $s_{um}/\bar{\sigma}_{vm}$ less than 0.4 and one for $s_{um}/\bar{\sigma}_{vm}$ greater than 0.4. In much of this data, the undrained

shear strength was representative of results from an unconfined compression test on a good quality sample. Hence, the correlations that follow are calibrated to this type of shear strength.

The rate of decrease in the pile capacity coefficient (α, β, λ) is expected to decrease with an increase in the independent parameter (Fig. 5). Therefore, the regression results in terms of the logarithm are thought to be more meaningful, even if the regression results in terms of π_3 or penetration are slightly more statistically significant than those in terms of the logarithm of these independent parameters. The arithmetric values of the independent parameters only provided a better correlation for the normally consolidated soils and then the differences were small. Therefore, the results of the regression analyses are summarized in Table 2 for only the logarithms of the independent parameters. Table 2 includes

TABLE 2.—Regression Lines

Case (1)	Number of data points (2)	Relationship (3)	Linear correlation coefficient (4)	Ratio of Computed to Measured: Mean $\bar{x}$ (5)	Ratio of Computed to Measured: Standard deviation σ (6)	Ratio of Computed to Measured: $\bar{x} + \sigma$ (7)
$s_{um}/\bar{\sigma}_{vm} < 0.4$						
1	51	$\lambda = 0.296–0.032 \ln (L)$[a]	−0.59	1.06	0.23	1.29
2	51	$\beta = 0.468–0.052 \ln (L)$[b]	−0.58	1.05	0.22	1.28
3	51	$\alpha = 1.486–0.126 \ln (L)$	−0.27	1.10	0.34	1.44
4	47	$\lambda = 0.178–0.016 \ln \pi_3$	−0.68	1.05	0.24	1.29
5	47	$\beta = 0.278–0.028 \ln \pi_3$	−0.71	1.03	0.19	1.22
6	47	$\alpha = 1.024–0.070 \ln \pi_3$	−0.33	1.09	0.31	1.40
$s_{um}/\bar{\sigma}_{vm} > 0.4$						
7	54	$\lambda = 0.488–0.078 \ln (L)$	−0.65	1.05	0.30	1.35
8	54	$\alpha = 1.012–0.103 \ln (L)$	−0.38	1.05	0.25	1.30
9	48	$\lambda = 0.232–0.032 \ln \pi_3$	−0.55	1.09	0.34	1.43
10	48	$\alpha = 0.685–0.061 \ln \pi_3$	−0.52	1.04	0.22	1.26

[a] Pile length, L, in feet.
[b] $\ln (x)$, natural logarithm.

also the correlation coefficients of the regression analyses.

The correlation coefficient provides a measure of the degree of fit for the assumed correlation function. Low absolute values of the correlation coefficient can be interpreted to mean that either the regression function does not represent the data or, if the standard deviation about the regression line (scatter) is small, that the dependent parameter is not significantly affected by the independent parameter. Standard deviations of the different methods cannot be directly compared as the magnitudes of the means of α, β, and λ differ by almost a magnitude. Therefore, the ratios of predicted to measured values α, β, and λ were computed. The mean and standard deviations of these ratios are also included in Table 2. Both the mean and standard deviation of the ratio of

computed to measured capacity must be considered when evaluating the confidence level of a predictive procedure. When the mean exceeds one, the sum of the mean and standard deviation provides a measure by which to compare the different methods: the smaller the sum, the better the method.

Evaluation of Results.—The following conclusions are supported by results of the regression analyses.

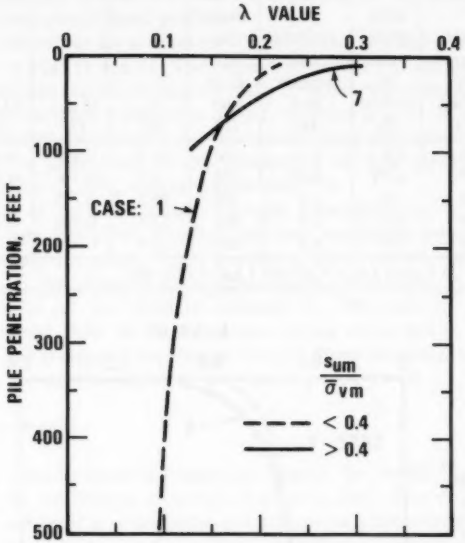

FIG. 11.—Comparison of Regression Curves (1 ft = 0.305 m)

1. For each dependent parameter, soil stress history affects the correlation equation.
2. For normally consolidated soils, the λ and β methods provide nearly equal correlations that are slightly better than the α method as reflected by the correlation coefficients and the sum of the mean and standard deviations of the ratio of computed to measured capacity.
3. For overconsolidated soils, the α and λ methods provide reasonable correlations.
4. The use of a soil-pile stiffness ratio as an independent parameter provides a slightly better correlation than pile penetration for normally consolidated soils.
5. The best correlations are the λ and β method with $\ln \pi_3$ for normally consolidated soils and the α method with $\ln \pi_3$ for overconsolidated soils.

The β values are highly sensitive to OCR, and this sensitivity contributes to a low correlation between β and either pile penetration or π_3. The λ value is also influenced by OCR, but the influence of OCR is less, as the λ method

uses both undrained shear strength and initial effective stress in the correlation; the β and α methods use only one of these two parameters.

TABLE 3.—Comparison of Methods

Example (1)	Diameter, in inches (2)	Wall thickness, in inches (3)	f_{max}, in kilopounds per square foot (4)	Pile penetration, L, in feet (5)	π_3 (6)	$\lambda\|_{\ln(L)}$ (7)	$\lambda\|_{\ln \pi_3}$ (8)	λ ratio $= \pi_3/L$ (9)
1	36	0.5	1	150	15.7	0.136	0.134	0.99
2	48	0.75	0.45	150	4.7	0.136	0.135	1.13
3	48	1.0	2.5	300	79.3	0.113	0.108	0.96
4	84	2.0	1.5	450	53.7	0.100	0.114	1.14
5	84	2.5	3.3	246	28.4	0.120	0.124	1.03

Note: 1 in. = 25.4 mm; 1 ft = 0.305 m; 1 ksf = 47.9 kPa.

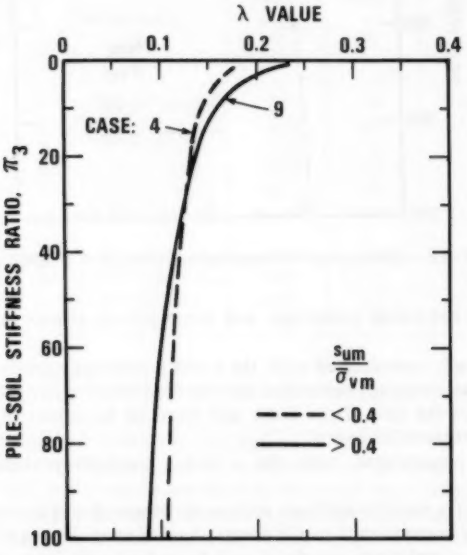

FIG. 12.—Comparison of Regression Curves

The magnitudes of α, β, and λ are not highly sensitive to soil strength for normally consolidated soils. Therefore, results from a correlation of these parameters with pile penetration or π_3, in normally consolidated soils, should

provide an indication of whether or not there is a length effect. The magnitude of β is influenced by the overconsolidation ratio (Table 1). Therefore, a correlation between measured β values and only pile penetration or π_3 in overconsolidated soils was found to be low, and the results are not included here. The load test data for overconsolidated clays are for short piles, and the large variations in the data are attributed in part to seasonal effects and construction details. Less data scatter and greater α values are expected for test results from long piles in deep, overconsolidated profiles.

The regression curves for λ in terms of pile penetration and pile-soil stiffness are compared in Fig. 11 and 12. The regression curves provide higher λ values for overconsolidated conditions than normally consolidated conditions for shallow penetrations, but at a pile penetration of 70 ft (21 m) or a π_3 of 24, the regression curves for normally consolidated and overconsolidated soils cross. This crossing is due in part to differences in the distribution of data points between the two conditions for $s_{um}/\bar{\sigma}_{vm}$ less or greater than 0.4.

The influence of the λ correlations with pile penetration and π_3 on computed pile capacity was examined for five offshore conditions encompassing the frequently encountered range. These examples, which are summarized in Table 3, show that π_3 for offshore piles ranges from about 5–80. A value of 0.1 in. (2.54 mm) for u^* was used to compute π_3. The ratio of average shaft friction determined from the π_3 correlation (Case 4) to that in terms of pile penetration (Case 1) ranges from about 0.95–1.15. From statistical considerations, both methods are equally reliable.

Concluding Comments

Theoretical considerations (t-z response) support the observation that a length effect exists on the friction capacity of piles in clay. The magnitude of the length effect influence is affected by soil stress-strain behavior (ξ, μ), pile-soil stiffness (π_3), lateral pile movements during installation, overconsolidation ratio, and other factors thought to be secondary. Parameter analyses demonstrate that average friction for a pile is not likely to be related to a single parameter representing pile-soil stiffness and soil stress-strain characteristics. Unfortunately, sufficient data are not available to test a theoretical model. Therefore, empirical approaches based on theoretical concepts must be used to evaluate pile capacity predictive models.

A statistical analysis of the available data show that the λ concept, either in terms of pile penetration or π_3, provides the most consistent and reliable single method for computing the axial capacity of piles in both normally consolidated and overconsolidated soils. The computed capacity is for loading rates where the failure load is reached within a few hours after initiating the test.

Until additional pile load test data become available in sufficient quantity to support alternative methods, we recommend that the axial static capacity of long piles driven into normally consolidated and lightly overconsolidated ($s_{um}/\bar{\sigma}_{vm} < 0.4$) clay formations be computed with the Lambda or β correlation with ln π_3 (Cases 4 or 5, Table 2) that provides the greater capacity. For piles in heavily overconsolidated clays, we recommend using either the Lambda or α correlation with ln π_3 (Cases 9 or 10, Table 2). The value of π_3 should

be computed in the same way as was done for the correlation study.

Because of short set-up times, oversized closure plates, reloading, and redriving for some of the test piles, especially those with large penetrations and large values of π_3, the regression curves tend to underestimate the actual capacity of long piles without closure plates and with long set-up. Therefore, we further recommend, based on personal judgment and the available data, that the minimum λ value be limited to 0.14 and the minimum β value be limited to 0.23.

Fig. 13 shows a comparison of β profiles in normally consolidated clays for Case 1, with λ limited to 0.14, Case 2, with β limited to 0.23, and the Flaate

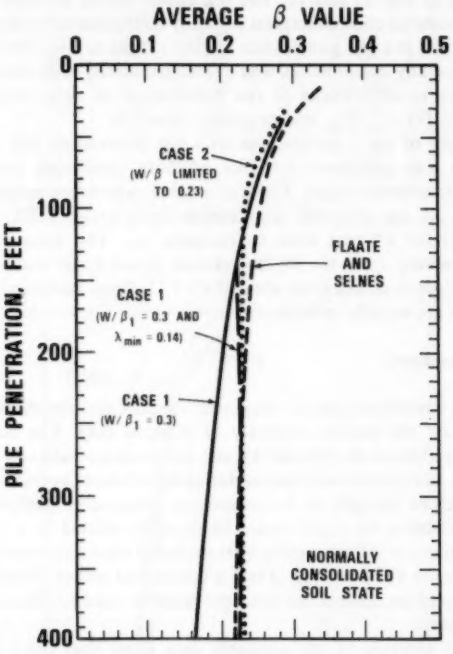

FIG. 13.—Comparison of β Values (1 ft = 0.305 m)

and Selnes method. A value of 0.3 for β_1 ($s_u/\bar{\sigma}_{vo}$) was used to generate the β curve for the Case 1 curves. Three methods (Cases 1 and 2 with limiting values and Flaate and Selnes) are in reasonably good agreement.

The recommendations in the preceding paragraph apply only to piles without oversized closure plates and piles with full set-up. The minimum value of $s_{um}/\bar{\sigma}_{vm}$ from the load test data was about 0.2, thus the recommended procedure may not be applicable to piles in soils with lower ratios of $s_{um}/\bar{\sigma}_{vm}$. The influence of loading rate and cyclic loading may justify alterations to the capacities computed in this way. Generally, pile capacity increases with an increase in loading rate

and decreases with cyclic loading due to degradation of the shear resistance (16,20).

The available data base of good quality pile load tests is very limited and inadequate to support significant or theoretical modifications to empirical methods applicable to the pile and soil conditions and the loading environment encountered in design of marine structures. Typical of the range in pile and soil conditions are pile lengths of 200 ft–600 ft (61 m–183 m), pile diameters of 3 ft (0.9 m)–12 ft (3.7 m), pile wall thicknesses of 0.5–3 in. (13–76 mm), soils in underconsolidated to heavily overconsolidated states, and soils with shear strengths of 0.05–15 ksf (2.4–718 kN/m^2). The cyclic nature and rate of wave loading experienced by piles supporting offshore structures are a strong contrast to the monotonic, slow loading rate on most test piles. Thus, the geotechnical engineer has been and will continue to be faced with the challenge of computing axial pile capacities for conditions for which there is little or no prior load test experience.

TABLE 4.—Uncertainty Analysis

Descriptions of factors (1)	Relative uncertainty between computed and actual capacity[a] (2)
Soil variability and disturbance of the soil surrounding the pile due to pile installation	±0.1
Distribution and magnitude of ultimate skin friction values in heavily overconsolidated soils	±0.1
Changes in the soil properties with time (consolidation, thixotropic and seasonal effects, and load history)	±0.2
Distribution and magnitude of residual stresses in the pile	±0
Pile installation details (displacement characteristics, time delays, sequence of installation)	±0.2

[a]Actual capacity may differ by ±10% from computed capacity.

Some of the major factors that contribute to differences between actual and computed capacities of static monotonically loaded piles driven into clay or in evaluating pile load test data are summarized in Table 4. Subjective estimates, which reflect our opinion of the present state-of-the-art, are shown in Table 4 for the relative uncertainty of each of these factors on pile capacity for pile and soil conditions where we have previous experience and where the piles are installed with good construction practices. Considering these factors and limitations of the analytic models, we expect measured capacities in most cases to be between 0.7 and 1.3 times predicted capacities.

Some methods may be more appropriate for certain soil conditions than others. The difficulty lay in establishing which method is the most appropriate for which conditions. The first step is to recognize the limitations of the available pile capacity methods. If a method is not appropriate or the uncertainty is unacceptably large, load tests may be needed to guide and confirm design. When load tests are not practical, the geotechnical engineer must make rational

decisions about pile capacities and select the most appropriate method based on his experience and analytic studies. Although recent research on effective stress methods with cavity expansion and reconsolidation offer promise, they are not yet ready for use as a standard design tool. Nevertheless, these methods can be a useful analytic tool to gain insight to aide the decision-making process. Still, the need continues for quality load tests on long piles to improve design procedures and increase the reliability and cost effectiveness of marine pile foundations.

Appendix.—References

1. American Petroleum Institute, *Recommended Practice for Planning, Designing, and Constructing Fixed Offshore Platforms*, API RP 2A, 11th edition, (1980).
2. Aurora, R. P., Peterson, E. H., and O'Neill, M. W., "Model Study of Load Transfer in Slender Pile," *Journal of the Geotechnical Engineering Division*, ASCE, Vol. 106, No. GT8, 1980, pp. 941–945.
3. Bergemann, H., "Alternating Loading and Pulling Tests on Steel I-beam Piles," *Proceedings of the Eighth International Conference on Soil Mechanics and Foundation Engineering*, Moscow, Vol. 2.1, 1973, pp. 13–17.
4. Blanchet, R., Tavenes, F., and Garneau, R., "Behaviour of Friction Piles in Soft Sensitive Clays," *Canadian Geotechnical Journal*, Vol. 17, No. 2, 1980, pp. 203–224, (See Discussions also).
5. Brand, E. W., Miktabhant, C., and Taechathummarak, A., "Load Tests on Small Foundations in Soft Clay," *Proceedings of the Specialty Conference on Performance of Earth and Earth-Supported Structures*, Purdue University, ASCE, Vol. I, Part 2, 1972, pp. 903–928.
6. Burland, J. B., "Shaft Friction of Piles in Clay—A Simple Fundamental Approach," *Ground Engineering*, Vol. 6, No. 3, 1973, pp. 30–42.
7. Cooke, P. W., Price, G., and Tarr, K., "Jacked Piles in London Clay: a Study of Load Transfer and Settlement Under Working Conditions," *Geotechnique*, Vol. 29, No. 2, 1979, pp. 113–147.
8. Coyle, H. M., and Reese, L. C., "Load Transfer for Axially Loaded Piles in Clay," *Journal of the Soil Mechanics and Foundations Division*, ASCE, Vol. 92, No. SM2, 1966, pp. 1–26.
9. Coyle, H. M., and Sulaiman, I. H., "Skin Friction for Steel Piles in Sand," *Journal of the Soil Mechanics and Foundations Division*, ASCE, Vol. 93, No. SM6, 1967, pp. 261–278.
10. Danys, J. V., "Light Pier on Friction Piles in Deep Soft Marine Clay," *Canadian Geotechnical Journal*, Vol. 8, No. 3, 1971, pp. 434–455.
11. Desai, C. S., and Holloway, D. M., "Load-Deformation Analysis of Deep Pile Foundations," *Proceedings of the Symposium on Applications of the Finite Element Method in Geotechnical Engineering*, Desai, Ed., U.S. Army Engineers, Waterways Experiment Station, Vicksburg, Mississippi, 1972, pp. 629–656.
12. Drewry, J. M., Weidler, J. B., and Hwong, S. T., "Predicting Axial Pile Capacities for Offshore Platforms," *Petroleum Engineer*, 1977, p. 41.
13. Endley, S. N., Ulrich, E. J., and Gray, J. B., "A Study of Axial Pile Load Tests," ASCE Meeting in Atlanta, Ga.
14. Esrig, M. I., and Kirby, R. C., "Advances in General Effective Stress Method for the Prediction of Axial Capacity for Driven Piles in Clay," *Proceedings of the Eleventh Offshore Technology Conference*, Houston, Tex., Vol. 1, 1979, pp. 437–448.
15. Flaate, K., and Selnes, P., "Side Friction of Piles in Clay," *Proceedings of the Ninth International Conference on Soil Mechanics and Foundation Engineering*, Tokyo, Japan, Vol. 1, 1977, pp. 517–522.
16. Grosch, J. J., and Reese, L. C., "Field Tests of Small-Scale Pile Segments in a Soft Clay Deposit Under Repeated Loading," *Proceedings of the Twelfth Offshore Technology Conference*, Houston, Tex., Vol. 4, 1980, pp. 143–151.
17. Hutchinson, J. N., and Jensen, E. V., "Loading Tests on Piles Driven into Estuarine

Clays at Port of Khorramshar, and Observations on the Effect of Bitumen Coatings on Shaft Bearing," *Norwegian Geotechnical Institute*, Oslo, Norway, 1968, No. 78.
18. Ito, K., and Koizumi, Y., "Field Tests with Regard to Pile Driving and Bearing Capacity of Piled Foundations," *Soils and Foundations*, Vol. VII, No. 3, 1967, pp. 30–53.
19. Janbu, N., "Static Bearing Capacity of Friction Piles," *Proceedings of the European Conference on Soil Mechanics and Foundation Engineering*, Vol. 1.2, 1976, pp. 479–488.
20. Kraft, L. M., Jr., Cox, W. R., and Verner, E. A., "Pile Load Tests: Cyclic Loads and Varying Loading Rates," *Journal of the Geotechnical Engineering Division*, ASCE, Vol. 107, No. GT1, 1981, pp. 1–19.
21. Kraft, L. M., Jr., "An Effective Stress Capacity Model for Piles in Clay," submitted to ASCE for publication.
22. Kraft, L. M., Jr., Ray, R. P., and Kagawa, T., "Theoretical Development of *t-z* Curves," *Journal of the Geotechnical Engineering Division*, ASCE, Vol. 107, No. GT11, 1981.
23. Kulhawy, F. H., and Peterson, M. S., "Behavior of Sand-Concrete Interfaces," *Proceedings of the Sixth Pan American Conference on Soil Mechanics and Foundation Engineering*, Lima, Peru, Vol. 2, 1979, pp. 225–236.
24. Meyerhof, G. G., "Bearing Capacity and Settlement of Pile Foundations," *Journal of the Geotechnical Engineering Division*, ASCE, Vol. 102, No. GT3, 1976, pp. 197–228.
25. Meyerhof, G. G., and Murdock, L. J., "An Investigation of the Bearing Capacity of Some Bored and Driven Piles in London Clay," *Geotechnique*, Vol. 3, No. 7, 1953, pp. 267–282.
26. Murff, J. D., "Pile Capacity in a Softening Soil," *Numerical and Analytical Methods in Geomechanics*, Vol. 4, No. 2, 1980, pp. 185–189.
27. Parry, R. H. G., and Swain, C. W., "A Study of Skin Friction on Piles in Stiff Clay," *Ground Engineering*, Vol. 10, No. 8, 1977, pp. 33–37.
28. Rigden, W. J., Pettit, J. J., St. John, H. D., and Poskitt, T. J., "Developments in Piling for Offshore Structures," *Proceedings of the Second International Conference on Behavior of Off-shore Structures*, 1979, pp. 279–296.
29. Steenfelt, J. S., Randolph, M. F., and Wroth, C. P., "Model Tests on Instrumented Piles Jacked into Clay," *Proceedings of the Tenth International Conference on Soil Mechanics and Foundation Engineering*, Stockholm, Sweden.
30. Stermac, A. G., Selby, K. G., and Devata, M., "Behavior of Various Types of Piles in a Stiff Clay," *Proceedings of the Seventh International Conference on Soil Mechanics and Foundation Engineering*, Mexico, Vol. 2, 1969, pp. 239–245.
31. Tomlinson, M. J., "Some Effects of Pile Driving on Skin Friction," *Behavior of Piles*, Institution of Civil Engineers, London, 1970, pp. 107–114.
32. Vijayvergiya, V. A., and Focht, J. A., Jr., "A New Way to Predict Capacity of Piles in Clays," *Proceedings of the Fourth Offshore Technology Conference*, Houston, Vol. 2, 1972, pp. 865–874.

THEORETICAL *t-z* CURVES

By Leland M. Kraft, Jr.,[1] M. ASCE, Richard P. Ray,[2] A. M. ASCE, and Takaaki Kagawa,[3] M. ASCE

INTRODUCTION

The subgrade reaction, or *t-z*, method suggested by Seed and Reese (19) is an expedient means of computing the axial movement of a pile under axial load. Procedures are available to generate the relationships between shear stress at the pile shaft (load transfer, t) and pile displacement, z, along the pile shaft and at the tip (3,4,6,8,9,10,13,16,21,22). The most commonly used procedures, however, are empirical and based on data from tests on short land piles, usually less than 100 ft (30 m) long, with diameters less than 18 in. (0.5 m). Pile diameter, axial pile stiffness, pile length, and distribution of soil strength and stiffness along the pile are all factors that influence the *t-z* behavior. Data from instrumented pile tests do not span a wide enough variety of conditions to establish a comprehensive data base for all the variables in the theory.

The theoretical concepts presented in this paper were developed to provide a basis for *t-z* criterion that would be applicable to a variety of pile and soil conditions. The validity of the criterion was tested with several case studies.

DEVELOPMENT OF *t-z* CURVES

General Comments.—The stress at and displacement of each point along a pile are influenced by the stress at every other point; the degree of influence decreases with distance from the point of interest. The subgrade-reaction approach assumes that the displacement at any point depends only on the stress at that point. Soil-pile interaction is represented by springs that relate shear stress on the soil-pile interface and displacement of the pile (Fig. 1).

Success in developing realistic *t-z* relationships for a pile depends on the accuracy of the ultimate load-transfer values of the soil (pile capacity), the distribution of those values along the pile, and the displacement characteristics

[1]Mgr., Special Projects Group, McClelland Engrs., Inc., Houston, Tex. 77081.
[2]Grad. Research Asst., Univ. of Michigan, Ann Arbor, Mich., formerly Geotechnical Engr. with McClelland Engrs., Inc., Houston, Tex. 77081.
[3]Sr. Geotechnical Engr., McClelland Engrs., Inc., Houston, Tex. 77081.

Note.—Discussion open until April 1, 1982. To extend the closing date one month, a written request must be filed with the Manager of Technical and Professional Publications, ASCE. Manuscript was submitted for review for possible publication on January 21, 1981. This paper is part of the Journal of the Geotechnical Engineering Division, Proceedings of the American Society of Civil Engineers, ©ASCE, Vol. 107, No. GT11, November, 1981. ISSN 0093-6405/81/0011-1543/$01.00.

of the soil during load transfer. For this study, available techniques were used to predict the ultimate values; therefore, only the load-transfer characteristics as they relate to displacement are discussed in detail.

To construct rational *t-z* curves, we considered separately prefailure and postfailure *t-z* responses. Prefailure *t-z* relationships were described by a theoretical model based on elasticity. Postfailure relationships were modeled considering the residual stress-deformation behavior at the soil-pile interface.

Prefailure *t-z* Curves.—The theoretical formulation discussed below uses a concentric cylinder approach with the following key assumptions and conclusions as described by Randolph and Wroth (18):

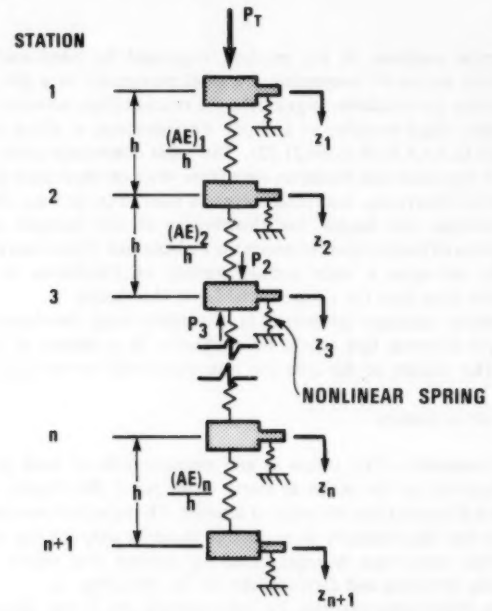

FIG. 1.—Finite Difference Model of Axially Loaded Pile

1. The displacement pattern of soil can be modeled as concentric cylinders in shear (Fig. 2).

2. Radial soil displacements due to pile loads are assumed negligible when compared to vertical soil deformations. Therefore, simple shear condition prevails in the soil.

3. Shear stress decreases with distance such that $\tau r = \tau_o r_o$; in which τ = the shear stress at distance r; τ_o = the shear stress on the pile-soil interface; and r_o = the pile radius.

4. Shear stresses are negligible beyond a radial distance r_m (or zone of influence), and the soil does not deform beyond that point.

5. The zone of influence is $r_m = 2.5\ l\ \rho\ (1 - \nu)$ and is an average value along the pile; in which l = pile length; ν = Poisson's ratio of soil; and ρ = the ratio of the soil shear moduli at depths $l/2$ and the pile tip.

These assumptions lead to load-displacement equation

$$z_s = \tau_o r_o \int_{r_o}^{r_m} \frac{dr}{Gr} \quad \text{(1)}$$

in which z_s = displacement of shaft element. G can be a function of radial distance as a result of disturbances caused by pile installation and nonlinear soil behavior. Both of these possibilities will be discussed in later sections. Following failure, the slip planes that develop invalidate Eq. 1. Up to the point of failure, however, variations in shear modulus with radial distance and modulus

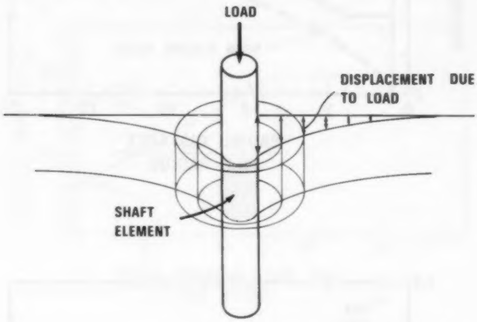

FIG. 2.—Settlement Modeled as Shearing of Concentric Cylinders

degradation with strain can be modeled with Eq. 1.

If G is constant, Eq. 1 reduces to

$$z_s = \left(\frac{\tau_o r_o}{G}\right) \ln \left(\frac{r_m}{r_o}\right) \quad \text{(2)}$$

Eq. 2 shows that the displacement is not only a function of shear stress and soil stiffness, but also pile radius and length (indirectly by r_m). These factors are not directly accounted for in empirical t-z criteria.

Variation of Shear Modulus with Depth.—The soil modulus varies along the pile, with radial distance from the pile, and with pile load as a result of natural soil variations, soil disturbance during pile installation, soil consolidation during setup, and nonlinear stress-strain response. The t-z response at a particular depth, however, is taken to be controlled by soil modulus conditions at that depth. Using this assumption, Randolph and Wroth (18) approximated a linear increasing variation in soil modulus along the pile shaft. The load-displacement response computed was in good agreement with more rigorous solutions. Therefore, this basic assumption in the t-z approach should account for vertical variations in soil modulus.

Radial Variation of Shear Modulus.—A typical distribution of the soil modulus is shown in Fig. 3 for four conditions: (1) Immediately after installation for pile loads that result in small soil strains; (2) immediately after installation for

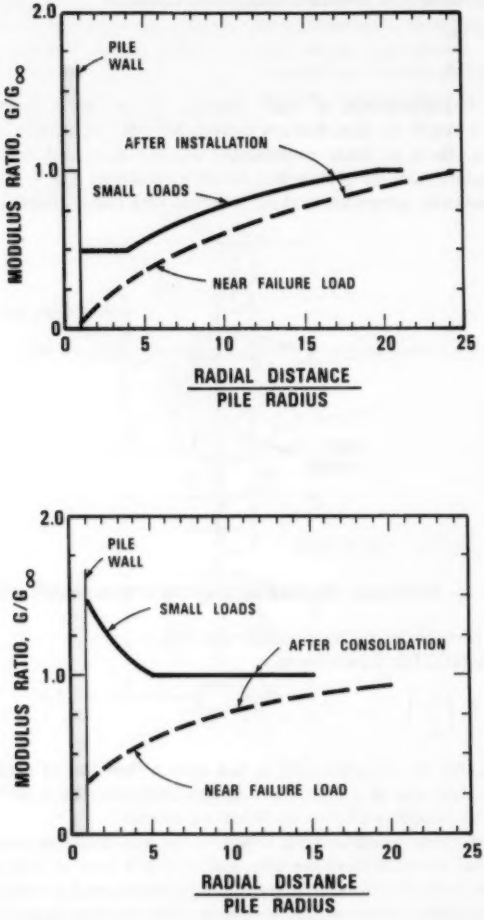

FIG. 3.—Variation in Soil Modulus Ratio

pile loads near failure that result in large soil strains; (3) after consolidation for small pile loads; and (4) after consolidation for pile loads near failure.

The variation in modulus due to pile installation and soil consolidation can

be estimated from results of cavity expansion to simulate changes in soil stresses during installation and consolidation theory to simulate the stress changes due to dissipation of pore pressures induced during installation. Available solutions (17) of cylindrical cavity expansion in Modified Cam-Clay soil with subsequent consolidation show that the size of the zone of disturbance (large stress changes) due to installation extends to about 20 pile radii from the pile, but soil failure extends only to about 4 pile radii. After consolidation, the shear strength next to the pile, which is predicted with the consolidation analyses, may exceed the original value with the strength decreasing away from the pile.

If the soil modulus is proportional to the undrained shear strength, then the distribution of the ratio of the shear strength after installation to initial shear strength can be used to adjust the initial in situ modulus at small strains to arrive at a representative distribution of the modulus next to the pile at any time after installation. The reduction in modulus with pile loading can then

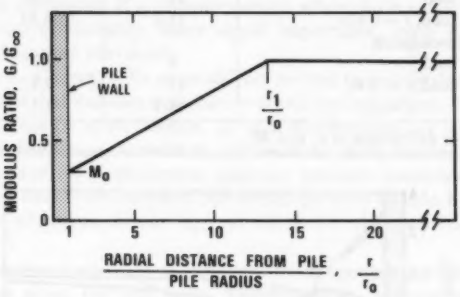

FIG. 4.—Idealized Radial Distribution of Soil Modulus Ratio

be estimated from the radial distribution of shear stress ($\tau = \tau_o r_o / r$) and knowledge of the stress-strain behavior of the soil.

Using Eq. 1 and a given radial distribution of modulus, we can compute an average modulus that will provide the same soil displacement, z_s, next to the pile wall as a solution for the actual distribution. For a linear variation in the modulus (Fig. 4) the average soil modulus is

$$G_{ave} = G_\infty \frac{\ln\left(\frac{r_m}{r_o}\right)}{\frac{\left(\frac{r_1}{r_o}\right) - 1}{\left(\frac{M_o r_1}{r_o}\right) - 1} \ln\left(\frac{M_o r_1}{r_o}\right) + \ln\left(\frac{r_m}{r_1}\right)} \quad \ldots\ldots\ldots\ldots\ldots\ldots (3)$$

in which G_{ave} = equivalent shear modulus for the pile-soil system; G_∞ = shear modulus a great distance from pile; and r_1 and M_o are defined in Fig. 4. The actual variation in modulus is not known with a high degree of precision. Therefore,

a linear approximation of this variation is adequate for most cases.

As an example, equivalent, weighted moduli were determined with Eq. 3 for a stiff, overconsolidated soil with a sensitivity of 1.5 and a maximum gain in strength after consolidation of 30%. The approximations to the radial variations of modulus ratio are shown in Fig. 5 for conditions after consolidation. These estimates were made using cavity expansion and consolidation results by Randolph, Carter, and Wroth (17) and a nonlinear stress-strain curve. Values of r_1/r_o, M_o, and G_{ave}/G_∞ at small and large strains are shown in Table 1.

TABLE 1.—Radial Variation of Soil Modulus Ratio Parameters[a] and Average Values

Condition (1)	r_1/r_o (2)	M_o (3)	G_{ave}/G_∞ (4)
Immediately after installation			
Small load	16	0.65	0.85
Large load, $f = 0.67s_u$	15.2	0.20	0.54
After consolidation			
Small load	4	1.3	1.04
Large load, $f = 0.4s_u$	12	0.8	0.96
$f = s_u$	14.4	0.4	0.73

[a]See Fig. 4 for definitions of r_1 and M_o.

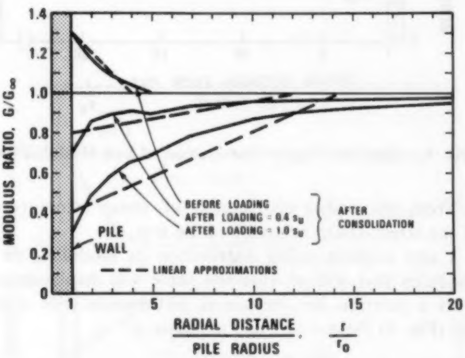

FIG. 5.—Estimated Radial Distribution of Soil Modulus Ratio

For conditions after consolidation, the nonlinear effects are more important than the installation effects. Therefore, further assessment and consideration of the effect due to installation will be neglected in the following work, and only the nonlinear effects are considered.

Nonlinear Stress-Strain.—The stress-strain behavior of some soils can be described by a hyperbolic expression.

$$G = G_i\left[1 - \left(\frac{\tau_o R_f}{\tau_{max}}\right)\right] \quad \text{(4)}$$

in which G = secant shear modulus at an applied shear stress τ_o; G_i = initial shear modulus at small strains; R_f = stress-strain curve-fitting constant; and τ_{max} = shear stress at failure. By combining Eqs. 4, 1, and the distribution of τ with r, the equation for t-z response becomes

$$z_s = \frac{\tau_o r_o}{G_i} \ln\left(\frac{\dfrac{r_m}{r_o} - \psi}{1 - \psi}\right) \qquad (5)$$

in which $\psi = \tau_o R_f / \tau_{max}$. A similar equation can be generated for a soil with a stress-strain behavior described by the Ramberg-Osgood model.

Eq. 5 can be used to generate prefailure t-z curves. Although this equation neglects radial heterogeneity caused by the installation process, these effects, after a long setup for driven piles, may be minor compared to uncertainties in the properties of the undisturbed soil and to the approximations used in developing the equations. If a situation arises where both radial heterogeneity and stress-strain nonlinearity share equal importance, both effects can be combined as discussed previously.

Post-Failure *t-z* Curves.—We must address several related problems to develop an analytic model that includes t-z behavior at and beyond failure. These problems include: (1) Maximum shaft friction; (2) pile displacement (or strain) at which the maximum friction is mobilized; (3) residual shaft friction at large pile displacements; and (4) displacement behavior between maximum and residual stresses. In this study, we computed the maximum shaft friction by conventional means and the pile displacement, z_{max}, at which the maximum friction is mobilized with Eq. 5.

Some conventional methods to compute shaft friction provide estimates of average values along the pile shaft. These methods account empirically for differences between maximum and residual load transfer and the degree of shear resistance between these values that is mobilized at maximum load on the pile. Also, these conventional methods provide average resistances along the shaft that may not reflect the actual distribution along the shaft. The distribution of shaft friction along the pile is important to the load-displacement behavior of the pile. For example, a shaft friction of 1 kip/sq ft (48 kN/m^2) may be used to compute the capacity of a pile in a stiff Beaumont clay. The distribution along the shaft, however, may be zero at the ground surface and increase linearly to 2 kip/sq ft (96 kN/m^2) near the pile tip. Some discretion should be used to establish the distribution of shaft friction along the pile when using conventional methods to compute the maximum shaft friction.

Once the soil reaches a state of incipient failure, additional deformation at the pile wall results from a shear strain in the soil with a rotation of principal planes, movements along slip planes, or a combination of these conditions. When slip planes develop, the soil behavior cannot be defined in terms of stress and strain. Therefore, Eq. 1 cannot be used to define the t-z response for postfailure conditions when slip planes develop. One approach to postfailure behavior is to model a section of the pile-soil system in a direct shear test or some other laboratory simulation. This is done by replacing one half of the soil sample normally used for the test with a representative piece of steel, concrete, or wood. If the failure is in the soil rather than at the soil-pile interface,

a conventional direct shear test may be more appropriate to define the load transfer-displacment response for post-failure conditions.

Direct Shear Tests on Sand and Concrete.—Desai and Holloway (5) and Kulhawy and Peterson (11) present load-displacement curves for sand and sand-concrete interfaces. The displacements at which the residual shear stress was reached are typically between 0.035 in. (0.9 mm) and 0.05 in. (1.3 mm) beyond the displacement at maximum shear stress. While the data from these studies are by no means inclusive, the data indicate that residual shear resistance in sand range between about 0.80–1.0 times the maximum shear strength.

Direct Shear Tests—Clay.—Residual resistances for undisturbed soils range from less than 60%–100% of the maximum resistance (12). The magnitude of strain softening of remolded material may differ from that of undisturbed material. The degree of softening may also be influenced by test type (simple shear, triaxial, direct shear).

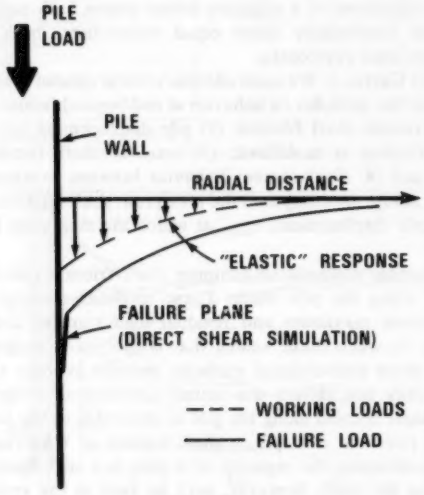

FIG. 6.—Exaggerated Displacement Profile

As part of this study, several consolidated-drained direct shear tests were performed on undisturbed and remolded samples of highly plastic clay. We tested a clay-clay interface instead of a clay-pile interface because several model and full-scale load tests have shown that the failure surface for piles in clay occurs within the clay, a small distance from the clay-pile interface (6).

Results of the direct-shear tests indicate a strength decrease of about 20% from peak to residual for this clay. The deformation necessary to develop the residual value after reaching the maximum stress was about 0.1 in. (2.5 mm).

Interpretation of Direct Shear Tests.—The direct shear test is not a perfect simulation of the load transfer-displacement behavior of a pile segment. The

total normal stress is held constant during the direct shear test. This stress boundary condition is different from the displacement boundary condition (nearly zero radial movement) during pile loading. The stress concentrations caused by the small contact area of the laboratory test and spacing between the shear boxes also result in differences between the simulation and prototype. Furthermore, the stress-displacement curve generated from a direct shear test simulates the condition along a failure plane (Fig. 6), and does not account for elastic strains that occur in the soil some distance away from the pile.

The displacement, δ_z, that occurs in moving from the maximum to residual stress in a direct shear test can be compared to the *t-z* displacement, Δz, that occurs in moving from the maximum to residual load-transfer value for a pile segment. The pile segment and adjoining soil exhibits *t-z* characteristics, to the point of failure, prescribed by Eq. 5. Once failure is reached, the *t-z* curve of the pile segment is governed by the direct shear test results along the failure surface, and by Eq. 5 for soil away from the failure surface. This implies that, once failure is reached and if the load transfer decreases with continued

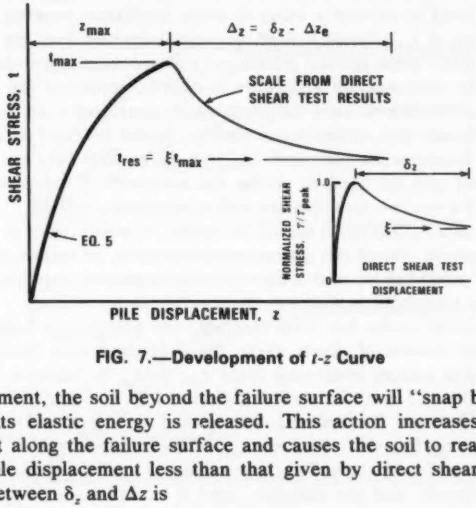

FIG. 7.—Development of *t-z* Curve

pile displacement, the soil beyond the failure surface will "snap back" a small amount as its elastic energy is released. This action increases the relative displacement along the failure surface and causes the soil to reach a residual level at a pile displacement less than that given by direct shear results. The difference between δ_z and Δz is

$$\delta_z - \Delta z = \Delta z_e \quad (6)$$

in which Δz_e = the elastic rebound, which is computed from Eq. 5, taking the difference for $\tau_o = t_{max}$ and $\tau_o = t_{residual}$.

The maximum difference between Δz and δ_z is less than 10% of δ_z for a 12-in. (0.3-m) diameter pile and typical soil conditions. The value of Δz_e increases with an increase in pile diameter, and δ_z is probably insensitive to pile diameter. Therefore, for pile diameters greater than about 18 in. (0.5 m), the magnitude of Δz_e should be evaluated to determine if a correction is needed. Otherwise, a value of δ_z from direct shear tests can be used directly for postfailure *t-z* construction.

Procedure to Construct Theoretical *t-z* Curve.—The *t-z* curve is constructed in two parts: prefailure and postfailure. The basic concept is summarized in Fig. 7. Prefailure *t-z* is governed by Eq. 5. This equation is flexible and can easily be altered to simulate changes of shear modulus with shear strain and changes of shear modulus with radial distance. An equivalent radius can be used for square or H-piles when using Eq. 5. The load-displacement relationships require a maximum unit load transfer value, t_{max}; shear strength, s_u; soil modulus, G_{max}; and stress-strain constant, R_f. The value of t_{max} may be less than s_u, for example, for piles in stiff, overconsolidated clays.

t_{max} is computed in the same way as it would be for shaft friction in pile capacity computations, but some discretion should be used to select the distribution of t_{max} along the pile. For example, a linear increasing distribution of t_{max} is probably more appropriate for short, driven piles in stiff, overconsolidated clays than a uniform value, even though the shear strength may be constant over the pile length. The average of the distribution should be consistent with the value obtained from conventional pile capacity procedures. If laboratory data show that the residual shear resistance is less than t_{max}, the pile capacity procedure is used to provide a value of shear resistance between t_{max} and t_{res}. Thus, the value of t_{max} should exceed the value obtained from the pile capacity procedures. Until more refined guidelines and procedures are developed, the value from the pile capacity procedure is used to represent the mean of t_{max} and t_{res}. The difference between the pile capacity generated from the *t-z* analysis, using this estimate and conventional theory, should be small except for very rigid or very compressible piles and for large differences between t_{max} and t_{res}. Trial and error can be used to revise the estimates, if necessary, until the pile capacity for the two methods are within acceptable limits.

The stress-strain parameters should be based on in situ tests at small strains (cross-hole, uphole, downhole), resonant column tests, or empirical correlations (7). Laboratory data can be used to determine the nonlinear response, as reflected by R_f with the hyperbolic model.

Once the failure stress has been reached, the post-failure behavior can be estimated from results of direct shear tests. Limited data indicate that the deformation that occurs in moving from t_{max} to t_{res} is between 0.03 in. (0.8 mm) and 0.05 in. (1.3 mm) for sand and about 0.1 in. (2.5 mm) for clay.

Comparison between Theoretical and Empirical *t-z* Curves.—The deformation needed to develop full shaft friction, z_{max}, varies considerably. This variation can be accounted for by the soil shear modulus, G, and the stress-strain parameter, R_f, pile length, and pile diameter, used in the theoretical approach. None of these factors are directly considered in empirical formulations.

Three examples of *t-z* construction (one each for sand; stiff clay, and soft clay) are shown in Fig. 8. For these examples, the post-peak response was approximated by a straight line from t_{max}–90% of the maximum for pile movements greater than z_{max}. The curves for a sand show that empirical procedures may result in a much softer *t-z* spring than indicated by the theory presented here. The curves for clay are within the range of the empirical curves, but the theoretical approach offers a sound method to develop *t-z* curves beyond the data base on which the empirical procedures were developed: 6-in. (152-mm)–18-in. (457-mm) diameter piles with less than 100-ft (30-m) penetration. The comparisons shown in Fig. 8 could be changed with changes in pile diameter and soil moduli.

***Q-z* Response at Pile Tip.**—The *Q-z* curves at the pile tip used in the subgrade reaction approach have been developed from instrumented pile tests and laboratory model tests. While the results of such tests yield useful information on overall load-settlement performance, a theoretical approach is needed to study the fundamental factors that influence the behavior of *Q-z* response and to apply the *Q-z* concepts to conditions beyond the data base on which the empirical procedures were developed.

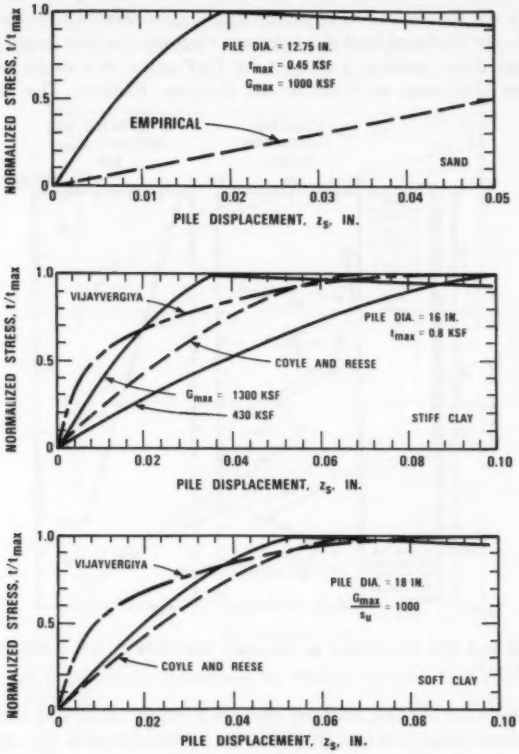

FIG. 8.—Comparison of *t-z* Curves (1 in. = 25.4 mm; 1 ksf = 47.9 kN/m²)

The elastic solution for a rigid punch (20) can be used to model *Q-z* behavior (21).

$$z = \frac{q_b D (1-\nu^2)}{E} I_b \quad \ldots\ldots\ldots\ldots\ldots\ldots\ldots\ldots\ldots\ldots\ldots\ldots\ldots\ldots (7)$$

in which q_b = stress on pile tip; D = tip diameter; E = Young's modulus of

soil; and I_b = influence coefficient. An appropriate secant Young's modulus is used in Eq. 7 to determine a value of z. For a rigid punch on an elastic half-space, the value of $I_b = 0.78$. Studies reported by Randolph and Wroth (18), in addition to those by Vesic (21), show that I_b is reduced, due to depth effects, to values typically between 0.5 and 0.78.

Case Studies

To verify the theoretical t-z approach and the procedures to select soil input parameters, we predicted load-displacement response for four single piles tested in a medium dense sand at a site on the Gulf coast, and single piles in stiff clays at the University of Houston and Hendon, England. The soil and pile

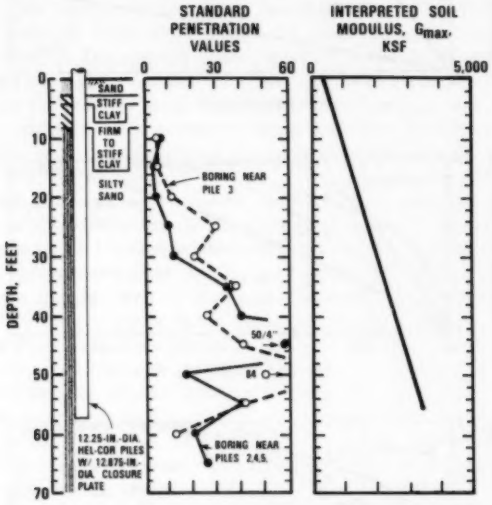

FIG. 9.—Soil and Pile Conditions at Houston Test Site (1 ft = 0.305 m; 1 kip/sq ft = 47.9 kN/m²)

conditions for each of these tests are described briefly along with a comparison of predicted and measured load-displacement curves for each test. All the case studies were for short-term loading. The computer program AXPILE was used for single pile analyses.

Houston Sand

Pile and Soil Conditions.—Load tests on four Armco Hel-Cor piles were performed in 1969 at a Houston site. Three of the 12.25-in. (311-mm) diameter piles (Piles 2, 4, and 5) were driven to 57.5-ft (17.5-m) penetration, and a fourth pile (Pile 3) was driven to 46-ft (14-m) penetration. The piles had an oversized closure plate (12.875-in. diameter). After driving, concrete was placed in the pile shells.

The soils at the site consist primarily of a loose-to-medium-dense silty sand. Profiles of standard penetration blow counts are shown in Fig. 9 for the two soil borings nearest the piles. The soil shear modulus profile, also included in Fig. 9, was developed from cross-hole tests. The shaft friction was computed with an earth pressure coefficient of 0.7 and a friction angle of 30°, except for depths greater than 41 ft (12.5 m) for Piles 2, 4, and 5 and for depths greater than 34.5 ft (10.5 m) for Pile 3 for which a friction angle of 35° was used. An end bearing coefficient of 40 was used to compute the tip resistance, which was about 50% of the computed capacity.

The t-z curves were generated with Eq. 5 using an R_f of 0.9 and the soil modulus profile (Fig. 9). Any loss of shear resistance for pile displacements

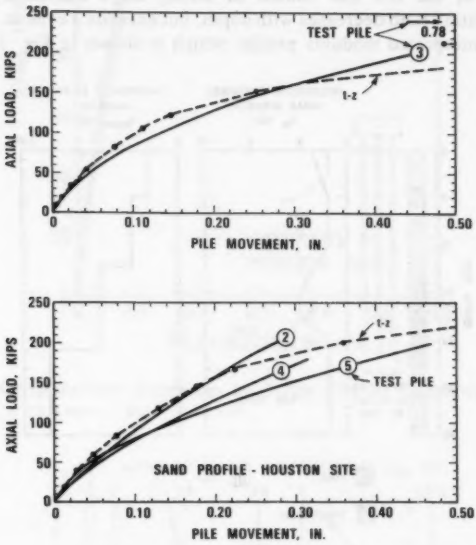

FIG. 10.—Load-Displacement Responses for Piles at Houston Test Site (1 in. = 25.4 mm; 1 kip = 4.45 kN)

greater than z_{max} was arbitrarily neglected. The load-displacement (Q-z) curve at the pile tip was computed using Eq. 7 with $E = E_{max}$ for values of Q up to 0.25 Q_{ult}, $E = 0.5\,E_{max}$ for $Q = 0.5\,Q_{ult}$, $E = 0.25\,E_{max}$ for $Q = Q_{ult}$, and straight line segments at intermediate points on the Q-z curve. A Poisson's ratio of 0.3 was used to convert G to E.

Load-Displacement Curves.—The measured and computed load-displacement curves are compared (Fig. 10). The computed results compare well with the measured data.

University of Houston Site

Pile and Soil Conditions.—A comprehensive testing program was conducted

in 1979 and 1980 at a site on the University of Houston Campus to study the performance of single piles and groups of piles driven into stiff, overconsolidated clays (14). Eleven 10.75-in. (279-mm) diameter closed end pipe piles were driven to 43-ft (13.1-m) penetration; nine in a square group with a 2.75-ft (0.84-m) center-to-center spacing; and two single piles located about 12 ft (3.7 m) from the center of the group and on opposite sides of the group. The geometry of the pile group and pile properties are shown in Fig. 11. Details of the instrumentation, installation, and testing are given by O'Neill (14) and are not repeated here. The piles were incrementally loaded at about 20, 82, and 110 days after installation. Measured and predicted results are compared for the first test.

The soils at the test site consist of strong clays and sandy clays. The overconsolidation ratio decreases with depth, but exceeds 3 even at 50-ft (15.3-m) depth. The interpreted modulus profile, which is shown in Fig. 11, was based

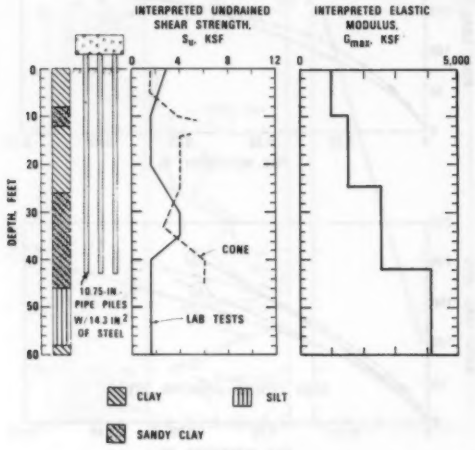

FIG. 11.—Soil Conditions at University of Houston Test Site (1 ft = 0.305 m; 1 kip/sq ft = 47.9 kN/m^2)

on cross-hole data. The interpreted shear strength profile was based primarily on unconsolidated-undrained tests, as the method used to predict pile capacity is based on this kind of strength test. The cone data, however, revealed a trend in the strength profile different from the laboratory data, as shown in Fig. 11. This difference would not affect the estimate of shaft resistance with the procedure used to compute pile capacity, but the difference would affect the estimate of end bearing.

An undrained shear strength of 6 kips/sq ft (287 kN/m^2) was used to compute the ultimate end bearing resistance. The average shaft friction was taken from local experience as 1 kips/sq ft (48 kN/m^2). The shaft friction was assumed to increase linearly with depth from zero at the ground surface.

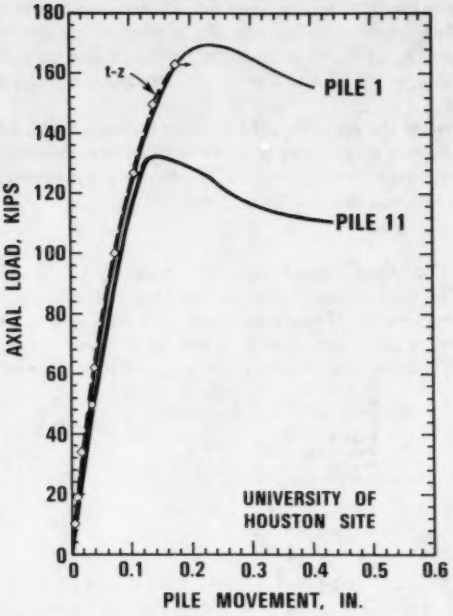

FIG. 12.—Load-Displacement Responses for Single Piles at University of Houston Test Site (1 in. = 25.4 mm; 1 kip = 4.45 kN)

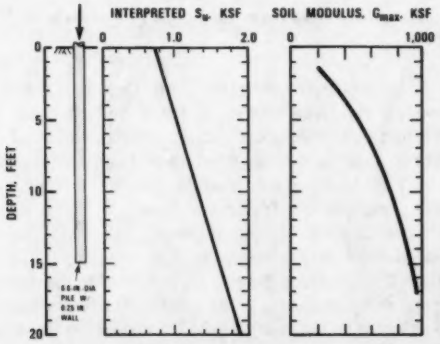

FIG. 13.—Soil Conditions at Hendon Site (1 ft = 0.305 m; 1 kip/sq ft = 47.9 kN/m^2)

The t-z curves were generated with Eq. 5 using an R_f of 0.9 and the soil modulus profile in Fig. 11. The development of the t-z curves arbitrarily neglected any loss of shear resistance for pile displacements greater than z_{max}. The load-displacement (Q-z) curve at the pile tip was taken as a binlinear curve using Eq. 7 with $q_b = q_b|_{max}$ and $E = E_{max}$ to compute Z_{max}. A Poisson's ratio of 0.5 was used.

Load-Displacement Curves.—Fig. 12 compares the measured load-displacement responses for the two single piles with the computed response. The measured and predicted responses at working loads are in excellent agreement. The predicted ultimate load is between the measured ultimate loads.

Hendon Site

Pile and Soil Conditions.—Load tests were made by Cooke, Price, and Tarr (2) on 6.6-in. (168-mm) diameter piles jacked 15 ft (4.6 m) into a stiff London clay at a site in Hendon, North London. Single piles and a pile group were tested. The piles in the group were in a line at a center-to-center spacing of 3 pile diameters. The two exterior piles of the group were load tested incrementally

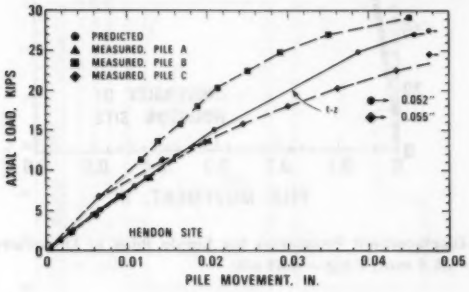

FIG. 14.—Load-Displacement Responses for Single Pile at Hendon Site (1 in. = 25.4 mm; 1 kip = 4.45 kN)

to failure, but the other tests were at working loads. Details of the instrumentation, installation, and testing are given by Cooke, Price, and Tarr (2).

The soil at the test site consists of stiff, overconsolidated London clay. Interpreted profiles of undrained shear strength and soil modulus at small strains are summarized in Fig. 13. The soil modulus profile was estimated with the empirical equations presented by Hardin and Drnevich (7).

The ultimate pile capacity was computed using s_u of 1.6 kips/sq ft (77 kN/m^2) at the pile tip, an average shaft friction of 0.94 kips/sq ft (45 kN/m^2), and a distribution of shaft friction along the pile proportional to the undrained strength profile. The average shaft friction and its distribution were based on the load test data. The procedures used to compute the t-z curves followed those described for the University of Houston site.

Load-Displacement Curves.—Fig. 14 compares the load-displacement response for three piles tested individually to working loads. The predicted and measured results were in excellent agreement for working load conditions. The measured

response of the two piles tested to failure were not in exact agreement with the predictions. These differences could have been caused by differences in the loading history and installation details between the two piles. Overall, the predicted and measured results were in good agreement.

Pile Group Tests.—Analyses were also made to compare computed and measured response of pile groups at the University of Houston site and Hendon site. The computer program PILGP1, which uses *t-z* curves to model pile response, was used with a shear modulus at small strains to account for the interaction effects (15). PILGP1 adjusts input single pile *t-z* curves for the interaction effects to account for group behavior. The predicted results were in general agreement with observed results.

Concluding Comments

Any assessment of the accuracy of the theoretical models must consider variability and accuracy of measured results as well as limitations of the theoretical models and our ability to define the input to the models. Variations in soil conditions across a site and in installation details of piles as well as changes in soil properties with time (consolidation, thixotropic and seasonal effects, and load history) can result in variations of ±30% in the measured displacement at working loads for supposedly identical piles. For example, load tests on four 6-in. (152-mm) diameter timber piles driven 20 ft (6.1 m) into a Bangkok clay show a variation of ±27% from the mean of the measured pile movement at a working load (safety factor of 2) (1). The variation in measured ultimate capacity can also be large as shown by the tests in Bangkok clay as well as the results in Fig. 12.

Accuracy of the measured data is affected by the care exercised in taking readings, the resolution and stability of the instrumentation, and the movement of the reference points. The emphasis and interest in production pile tests are with capacity more than pile movements. Therefore, the accuracy of the displacement readings in production pile tests may not always be sufficient to evaluate the analytic models. The cases used in this study to test the theoretical model were, with the exception of the pile tests in sand at a Houston site, for research studies where the accuracy of the measured displacements were thought to be quite reliable.

Predicted and measured load-displacement curves were generally in good agreement. Improvements are still needed, however, to: (1) Define the distribution and magnitude of the ultimate load transfer along the pile shaft and at the pile tip; (2) predict the soil movements (and, thus, negative shaft friction) caused by consolidation as excess pore pressure, which is induced with pile installation, dissipates (especially in soft clays); (3) incorporate the effects of soil creep; (4) evaluate changes in soil properties when piles are installed in sands; and (5) evaluate group efficiencies, especially if load-displacement predictions are needed at loads near failure.

The theoretical *t-z* curves described here can provide reasonable estimates of the load-displacement response of single piles and pile groups, especially for working loads. These mathematical tools should be used with judgment and knowledge of their limitations. The areas identified as needing further improvements provide a guide to these limitations. Our understanding of both

the limitations and attributes of the theories will improve as we gain more experience with their use and make efforts to compare predicted and measured results.

Appendix I.—References

1. Brand, E. W., Muktabhant, C., and Taechathummarak, A., "Load Tests on Small Foundations in Soft Clay," *Proceedings, Specialty Conference on Performance of Earth and Earth-Supported Structures,* ASCE, Purdue Univ., Vol. I, Part 2, June 1–14, 1972, pp. 903–928.
2. Cooke, P. W., Price, G., and Tarr, K., "Jacked Piles in London Clay: a Study of Load Transfer and Settlement Under Working Conditions," *Geotechnique,* Vol. 29, No. 2, June, 1979, pp. 113–147.
3. Coyle, H. M., and Reese, L. C., "Load Transfer for Axially Loaded Piles in Clay," *Journal of the Soil Mechanics and Foundations Division,* ASCE, Vol. 92, No. SM2, Mar., 1966, pp. 1–26.
4. Coyle, H. M., and Sulaiman, I. H., "Skin Friction for Steel Piles in Sand," *Journal of the Soil Mechanics and Foundations Division,* ASCE, Vol. 93, No. SM6, Nov., 1967, pp. 261–278.
5. Desai, C. S., and Holloway, D. M., "Load-Deformation Analysis of Deep Pile Foundations," *Proceedings, Symposium on Applications of the Finite Element Method in Geotechnical Engineering,* Desai, C. S., ed., U.S. Army Engineers, Waterways Experiment Station, Vicksburg, Miss., Sept., 1972, pp. 629–656.
6. Grosch, J. J., and Reese, L. C., "Field Tests of Small-Scale Pile Segments in a Soft Clay Deposit Under Repeated Loading," *Proceedings, 12th Offshore Technology Conference,* Houston, Tex., Vol. 4, May, 1980, pp. 143–151.
7. Hardin, B. O., and Drnevich, V. P., "Shear Modulus and Damping in Soils: Design Equations and Curves," *Journal of the Soil Mechanics and Foundations Division,* ASCE, Vol. 98, No. SM7, July, 1972, pp. 667–692.
8. Holloway, D. M., "Mechanics of Pile-Soil Interaction in Cohesionless Soil," thesis presented to Duke University, at Durham, N.C., in 1975, in partial fulfillment of the requirements for the degree of Doctor of Philosophy.
9. Holmquist, D. V., and Matlock, H., "Resistance-Displacement Relationships for Axially-Loaded Piles in Soft Clay," *Proceedings, 8th Offshore Technology Conference,* Houston, Tex., Vol. 1, May 3–6, 1976, pp. 553–569.
10. Kezdi, A., "The Bearing Capacity of Piles and Pile Groups," *Proceedings, 4th International Conference on Soil Mechanics and Foundation Engineering,* London, Vol. 2, Aug., 1957, pp. 46–51.
11. Kulhawy, F. H., and Peterson, M. S., "Behavior of Sand-Concrete Interfaces," *Proceedings, 6th Pan American Conference on Soil Mechanics and Foundation Engineering,* Lima, Peru, Vol. 2, 1979, pp. 225–236.
12. Ladd, C. C., and Edgers, L., "Consolidated-Undrained Direct-Simple Shear Tests on Saturated Clays," *Research Report 72–82,* Soils Publication 284, Dept. of Civ. Engrg., Massachusetts Inst. of Tech., Cambridge, Mass., 1972.
13. Meyerhof, G. G., "Composition of Sands and Bearing Capacity of Piles," *Journal of the Soil Mechanics and Foundations Division,* ASCE, Vol. 85, No. SM6, Part 1, June, 1959, pp. 1–29.
14. O'Neill, M. W., "Mechanical Modeling and Field Testing of Full Sized Pile Group," Chapter 5, University of Houston, Interim Report to the Federal Highway Administration, Offices of Research and Development, Washington, D.C., Mar., 1979.
15. O'Neill, M. W., *Program PILGP1 User's Guide,* Univ. of Houston, Civ. Engrg. Dept., Houston, Tex., 1980.
16. Parker, F., Jr., and Reese, L. C., "Experimental and Analytical Studies of Behavior of Single Piles in Sand Under Lateral and Axial Loading," *Research Report 117-2,* Center for Highway Research, The University of Texas, Austin, Tex., 1970.
17. Randolph, M. F., Carter, J. P., and Wroth, C. P., "Driven Piles in Clay—The Effects of Installation and Subsequent Consolidation," *Geotechnique,* Vol. 29, No. 4, Apr., 1979, pp. 361–393.
18. Randolph, M. F., and Wroth, C. P., "Analysis of Deformation of Vertically Loaded

Piles," *Journal of the Geotechnical Engineering Division*, ASCE, Vol. 104, No. GT12, Dec., 1978, pp. 1465–1488.
19. Seed, H. B., and Reese, L. C., "The Action of Soft Clay Along Friction Piles," *Transactions*, ASCE, Vol. 122, 1957, pp. 731–754.
20. Timoshenko, S. P., and Goodier, J. N., *Theory of Elasticity*, McGraw-Hill Book Co., New York, N.Y., 1970.
21. Vesic, A. S., *Principles of Pile Foundation Design*, Soil Mechanics Series No. 38, Duke University, Durham, N.C., 1975.
22. Vijayvergiya, V. N., "Load-Movement Characteristics of Piles," *4th Symposium of Waterway, Port, Coastal and Ocean Division*, ASCE, Long Beach, Calif., Vol. 2, 1977, pp. 269–284.

Appendix II.—Notation

The following symbols are used in this paper:

D = tip diameter;
D_r = relative density;
E = Young's modulus of soil;
E_{max} = E at small strains;
G = shear modulus of soil;
G_{ave} = average G for equivalent homogeneous conditions;
G_∞ = shear modulus at small strains and remote from pile;
G_i = shear modulus at small strains;
I_b = influence coefficient;
l = length of pile;
M_o = modulus ratio of soil at pile shaft;
Q = pile tip force;
Q_{ult} = ultimate Q;
q_b = stress on pile tip;
R_f = empirical parameter of a hyperbolic model;
r = radial distance;
r_m = radius of zone of influence;
r_o = pile radius;
s_u = undrained shear strength of soil;
t = shear stress along pile;
t_{max} = maximum t;
t_{res} = t at large z;
z = axial pile displacement;
z_s = axial pile displacement at pile shaft;
z_{max} = z at max t;
Δz_e = elastic rebound;
Δz = $\delta_z - \Delta z_e$;
δ_z = shear displacement from peak to residual conditions in direct shear test;
ν = Poisson's ratio of soil;
ρ = ratio of soil shear moduli at depths $l/2$ and l;
τ = shear stress;
τ_o = shear stress at pile shaft;
τ_{max} = max shear resistance; and
ψ = $\tau_o R_f / \tau_{max}$.

SEEPAGE FROM FREE WATER ABOVE IMPERMEABLE TAILINGS

By Lewis T. Isaacs[1] and Bruce Hunt[2]

INTRODUCTION

Tailings are the residue from the treatment of ore after the recoverable values have been removed. Coarse, dry tailings are usually stacked on a tailings dump, while the fine material is pumped as a slurry to a tailings pond or dam where the waste material settles. Free water from the slurry, and from any runoff from the catchment area upstream of the tailings dam, may be ponded above the tailings. The dam embankment is usually constructed of readily available materials which can include spoil from strip mining and dried tailings. Conventional practices and typical dams are described by Casagrande and McIver (3), Klohn (8), and in a number of contributions in Aplin and Argall (1).

Seepage analyses of tailings dams may be done for a number of reasons. The analyses are used to estimate the amount of water leaving a tailings structure as seepage water, to determine pore pressures for stability analysis, to estimate the exit point and the seepage velocities. Methods for seepage analysis of tailings dams are discussed by Osler (9), Galpin (4), Swaisgood and Toland (13), and Pettibone and Kealy (10).

Because of the wide range of materials that occur as tailings and embankment materials, the conditions for seepage analyses vary from situations in which the permeability of the tailings is much greater than that of the embankment, to situations in which the reverse is true. It is good practice to manage a tailings dam in such a way that the tailings deposits slope away from the embankment, and the pond of free water is not in contact with the embankment. This reduces the seepage discharge into the embankment and improves its stability. However, it may not be possible to guarantee this condition, and a designer may have to consider the possibility of the pond water being in contact with the embankment. When the tailings are impermeable relative to the bank, the seepage analysis requires an estimate of the seepage discharge from the free water into the embankment. An approximate solution for this discharge has been given by Thomson and Rodin (14). Another approximate solution is the "half triangular

[1]Sr. Lect., Dept. of Civ. Engrg., Univ. of Queensland, Brisbane, Australia.
[2]Reader, Dept. of Civ. Engrg., Univ. of Canterbury, Christchurch, New Zealand.

Note.—Discussion open until April 1, 1982. To extend the closing date one month, a written request must be filed with the Manager of Technical and Professional Publications, ASCE. Manuscript was submitted for review for possible publication on October 10, 1980. This paper is part of the Journal of the Geotechnical Engineering Division, Proceedings of the American Society of Civil Engineers, ©ASCE, Vol. 107, No. GT11, November, 1981. ISSN 0093-6405/81/0011-1563/$01.00.

ditch" solution in which the discharge is assumed to equal half the discharge from a triangular ditch. The discharge for a triangular ditch can be determined from the calculations of Vedernikov (5).

This paper describes a proposed model for the entry region of the discharge from free water above impermeable tailings, and presents an analytical solution based on the model. The results are compared with those of Thomson and Rodin (14), and with the "half triangular ditch" solution. An experimental investigation is described, and experimental and theoretical results are compared. The application of the theory and the results to design studies is examined.

Proposed Model

When the tailings are impermeable, seepage discharge enters the embankment through the part of the embankment face in contact with the free water. Under gravity, the water falls as unsaturated flow to the saturated zone at the bottom of the embankment (Fig. 1). In the proposed model, it is assumed that the flow in the entry zone is saturated and that this region controls the discharge. The side boundaries of the entry zone are surfaces where the pore pressure is zero relative to atmospheric pressure. In the core of the flow, the pore pressures at the top of the entry zone are positive, and transition to unsaturated flow under gravity occurs at the bottom of the entry zone when the pore pressures become nearly zero throughout the core. In the analytical solution, this boundary was located at minus infinity, and the results are applicable only when the saturated region at the bottom of the embankment is some distance below the entry region.

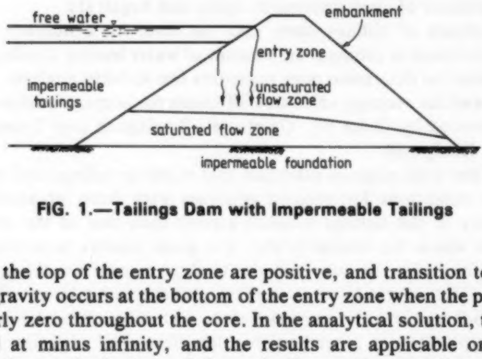

FIG. 1.—Tailings Dam with Impermeable Tailings

Problem Formulation

The problem for which a solution is sought is shown in Fig. 2. It is assumed that saturated, two-dimensional seepage occurs within the region $D_\infty CBAD_\infty$, that the embankment is homogeneous and isotropic, and that Darcy's law applies. The complex potential function is defined by

$$w(z) = \phi(x,y) + i\psi(x,y) \qquad (1)$$

in which $z = x + iy$; $i = \sqrt{-1}$; x,y = Cartesian coordinates; ψ = stream function; and the velocity potential, ϕ, is defined by

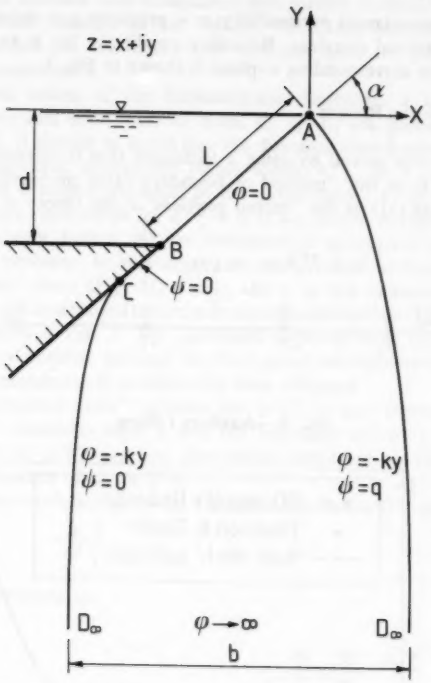

FIG. 2.—Entry-Zone Model in z-Plane

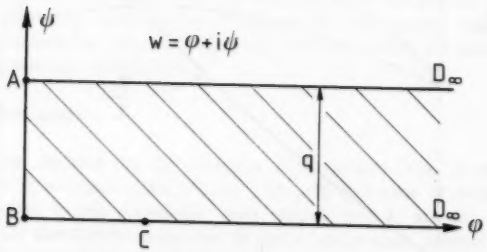

FIG. 3.—Complex Potential Plane

$$\phi(x,y) = -k\left(\frac{p}{\rho g} + y\right) \quad \text{(2)}$$

in which k = embankment permeability; p = pressure; ρ = water mass density; and g = gravitational constant. Boundary conditions for ϕ and ψ are shown in Fig. 2, and the corresponding w-plane is shown in Fig. 3.

Problem Solution and Results

The problem was solved by using a technique that is referred to by Aravin and Numerov (2) as the "method of boundary-value problems," or by Polubarinova-Kochina (11) as the "mixed problem of the theory of functions." In

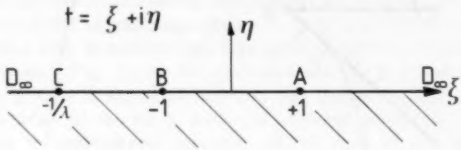

FIG. 4.—Auxiliary t-Plane

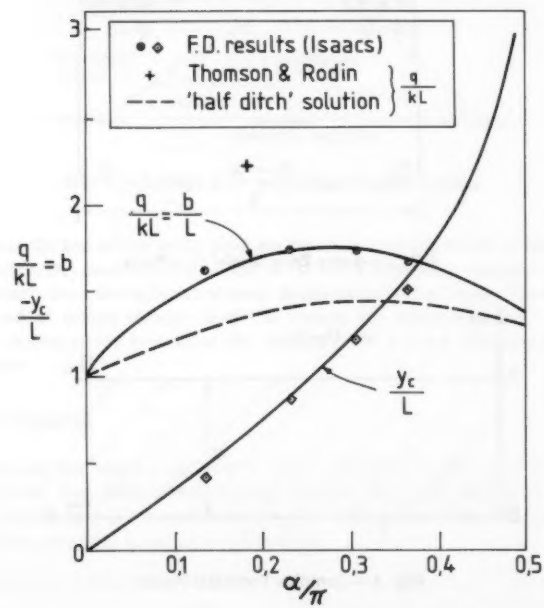

FIG. 5.—q/kL, y_c/L, and b/L Plotted as Functions of α/π

this application, the method proceeded by mapping the w-plane in Fig. 3 into the lower half of an auxiliary t-plane, which is shown in Fig. 4. Then a Riemann-Hilbert problem was formulated and solved to obtain an expression for the Zhukovskii function in the t-plane. Thus, the mapping function for w, and the solution for the Zhukovskii function, gave the problem in terms of a complex parameter, t.

The calculated values of the dimensionless discharge, q/kL, and of the dimensionless vertical coordinate of point C, y_c/L, are plotted as functions of α/π in Fig. 5. It should be noted that the dimensionless discharge is identical with the dimensionless, asymptotic plume width, b/L, as $y \rightarrow -\infty$ since the flux velocity has a magnitude equal to the permeability, k, as $y \rightarrow -\infty$. Plots of the free surfaces calculated for $\alpha/\pi = 0.23$ are shown in Fig. 2.

One of the writers, Isaacs, (6) has presented an alternative approach to the solution of the problem. In this approach, the problem is formulated on the complex potential plane (Fig. 3), with x and y as the unknown variables. A finite difference method is used to compute numerical solutions. The four solutions obtained are shown in Fig. 5. The agreement between these results, and those from the complex variable method, are very good and indicate that the correct solution to the mathematical problem has been obtained.

The "half triangular ditch" solution for q/kL is also shown in Fig. 5. In this solution, C coincides with B and the boundary for $\psi = 0$ is a vertical line. The values of q/kL are less than those calculated by the writers, with a maximum difference of about 19%.

The approximate solution given by Thomson and Rodin (14) is

$$\frac{q}{k} = 4d \quad \text{(3)}$$

which may be rewritten as

$$\frac{q}{kL} = 4 \sin \alpha \quad \text{(4)}$$

We sought further details of their work and were informed that Eq. 3 was based on flow net and electrical analogue solutions for $\alpha/\pi = 0.187$, which gives a result about 27% larger than the corresponding value from our results.

These checks and comparisons suggest that the correct solution to the formulated problem has been obtained, and that the results are accurate enough for most engineering calculations.

Anisotropic Embankment

The symbols defined for the isotropic embankment (Fig. 2) are used with a bar for the anisotropic embankment. The principal axes of permeability are assumed parallel to the coordinate axes, and $\bar{k}_x$ and $\bar{k}_y$ are the permeability coefficients for the directions parallel to the $\bar{x}$- and $\bar{y}$-axes, respectively.

The transformation from the $\bar{x}$-$\bar{y}$ plane to an isotropic x-y plane is given by

$$x = \left(\frac{\bar{k}_y}{\bar{k}_x}\right)^{1/2} \bar{x}, \; y = \bar{y} \quad \text{(5)}$$

This transformation leaves vertical distances and $p/\rho g + y$ the same on both planes.

The slope of the upstream face, the length of the wetted surface, and the permeability coefficient for the transformed problem are

$$\alpha = \tan^{-1}\left[\left(\frac{\bar{k}_x}{k_y}\right)^{1/2} \tan \bar{\alpha}\right] \quad \ldots\ldots\ldots\ldots\ldots\ldots\ldots\ldots\ldots\ldots (6)$$

$$L = \bar{L}\frac{\sin \bar{\alpha}}{\sin \alpha} \quad \ldots\ldots\ldots\ldots\ldots\ldots\ldots\ldots\ldots\ldots\ldots\ldots\ldots\ldots (7)$$

$$k = (\bar{k}_x \bar{k}_y)^{1/2} \quad \ldots\ldots\ldots\ldots\ldots\ldots\ldots\ldots\ldots\ldots\ldots\ldots\ldots\ldots (8)$$

The transformation (Eq. 5) and the choice for k (Eq. 8) are such that the discharge for the anisotropic problem, $\bar{q}$, equals the discharge for the isotropic problem, q. The value for q ($= \bar{q}$) is found from Fig. 5 for the values of α, L, and k obtained from Eqs. 6–8.

Experimental Investigation

An experimental investigation was carried out in the apparatus shown in elevation in Fig. 6. The dimension normal to this view was 1.09 ft (333 mm). The choice of a material to model the embankment was influenced by the condition that: (1) The capillary fringe was to be as small as possible; (2) the seepage flow had to be laminar so that Darcy's law was valid; and (3) a homogeneous material was required.

There was a conflict between (1) and (2) because the capillary fringe could be reduced by an increase in particle size, but an increase in particle size would have increased the seepage velocity. The material chosen was a well-graded, medium-to-coarse sand which was estimated to be about the upper limit of grain size for laminar flow. The measured capillary rise for this material was approximately 1.6 in. (40 mm). The sand was carefully placed in layers of approximately 6 in. (150 mm). It was compacted with a vibrator during placing to prevent settlement when the seepage experiments were run. A perspex plate was used to model the impermeable layer, and a sealant was applied around the edges of the plate to prevent leakage.

Air trapped in the sand voids presented considerable difficulties during the experimental investigation. The presence of air in the voids near the surface was observed to cause large, approx 50%, increases in the depth for any given discharge because of the reduction in the effective permeability. The results presented in Fig. 7 were obtained under conditions in which the air had been removed.

It was decided that the best values for the permeability coefficients of the model embankment would be obtained from an in situ test. A steady-state test was run in which the upper water level covered all the sand, and the lower water level was above the top level of the outlet from the sand. Under these conditions, saturated seepage occurred throughout the sand. The seepage heads at 16 positions were measured with piezometers attached to tappings in the side wall. The experimental values of seepage head were compared with the contours of seepage head obtained from three finite element analysis, with k_x/k_y

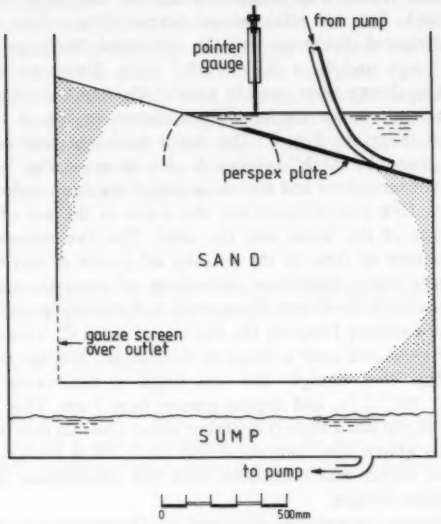

FIG. 6.—Experimental Apparatus

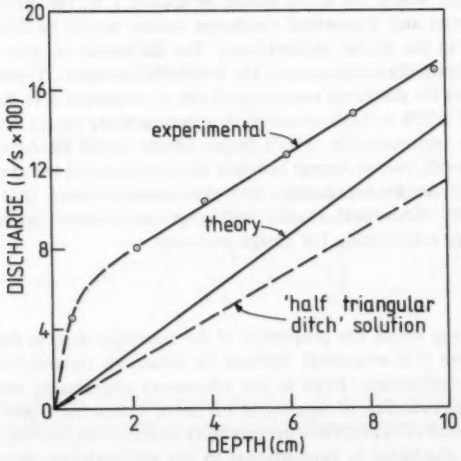

FIG. 7.—Experimental Results for Discharge Versus Depth

ratios 1.0, 2.25, and 4.0. The best overall agreement between the experimental and the analytical results was obtained when the analytical results for $k_x/k_y = 2.25$ were used. For this ratio, actual permeability values were calculated from the experimental discharge and the analytical discharge and yielded $k_x = 1.64 \times 10^{-3}$ m/s and $k_y = 0.73 \times 10^{-3}$ m/s. These permeability values and the preceding theory were used to predict the depth-discharge relationship for this embankment under the conditions shown in Fig. 2. The result was the line marked *theory* in Fig. 7. The depth-discharge relationship predicted from the "half triangular ditch" solution is also shown in Fig. 7.

Experimental observations and measurements were done under the conditions shown in Fig. 6. Dye was injected into the water at the top of the plate, and where the surface of the water met the sand. The dye movement confirmed the expected pattern of flow in the vicinity of points A and C (Fig. 2), and showed that there was a significant movement of water through the capillary fringe, which rose some 35–40 mm above point A. It was not possible to determine the extent of the capillary fringe in the vicinity of point C. Values for discharge and depth were measured over a range of discharges, and the measured values are shown in Fig. 7. A straight line was fitted to the results for discharges greater than 8×10^{-2} L/s, and depths greater than 2 cm. This line was above the theoretical line and had a slightly different slope. The fact that the experimental straight line was above the theoretical line and, when extrapolated, did not pass through the origin was consistent with the observation of a significant flow in the capillary fringes.

While the difference between experimental and theoretical values was relatively large at the experimental scale, the amount of discharge through the capillary fringe would remain relatively constant as the depth increased. Therefore, under field conditions, where the depth would be approx 1 m, the difference between the experimental and theoretical discharge values would be about 2% for the material used in the model embankment. The difference in slope was probably caused by errors in the assessment of the permeability values. The theory indicates that the slope of the discharge versus depth line is proportional to the permeability, and an error of ±20% in the determination of permeability values in this experiment would not be unreasonable. Much larger errors could be expected for field situations. Overall, the agreement between the experimental and theoretical results was considered to be acceptable, and the writers believe that the proposed model and the theoretical results will give satisfactory predictions of the depth-discharge relationship for design purposes.

Applications

In most tailings dams, the properties of the materials used in the embankment are variable and it is extremely difficult to obtain an accurate estimate of the permeability coefficients. Even in the laboratory experiment described in this paper there was evidence of significant variation within the model embankment, and the evaluation of appropriate permeability coefficients proved difficult. Since the computed discharge is proportional to the permeability, it may be argued that an overly sophisticated analysis cannot be justified in most design situations. The theoretical analysis has shown that q/kL lies between 1.5 and 1.7 over most of the range of α/π. Therefore, for design purposes, the use of q/kL

= 1.6 will generally be sufficiently accurate.

The theory is applicable only if the saturated zone at the bottom of the embankment is some distance below the level of the free water surface (Fig. 1). The writers' opinion is that the theory may be used when the top of the saturated zone is more than about $5d$ below the free water surface.

In general, there will also be some seepage through the railings into the embankment. If this seepage discharge is judged to be significant, it should be estimated by an analysis of the tailings and added to the discharge from the free water. The saturated zone at the bottom of the embankment should be analyzed for the combined discharge.

Mathematical Details

A straightforward application of the Schwartz-Christoffel transformation gives the mapping of the w-plane upon the t-plane as

$$w = q\left[\frac{1}{\pi}\ln\left(t + \sqrt{t^2 - 1}\right) + i\right] \quad \ldots\ldots\ldots\ldots\ldots\ldots\ldots\ldots\ldots\ldots (9)$$

in which q = two-dimensional flow rate. The real and imaginary parts of Eq. 9 give expressions for ϕ and ψ, respectively, in the lower half of the t-plane.

The Zhukovskii function, $\theta(t) = \theta_1(\xi,\eta) + i\,\theta_2(\xi,\eta)$, is defined as

$$\theta = w - ikz \quad \ldots\ldots\ldots\ldots\ldots\ldots\ldots\ldots\ldots\ldots\ldots\ldots\ldots\ldots (10)$$

Since $\phi + ky = 0$ along CD_∞ and AD_∞, and since $y\cos\alpha - x\sin\alpha = 0$ along ABC, the problem for $\theta(t)$ reduces to finding a function that is analytic in the lower half of the t-plane, and that satisfies the following boundary conditions along the real axis:

$$\theta_1(\xi,0) = 0 \left(-\infty < \xi < \frac{-1}{\lambda},\ 1 < \xi < \infty\right) \quad \ldots\ldots\ldots\ldots\ldots\ldots (11)$$

$$\theta_1(\xi,0)\cos\alpha + \theta_2(\xi,0)\sin\alpha = qG(\xi) \quad \left(\frac{-1}{\lambda} < \xi < 1\right) \quad \ldots\ldots\ldots\ldots (12)$$

The function $G(\xi)$ is continuous with a discontinuity in its derivative at $\xi = -1$, and can be calculated from Eqs. 9 and 10 in the form

$$G(\xi) = \frac{\cos\alpha}{\pi}\ln\left(-\xi + \sqrt{\xi^2 - 1}\right) \quad \left(\frac{-1}{\lambda} < \xi < -1\right)$$

$$= \frac{\sin\alpha}{\pi}\left(\sin^{-1}\xi + \frac{\pi}{2}\right) \quad (-1 < \xi < 1) \quad \ldots\ldots\ldots\ldots\ldots\ldots (13)$$

The Reimann-Hilbert problem given by Eqs. 11–12 for $\theta(t)$ can be reduced to a Dirichlet problem by using an auxiliary function defined as

$$F(t) = \left(t + \frac{1}{\lambda}\right)^{-\alpha/\pi}(t-1)^{-1+\alpha/\pi} \quad \ldots\ldots\ldots\ldots\ldots\ldots\ldots\ldots (14)$$

in which α = embankment slope. Thus, Eqs. 11–14 show that the product

$\theta(t)\,F(t)$ is analytic in the lower t-plane and vanishes as $|t| \to \infty$, and that the real part of this product satisfies the following boundary conditions along the real axis:

$$\text{Re}\,[\theta(\xi)\,F(\xi)] = 0 \quad \left(-\infty < \xi < \frac{-1}{\lambda},\ 1 < \xi < \infty\right)$$

$$= -q|F(\xi)|\,G(\xi), \quad \left(\frac{-1}{\lambda} < \xi < 1\right) \ldots\ldots\ldots\ldots\ldots\ldots\ldots\ldots\ldots\ldots (15)$$

The general solution of a Dirichlet problem in a lower half plane is given by

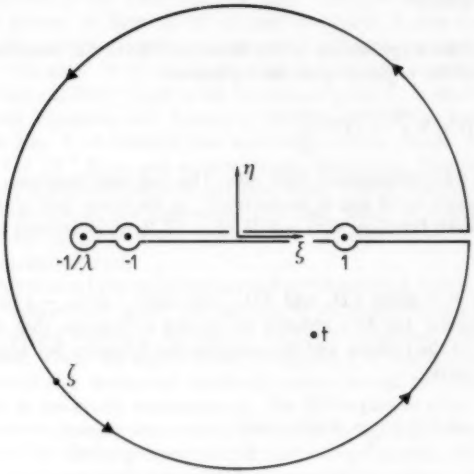

FIG. 8.—Integration Contour used to Obtain Eq. 11

Polubarinova-Kochina (11), and the use of Eq. 15 in that result gives

$$\theta(t)\,F(t) = \frac{q}{\pi i}\int_{-1/\lambda}^{1} \frac{|F(\xi)|\,G(\xi)}{\xi - t}\,d\xi \ldots\ldots\ldots\ldots\ldots\ldots\ldots\ldots\ldots\ldots (16)$$

The symbol $|F(\xi)|$ denotes the magnitude, or modulus, of the complex function $F(t)$ on the real axis. Eq. 16 gives the solution for $\theta(t)$ once the unknown constants q and λ have been calculated.

Eq. 16 can be rewritten in an alternative way by integrating the function $F(\zeta)\ln(\zeta + \sqrt{\zeta^2 - 1})/(\zeta - t)$ around the contour shown in Fig. 8. This leads to the identity

$$\int_{-1/\lambda}^{-1} \frac{|F(\xi)|\,G(\xi)}{\xi - t}\,d\xi = \cot^2\alpha \int_{-1}^{-1} \frac{|F(\xi)|\,G(\xi)}{\xi - t}\,d\xi$$

$$- \cot\alpha \int_1^\infty \frac{|F(\xi)|}{\xi - t}\, d\xi - F(t)\cot\alpha\, [\ln(t + \sqrt{t^2-1}) + i\pi] \quad \ldots\ldots\ldots (17)$$

Thus, Eq. 17 can be used to rewrite Eq. 16 in the form

$$\theta(t)\,F(t) = \frac{q}{\pi i}\left\{\csc^2\alpha \int_{-1}^{1} \frac{|F(\xi)|\,G(\xi)}{\xi - t}\, d\xi - \cot\alpha \int_1^\infty \frac{|F(\xi)|}{\xi - t}\, d\xi \right.$$

$$\left. - F(t)\cot\alpha\, [\ln(t + \sqrt{t^2-1}) + i\pi]\right\} \quad \ldots\ldots\ldots\ldots\ldots\ldots (18)$$

Eq. 18 is a useful alternative to Eq. 16 when $t \to -1/\lambda$.

Construction of the velocity hodograph for this problem shows that

$$\underset{\substack{t\to -1\\ \lambda}}{\text{Limit}} \frac{dz}{dw} = -\frac{(\cot\alpha + i)}{k} \quad \ldots\ldots\ldots\ldots\ldots\ldots\ldots\ldots (19)$$

Thus, Eqs. 9, 10 and 19 give

$$\underset{\substack{t\to -1\\ \lambda}}{\text{Limit}} \frac{d\theta}{dt} = \underset{\substack{t\to -1\\ \lambda}}{\text{Limit}} \frac{dw}{dt}\left(1 - ik\frac{dz}{dw}\right) = \frac{i\,q\cot\alpha}{\pi\sqrt{\dfrac{1}{\lambda^2 - 1}}} \quad \ldots\ldots\ldots (20)$$

Inspection of Eq. 18 shows that it will give the correct result when substituted into Eq. 20 if, and only if,

$$\csc^2\alpha \int_{-1}^{1} \frac{|F(\xi)|\,G(\xi)}{\xi + \dfrac{1}{\lambda}}\, d\xi - \cot\alpha \int_1^\infty \frac{|F(\xi)|}{\xi + \dfrac{1}{\xi}}\, d\xi = 0 \quad \ldots\ldots\ldots\ldots (21)$$

Eq. 21 allows λ to be calculated as a function of α.

An expression for q/kL can also be obtained from Eq. 18 by setting $w = 0$; $z = -Le^{i\alpha}$; $\theta = iLke^{i\alpha}$; and $F(t) = |F(-1)|e^{i(\pi-\alpha)}$ as $t \to -1$. This leads to the result

$$\frac{q}{kL} = \frac{\pi|F(-1)|}{\left[\csc^2\alpha \displaystyle\int_{-1}^{1} \frac{|F(\xi)|\,G(\xi)}{\xi + 1}\, d\xi - \cot\alpha \int_1^\infty \frac{|F(\xi)|}{\xi + 1}\, d\xi\right]} \quad \ldots\ldots\ldots (22)$$

Thus, Eq. 22 allows q/kL to be calculated as a function of α.

Finally, parametric equations of the free surface coordinates along CD_∞ and AD_∞ can be calculated by letting $t \to \xi$ for $-\infty < \xi < -1/\lambda$ and $1 < \xi < \infty$ in Eqs. 9, 10 and 16 after setting $w = -ky$ and $w = -ky + iq$, respectively. This leads to the result

$$\frac{yk}{q} = \frac{-1}{\pi}\ln(|\xi| + \sqrt{\xi^2 - 1}) \quad \left(-\infty < \xi < \frac{-1}{\lambda}\; 1 < \xi < \infty\right) \quad \ldots\ldots\ldots (23)$$

$$\frac{xk}{q} = 1 + \frac{1}{\pi F(\xi)} \int_{-1/\lambda}^{1} \frac{|F(\xi')|\, G(\xi')}{\xi' - \xi}\, d\xi' \quad (1 < \xi < \infty)$$

$$= \frac{-1}{\pi |F(\xi)|} \int_{-1/\lambda}^{1} \frac{|F(\xi')|\, G(\xi')}{\xi' - \xi}\, d\xi' \quad \left(-\infty < \xi < \frac{-1}{\lambda}\right) \quad \ldots\ldots\ldots\ldots \quad (24)$$

The variable ξ' in Eq. 24 is a dummy integration variable.

Numerical Evaluation

One of the most difficult parts of the analysis consisted of calculating numerical values for the singular integrals. Infinite limits of integration were converted to finite limits by using the change in variable $\xi = 1/\xi'$. Then a few of the simpler integrals were computed by using a Taylor's series expansion of the integrands. However, most of the integrals were computed by a process known as "subtracting the singularity." This relatively little-used method is explained by Scheid (12) and Kantorovich and Krylow (7) and will be shown herein by considering

$$I = \int_{-1}^{1} \frac{|F(\xi)|\, G(\xi)}{\xi + \frac{1}{\lambda}}\, d\xi \quad \ldots\ldots\ldots\ldots\ldots\ldots\ldots\ldots\ldots\ldots\ldots\ldots \quad (25)$$

The integrand has a singularity as $\xi \to 1$

$$\frac{|F(\xi)|\, G(\xi)}{\xi + \frac{1}{\lambda}} \sim \frac{\sin\alpha}{\left(1 + \frac{1}{\lambda}\right)^{1+\alpha/\pi} (1-\xi)^{1+\alpha/\pi}} \left[1 - \frac{\sqrt{2}}{\pi} (1-\xi)^{1/2} \right.$$

$$\left. + \frac{1 + \frac{\alpha}{\pi}}{1 + \frac{1}{\lambda}} (1-\xi) - \frac{\sqrt{2}}{\pi} \left(\frac{1}{12} + \frac{1 + \frac{\alpha}{\pi}}{1 + \frac{1}{\lambda}} \right) (1-\xi)^{3/2} + \ldots \right] \quad \ldots\ldots\ldots \quad (26)$$

and an infinite derivative as $\xi \to -1$

$$\frac{|F(\xi)|\, G(\xi)}{\xi + \frac{1}{\lambda}} \sim \frac{\sin\alpha}{\pi (2)^{1/2 - \alpha/\pi} \left(\frac{1}{\lambda} - 1 \right)^{1+\alpha/\pi}} (\xi + 1)^{1/2} + \ldots \quad \ldots\ldots\ldots \quad (27)$$

The right sides of Eqs. 26–27 can be subtracted from the integrand of Eq. 25, and then the result of integrating the right sides of Eqs. 26–27 can be added to obtain the exact result

$$I = \int_{-1}^{1} f(\xi)\,d\xi + \frac{\sin\alpha}{\left(1+\frac{1}{\lambda}\right)^{1+\alpha/\pi}}\left[\frac{(2)^{\alpha/\pi}}{\frac{\alpha}{\pi}} - \frac{(2)^{1+\alpha/\pi}}{\pi\left(\frac{1}{2}+\frac{\alpha}{\pi}\right)} + \frac{(2)^{1+\alpha/\pi}}{1+\frac{1}{\lambda}}\right.$$

$$\left. - \left(\frac{\frac{1}{12}+\frac{1+\frac{\alpha}{\pi}}{1+\frac{1}{\lambda}}}{\pi\left(\frac{3}{2}+\frac{\alpha}{\pi}\right)}\right)(2)^{2+\alpha/\pi}\right] + \frac{(2)^{1+\alpha/\pi}\sin\alpha}{3\pi\left(\frac{1}{\lambda}-1\right)^{1+\alpha/\pi}} \quad \ldots\ldots\ldots \quad (28)$$

The function $f(\xi)$ is given by

$$f(\xi) = \frac{|F(\xi)|\,G(\xi)}{\xi+\frac{1}{\lambda}} - \frac{\sin\alpha}{\left(1+\frac{1}{\lambda}\right)^{1+\alpha/\pi}(1-\xi)^{1-\alpha/\pi}}\left[1 - \frac{\sqrt{2}}{\pi}(1-\xi)^{1/2}\right.$$

$$\left. + \frac{1+\frac{\alpha}{\pi}}{1+\frac{1}{\lambda}}(1-\xi) - \frac{\sqrt{2}}{\pi}\left(\frac{1}{12}+\frac{1+\frac{\alpha}{\pi}}{1+\frac{1}{\lambda}}\right)(1-\xi)^{3/2}\right]$$

$$- \frac{\sin\alpha}{\pi(2)^{1/2-\alpha/\pi}\left(\frac{1}{\lambda}-1\right)^{1+\alpha/\pi}}(\xi+1)^{1/2} \quad \ldots\ldots\ldots\ldots\ldots \quad (29)$$

Since $f(\xi)$ and its first derivative are both finite at $\xi = -1$, and at $\xi = 1$, low-order quadrature formula, such as the trapezoidal rule or Simpson's rule, can be used to approximate the integral in Eq. 28. Furthermore, since the remaining terms in Eq. 28 are the leading terms in a Taylor's series evaluation of Eq. 21, the approximate value of the integral in Eq. 28 is only a small portion of the numerical value of I. In fact, the relative contribution of the integral in Eq. 28 becomes negligible as $\alpha \to 0$, which means that the use of Eq. 28 leads to an approximate calculation of I that becomes more accurate as the strength of the singularity in the integrand of Eq. 25 increases.

Summary and Conclusions

A model has been proposed for the entry zone of seepage into an embankment from free water above impermeable tailings. A theoretical solution for this model for two-dimensional, isotropic, Darcy flows has been presented, and the transformation required if the theory is to be applied to anisotropic embankments has been given.

The results of an experimental study indicate that the theory will yield

reasonably accurate estimates of the discharge provided that the field conditions are close to the conditions assumed in the model.

Appendix I.—References

1. Aplin, C. L., and Argall, G. O., eds., "Tailing Disposal Today," *Proceedings First International Tailing Symposium*, Tuscon, Ariz., 1972.
2. Aravin, V. I., and Numerov, S. N., *Theory of Fluid Flow in Undeformable Porous Media*, Chapter 8, (translated by A. Moscana), printed in Jerusalem by S. Monson, 1965.
3. Casagrande, L., and McIver, B. N., "Design and Construction of Tailings Dams," *Stability in Open Pit Mining*, G. O. Brawner, and V. Milligan, eds., American Institute of Mining, Metallurgical, and Petroleum Engineers, Inc., New York, N.Y., 1971, pp. 181–203.
4. Galpin, A. L., "The Control of Water in Tailings Ponds," *Geotechnical Practice for Stability in Open Pit Mining*, C. O. Brawner, and V. Milligan, eds., American Institute of Mining, Metallurgical, and Petroleum Engineers, Inc., New York, N.Y., 1971, pp. 173–195.
5. Harr, M. E., *Groundwater and Seepage*, McGraw-Hill, New York, N.Y., 1962.
6. Isaacs, L. T., "Numerical Solution of a Special Seepage Infiltration Problem," *Research Report No CE17*, Department of Civil Engineering, University of Queensland, Brisbane, Australia, Sept., 1980.
7. Kantorovich, L. V., and Krylov, V. I., *Approximate Methods of Higher Analysis*, (Translated by C. D. Benster), P. Noordhoff Ltd., Groningen, 1958, pp. 528–534.
8. Klohn, E. J., "Tailings Dams in British Columbia," *Geotechnical Practice for Stability in Open Pit Mining*, C. O. Brawner, and V. Milligan, eds., American Institute of Mining, Metallurgical, and Petroleum Engineers, Inc., New York, N.Y., 1971, pp. 151–171.
9. Osler, J. C., "Stability Investigations for Tailings Dams," *Geotechnical Practice for Stability in Open Pit Mining*, C. O. Brawner, and V. Milligan, American Institute of Mining, Metallurgical, and Petroleum Engineering, Inc., New York, N.Y., 1971, pp. 107–124.
10. Pettibone, H. C., and Kealy, C. D., "Engineering Properties of Mine Tailings," *Journal of Soil Mechanics and Foundations Division*, ASCE, Vol. 97, No. SM9, 1971, pp. 1207–1225.
11. Polubarinova-Kochina, P. Ya., Chapter 6, *Theory of Ground Water Movement*, (translated by J. M. R. de Wiest), Princeton University Press, Princeton, N.J., 1962.
12. Scheid, F., Chapter 16, *Numerical Analysis, Schaum's Outline Series in Mathematics*, McGraw-Hill, New York, N.Y., 1968.
13. Swaisgood, J. R., and Toland, G. C., "The Control of Water in Tailings Structures," *Proceedings First International Tailing Symposium*, C. L. Aplin, and G. O. Argall, eds., Tuscon, Ariz., 1972, pp. 138–163.
14. Thomson, G. M., and Robin, S., *Colliery Spoil Tips—After Aberfan*, Institute of Civil Engineering, London, 1972.

Appendix II.—Notation

The following symbols are used in this paper:

b = asymptotic width of saturated plume;
d = depth of free water;
g = gravity constant;
k = permeability coefficient (isotropic);
k_x, k_y = permeability coefficients for directions parallel to x- and y-axes;
L = length of wetted face of embankment;
p = pressure relative to atmospheric pressure;

q = two-dimensional seepage discharge;
t = $\xi + i\eta$;
u = horizontal component of velocity;
V = magnitude of velocity vector;
v = vertical component of velocity;
w = complex potential;
x = horizontal distance from origin;
y = vertical distance from origin;
z = $x + iy$;
α = slope of upstream face of embankment;
λ = dummy variable defined in Fig. 4;
ζ = dummy variable of integration;
η, ξ = Cartesian coordinates;
θ = $w - ikz$;
ξ' = dummy integration variable;
ρ = density of water;
ϕ = velocity potential, real part of w; and
ψ = stream function, imaginary part of w.

A bar superscript is used to distinguish values that apply to an anisotropic plane, e.g. $\bar{x}$, $\bar{y}$, $\bar{q}$.

DISCUSSION

Note.—This paper is part of the Journal of the Geotechnical Engineering Division, Proceedings of the American Society of Civil Engineers, ©ASCE, Vol. 107, No. GT11, November, 1981. ISSN 0093-6405/81/0011-1581/$01.00.

Discussions

Discussions may be submitted on any Proceedings paper or technical note published in any *Journal* or on any paper presented at any Specialty Conference or other meeting, the *Proceedings* of which have been published by ASCE. Discussion of a paper/technical note is open to anyone who has significant comments or questions regarding the content of the paper/technical note. Discussions are accepted for a period of 4 months following the date of publication of a paper/technical note and they should be sent to the Manager of Technical and Professional Publications, ASCE, 345 East 47th Street, New York, N.Y. 10017. The discussion period may be extended by a written request from a discusser.

The original and three copies of the Discussion should be submitted on 8-1/2-in. (220-mm) by 11-in. (280-mm) white bond paper, typed double-spaced with wide margins. The length of a Discussion is restricted to two *Journal* pages (about four typewritten double-spaced pages of manuscript including figures and tables); the editors will delete matter extraneous to the subject under discussion. If a Discussion is over two pages long it will be returned for shortening. All Discussions will be reviewed by the editors and the Division's or Council's Publications Committees. In some cases, Discussions will be returned to discussers for rewriting, or they may be encouraged to submit a paper or technical note rather than a Discussion.

Standards for Discussions are the same as those for Proceedings Papers. A Discussion is subject to rejection if it contains matter readily found elsewhere, advocates special interests, is carelessly prepared, controverts established fact, is purely speculative, introduces personalities, or is foreign to the purposes of the Society. All Discussions should be written in the third person, and the discusser should use the term "the writer" when referring to himself. The author of the original paper/technical note is referred to as "the author."

Discussions have a specific format. The title of the original paper/technical note appears at the top of the first page with a superscript that corresponds to a footnote indicating the month, year, author(s), and number of the original paper/technical note. The discusser's full name should be indicated below the title (see Discussions herein as an example) together with his ASCE membership grade (if applicable).

The discusser's title, company affiliation, and business address should appear on the first page of the manuscript, along with the *Proceedings* paper number of the original paper/technical note, the date and name of the *Journal* in which it appeared, and the original author's name.

Note that the discusser's identification footnote should follow consecutively from the original paper/technical note. If the paper/technical note under discussion contained footnote numbers 1 and 2, the first Discussion would begin with footnote 3, and subsequent Discussions would continue in sequence.

Figures supplied by the discusser should be designated by letters, starting with A. This also applies separately to tables and references. In referring to a figure, table, or reference that appeared in the original paper/technical note use the same number used in the original.

It is suggested that potential discussers request a copy of the *ASCE Authors' Guide to the Publications of ASCE* for more detailed information on preparation and submission of manuscripts.

Soil-Bentonite Slurry Trench Cutoffs[a]

Discussion by S. A. Jefferis[2]

The author has presented some very interesting data on the behavior of soil-bentonite cutoffs. In particular, the concept of filter cake permeability to thickness ratio, k_c/t_c provides a most useful design parameter. However, it may be of interest that some additional theory on filtration of slurries can be used to link and extend the data presented.

Using the filtration model presented by Nash, Eq. 3, it can be shown that the volume of filtrate, V, obtained up to time, t, during formation of a filter cake of area, A, is given by

$$V = C(h,b)At^{1/2} + v \quad \ldots\ldots\ldots\ldots\ldots\ldots\ldots\ldots\ldots\ldots\ldots\ldots\ldots\ldots (3)$$

in which $C(h,b)$ is a function of h, the formation head and b, a more general variable used to describe the type, condition, and concentration of the bentonite slurry. $C(h,b)$ is independent of time and thus can be regarded as a constant for tests on a given slurry under a constant formation head. The term v is not obtained from the theory but is included to represent the small excess flow which sometimes occurs in practice during the first moments of filtration. v is often attributed to the flow necessary to establish a filter cake. For times greater than about one minute, Eq. 3 has been found to hold very well in practice. Differentiating Eq. 3 gives the flow rate through the cake dV/dt. Substituting this into Darcy's law then gives

$$\frac{k_c}{t_c} = \frac{C(h,b)}{2h}\, t^{-1/2} \quad \ldots\ldots\ldots\ldots\ldots\ldots\ldots\ldots\ldots\ldots\ldots\ldots\ldots\ldots (4)$$

If, during a cake formation test, V is recorded as a function of time, $C(h,b)$ can be evaluated from Eq. 3. Eq. 4 can then be used to calculate k_c/t_c for any formation time. In this way, k_c/t_c can be obtained directly from cake formation tests. Thus, it is not necessary to use the full procedure outlined by the author of forming the cake for the required time, decanting excess slurry, and then permeating the cake with water under constant head. The fact that during a cake formation test there is slurry above the cake, and that during permeation there is just water, will not affect the value of k_c/t_c obtained, as filter cake formation is controlled by the permeation of water through the existing cake. Strictly, if the author's procedure is used, the same head should be used for formation and permeation. If the heads are significantly different, the value of k_c/t_c could be affected. Perhaps the author could confirm that comparable heads were used in his tests.

The validity of Eq. 4 can be checked by replotting the author's data from

[a]April, 1980, by David J. D'Appolonia (Proc. Paper 15372).

[2]Lecturer in Civ. Engrg., King's College London, London, England.

Fig. 7 as k_c/t_c against $t^{-1/2}$ for constant formation heads. Fig. 16 shows the replotted data. As far as possible, the author's actual data points have been used. Where data have been obtained from the interpolated curves, the corresponding points in Fig. 16 are shown surrounded by a dotted circle. From Fig. 16 it can be seen that the agreement with Eq. 4 is very good with the slight exception of the 24 hr data. This could imply a breakdown in the theory for long formation times, but this seems unlikely as the fit at 16 hr is still good and the fit for the one point at 48 hr is also good.

While the value of k_c/t_c will obviously depend on the type of bentonite and its concentration, etc., the dependence of k_c/t_c on $t^{-1/2}$ may, in part, explain the relatively narrow practical limits for it found by the author (5×10^{-9} sec to 25×10^{-9} sec^{-1}). A factor of 5 for k_c/t_c corresponds to a factor of

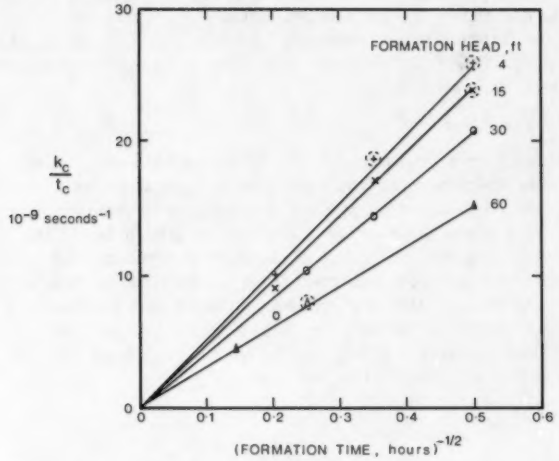

FIG. 16.—Replotted Data for Relationship Between Filter Cake Permeability and Cake Formation Pressure and Time

25 for formation time (e.g., this could be changed from 50 hr to 2 hr).

The author states that filtrate loss, as measured under the standard American Petroleum Institute conditions, is not a useful design parameter. This is in agreement with the writer's experience. Filtrate loss can be related to k_c/t_c (a paper is currently being prepared which includes this analysis), but even this provides little further information relevant to practice.

The author's observations, that the downstream filter cake may be lost when the cutoff is put into service, but that the upstream cake is normally stable, are most interesting. During formation (excavation), the cakes may be subjected to a head comparable to that which they will experience in service (especially if allowance is made for the head loss across the soil-bentonite fill). Also, after formation, the cakes will gain in strength due to thixotropic gelation of the bentonite. Thus, from a desk study, one could conclude that the downstream

cake should be stable. In contrast, the upstream cake might be expected to be unstable, as any consolidation of the soil-bentonite fill under the applied hydraulic gradient could allow movement and possible rupture of the cake.

APPENDIX.—REFERENCE

1. Nash, Kevin L., "Stability of Trenches Filled with Fluids," *Journal of the Construction Division*, ASCE, Vol. 100, No. CO4, Proc. Paper 11006, Dec., 1974, pp. 533–542.

CONE PENETRATION IN SOIL PROFILING[a]

Discussion by Marius Roy[4]

The authors have presented an interesting approach to describing the clay behavior and, in particular, the degree of overconsolidation on the base that the ratio u/q_c close to one should be associated with normally consolidated clays and lower values occuring at high OCR. Also, they have shown that u/q_c decreases as the cone angle decreases. Therefore, in order to experimentally define a good relationship between u/q_c and the OCR, it is appropriate to comment on the use of the ratio u/q_c in the function of the geometry and location of the porous element on the pore pressure probe.

The piezometer probes developed by Wissa, et al. (31), and Torstensson (27), bear a striking resemblance in their shape (Fig. 9). However, as there is a small difference in the shape and in the location of the porous element behind the lower end of the cone, the writer presumes the magnitude of pore pressures measured with these apparati will be different. On the other hand, if the cone resistance and pore pressures are not measured simultaneously, it will be more difficult to establish reliably good predictions of the OCR in practice.

During the last few years, the writer has worked to solve these problems and has built an apparatus called a "piezo-penetrometer" to investigate the soil properties of sensitive clays. The basic aim of the piezo-penetrometer is the simultaneous measurement of cone resistance and pore pressures when the apparatus is pushed down at a constant rate of penetration. The instrument consists of the well-known Fugro penetrometer, developed in Holland by de Ruiter (7), fitted with a porous pore pressure pick up and transducer. The point has the classical shape of a cone with an apex of 60° and a base area of 100 mm^2. It has a straight cylindrical shaft above the point with the same diameter as the base of the conical tip. The pore pressure is measured by a pore pressure transducer installed between the cone tip and the load cell. The piezo-penetrometer is equipped with a detachable point in order to easily

[a] April, 1980, by Mohsen M. Baligh, Vitoon Vivatrat, and Charles C. Ladd (Proc. Paper 15377).

[4] Prof. of Civ. Engrg., Université Laval, Québec, Canada.

vary the position of the pore pressure pick up and to study the pattern of pore pressure generation at or above the cone tip.

Five types of tips were used in this study, and details are presented in Fig. 10. The three tips identified as PPA, DPA, and PPS are fitted with a filter in the cone tip, while the two other tips, PA or PS and RA are equipped with a cylindrical filter installed immediately above the cone and about one diameter above the cone, respectively. The results obtained on the well-known St. Alban test site and reported by Roy, et al. (32), show that maximum pore pressures are measured with the tips PPA, DPA, and PPS as the result of the strong deformation required to let the piezo-penetrometer penetrate the intact clay. Pore pressures measured with the tip RA correspond to the new stress condition along the shaft after the failure was developed around the conical part of the piezo-penetrometer. Tip PA-PS measures pore pressures prevailing

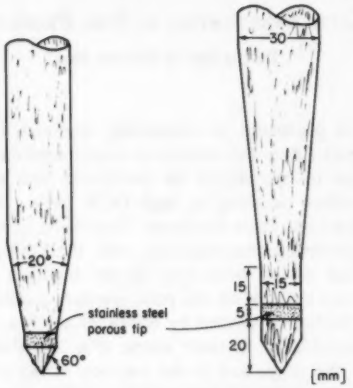

a) After Wissa et al (1975). b) After Torstensson (1975).

FIG. 9.—Schematic Drawing of Pore Pressure Probe, (*a*) after Wissa, et al., (1975); (*b*) after Torstensson, (1975)

in the transition zone between the failure zone around the cone and the disturbed zone around the shaft.

The magnitude of the pore pressure to cone resistance ratio, u/q_c, was calculated by using the pore pressure results obtained with the tips PPA, DPA, and PPS, the tip PA or PS and the tip RA, and the average of the cone resistance profile (side friction is nearly zero in the St. Alban sensitive clay). The average values u/q_c of 0.56, 0.51, and 0.41 respectively indicate a large variation in the function of the location of the porous element of the piezo-penetrometer. It is well indicated from the results of the authors and the writer that the magnitude of pore pressures during penetration varies with the shape of the tip and the location of the porous element on the probe. Therefore, it seems important to note that a soil profiling should be established with an appropriate tip in order to measure the maximum pore pressures induced during the driving, i.e. those measured in the failure zone of the intact clay around the tip. Also,

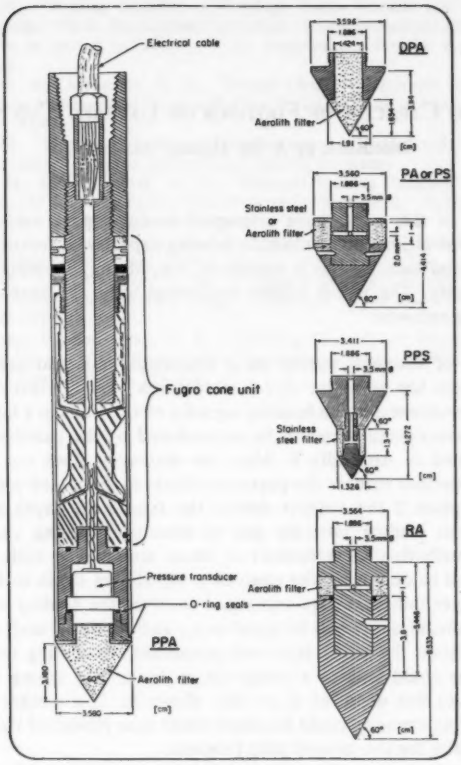

FIG. 10.—Details of Piezo-Penetrometer

the shape should correspond to the recommended standard for the cone penetration test (CPT) presented to the Tokyo Conference in 1977.

APPENDIX.—REFERENCE

33. Roy, M., Tremblay, M., Tavenas, F., and LaRochelle, P., "Induced Pore Pressures in Static Penetration Tests in Sensitive Clay," Preprint volume, 33rd Canadian Geotechnical Conference, Sept. 24–26, 1980, Calgary, Canada.

Bearing Capacity of Footings on Layered C-ϕ Soils[a]

Discussion by A. M. Hanna,[3] M. ASCE

The authors of this paper have attempted to develop an empirical method for the numerical estimation of ultimate bearing capacity of footings on layered soils. The method incorporates a variety of simplifying assumptions that may reduce its validity. The writer wishes to discuss some of these assumptions, in the following sections:

1. The case of footings resting on a foundation material consisting of a multilayer system has been the object of research over the last two decades. The authors' statement that the bearing capacity of C-ϕ soils in a layered system has not been investigated seems to be contradicted by the existence of several publications listed in Appendix I. Also, the statement does not bring to the attention of interested readers the previous efforts to the stated problem.

2. In Assumption 2 the authors define the significant depth as the depth to which the net loading intensity due to structural loading can produce a perceptible contribution to settlement or shear stress. The authors proposed Eq. 7 to be used to determine the equivalent significant depth in layered soils. If the upper layer thickness, z_1, was equal to twice the footing width, B, the equivalent significant depth will be equal to z_1, and design of such a foundation will depend only on the upper layer soil properties. According to the writer's test results, this could lead to a conservative design if a strong soil layer or rockbed underlies this depth of $Z_1(=2B)$. However, if a weaker layer exists below, the bearing capacity could be much lower than predicted by the authors' method, especially for the case of strip footings.

3. The writers have some reservations about the use of shear box test results which have no theoretical verification in predicting the ultimate bearing capacity of square or circular footings. Also, the size of the testing box and footing models seemed to be very small.

In conclusion, the writer wishes to suggest that a purely empirical method in geotechnical engineering is acceptable provided that the method is first compared with all available test results, and tested with some field data before it be recommended for the designer.

Appendix.—References

6. Brown, J. D., and Meyerhof, G. G., "An Experimental Study of the Ultimate Bearing Capacity of Layered Clay Foundations," *Proceedings*, Seventh International Conference on Soil Mechanics and Foundation Engineering, Mexico, Vol. 2, 1969, pp. 45–51.

[a]July, 1980, by B. Satyanarayana and R. K. Garg (Proc. Paper 15578).

[3]Assoc. Prof., Concordia Univ., Civ. Engrg. Dept., 1455 De Maisonneuve West, Montreal, Quebec, Canada H3G-1M8.

7. Hanna, A. M., "Bearing Capacity of Footings Under Vertical and Inclined Loads on Layered Soils," Ph.D. thesis presented to Nova Scotia Technical College, at Halifax, N.S, in 1978, in partial fulfillment of the requirements for the degree of Doctor of Philosophy.
8. Hanna, A. M., and Meyerhof, G. G., "Design Charts for Ultimate Bearing Capacity of Foundations on Sand Overlying Soft Clay," *Canadian Geotechnical Journal*, No. 17, 1980, pp. 300–303.
9. Hanna, A. M., "Bearing Capacity of Foundations on a Weak Sand Layer Overlying a Strong Deposit," *Canadian Geotechnical Journal* (in press).
10. Hanna, A. M., and Meyerhof, G. G., "Ultimate Bearing Capacity of Foundations on a Three-Layer Soil, with Special Reference to Layered Sand," *Canadian Geotechnical Journal*, No. 16, 1979, pp. 412–414.
11. Meyerhof, G. G., "Ultimate Bearing Capacity of Footings on Sand Layer Overlying Clay," *Canadian Geotechnical Journal*, No. 11, 1974, pp. 223–229.
12. Meyerhof, G. G., and Hanna, A. M., "Ultimate Bearing Capacity of Foundations on Layered Soils under Inclined Load," *Canadian Geotechnical Journal*, No. 15, 1978, pp. 565–572.
13. Satyanarayana, B., and Gray, R. K., "Bearing Capacity of Footings on Layered C-ϕ Soils," *Journal of the Geotechnical Engineering Division*, ASCE, Vol. 106, No. GT7, Proc. Paper 15578, pp. 819–824.

Resorcinolic Grout for Injecting Sandy Foundations[a]

Discussion by Anthony Noel James[3]

The authors have presented an interesting technical note describing an acid catalyzed resorcinol grout. The writer has several comments to make. First of all, the practical history of chemical grouts is rather longer than the authors indicate. Silicate grouts have been in use for 65 yr and the previous use of resorcinol formaldehyde (RF) grouts with both acid and alkaline catalysts was first described in patents (U.K. Patent 918,641, and amendment, 1963 to Soletanche Ltd.) Alkaline catalysed RF grouts, e.g., MQ 14, from Borden (UK) Ltd., typically contain 5%–10% of resorcinol, have low viscosities of about 2 cp at 20° C, and gel times ranging from about 20 min to a few hours. They set to form as very hard, durable, translucent pink solids. Formulation data is given in the aforementioned patent specification, but comparisons of technical properties and costs with the acid catalyzed grout described by the authors cannot be made because they give no mix compositions. The alkaline RF grouts certainly meet the aims expressed by the authors.

Acidic RF grouts were used successfully for grouting the Woolwich and Reading beds at Blackwall Tunnel in 1961 (14). The alkaline RF grouts used for grouting deep rock for mine shaft sinking in North Yorkshire (15) are highly exothermic and require special batching and proportioning arrangements to prevent premature gelation. Fig. 3 of the authors' paper suggests that the acidic RF grout is also exothermic. Furthermore, Resorcinol is highly dermatitic and requires great care in handling, as the authors indicate; its unreacted presence in the ground is also undesirable as potential toxic material (20).

Use of Grouts for Strengthening Ground.—It is undoubtedly possible to considerably increase the strength of granular deposits with selected chemical grouts and they have been used for this purpose in a number of cases (19). Nevertheless, designs which seek to use the high strength and durability of grouts such as RF must be considered with great care. Virtually all granular soils are heterogeneous and usually contain zones of low permeability such as fine silts, clayey silts, or clays which cannot be effectively impregnated with any form of grout. There have been several basic chemical grout formulations previously proposed for use in providing high strength. For example, high concentration sodium silicate grouts (16), urea-formaldehyde (U.K. Patent 876,441, 1960, Soil Mechanics Ltd.), and epoxy grouts (U.K. Patents 1,019,122 and 1,021,528, 1966, Shell.)

Chemical Grout Requirements.—The authors show that they are aware of some of the required properties of a satisfactory grout, but they do not clarify the restraints which currently apply in practical engineering. During the past

[a]October, 1980, by Arvind V. Shroff and Dhananjay L. Shah (Proc. Paper 15724).

[3]———, Binnie & Partners, Artillery House, Artillery Row, Westminster, London, England.

ten years, a number of authorities, c.f. (17), have placed severe limitations on the use of chemical grouts, largely because of their potential for polluting groundwater. Two examples may be cited:

1. Grouts such as AM-9 based on acrylamides have excellent technical properties (5). However, there are well-defined and very low limits for acrylamides in drinking water (21). Many authorities will no longer accept the risk of pollution by such grouts and their use has declined greatly in recent years.
2. Lignochromes first used for engineering purposes in 1957 (19) are prepared from lignosulphonates, sodium dichromate, and inorganic catalysts. They, too, are excellent and cheap chemical grouts and were used successfully for several major projects (13). Their use has since been in part discontinued because of fears of pollution by chromium. The acceptability of RF grouts must be in some doubt for similar reasons.

There are, in fact, very few penetrating, strong, durable, and economic grouts which would nowadays be accepted for the great majority of ground engineering projects. Of these, the most notable are the silicates, though there are some doubts about their durability. A further class is based on tannins and formaldehyde, of which commercial examples are manufactured in the form of "Geoseal" and "Terranier." These grouts tend to contain small particles which limit their use in fine-grained soils unless costly clarification procedures are used. A third class is the RF grouts which are also costly.

Mechanisms of Ground Strengthening.—The reaction of resorcinol with formaldehyde under alkaline conditions produces continuous hydro gels which fill the pore space of granular soils. The resultant product may be regarded as a matrix of set grout densely filled with sand. Indeed, the same description can be used for the majority of chemical grouts because they also set to form hydro gels.

There are two types of grout known to the writer which confer strength on the ground by depositing adhesive material at the contacts of the soil particles: They are (1) the more dilute urea-formaldehyde (UF) grouts; and (2) the special nonaqueous epoxy grouts of low viscosity described in the patent literature of oil well drilling. From the authors' description, it would seem that the acidic RF grouts behave similarly to the UF systems.

Further Comments.—No hydro gel chemical grout can satisfactorily endure dessicating conditions for any length of time in the ground and it is probably inadvisable to use RF grouts in these conditions. The hydrochloric acid RF grout described by the authors has a pH of 1.5–2.5. The writer would expect this grout to be very corrosive to the steels commonly used in field grouting equipment, especially to conventional grout pumps.

APPENDIX.—REFERENCES

13. Black, J. C., Kelland, J. D., "Cominco's Saskatchewan Potash Shafts," *Proceedings of the Ninth Commonwealth and Mining Congress* London, England, Vol. I, Mining and Metallurgy 1969, pp. 883–902.
14. Caron C., Deslisle J. P., et al., "Resin Grouting with Special Reference to the Treatment of Woolwich and Reading Beds at the New Blackwall Tunnel," Grouts & Drilling Muds in Engineering Practice, Butterworth, 1963.

15. Cleasley, J. V., Pearse, G. E., et al., "Shaft Sinking at Boulby Mine Cleveland Potash Ltd.," *Institute Mining & Metallurgy*, Vol. 85, 1975, pp. A7-A28.
16. Clough, Wayne G., Kück, W. M., et al., "Silicate-Stabilised Sands," *Journal of the Geotechnical Engineering Division*, ASCE, Vol. 106, No. GT1, Proc. Paper 14335, Jan., 1979, pp. 65–82.
17. European Standards for Drinking Water, Second Edition WHO, 1970.
18. Golden, J., Ouellete, R. P., et al., "Environmental Impact Data Book," *Anne Arbour Science*, 1979, pp. 462–480.
19. James, A. N., and Neelands, R. J., "Formulation and Selection of Chemical Grouts with Typical Examples of their Field Use," Grouts and Muds in Engineering Practice, Butterworth, 1963.
20. Russian Toxicological Data for Chemicals in Drinking Water, Technical Note No. 20, Central Water Planning Unit.
21. U.S. Food & Drug Administration Code of Federal Regulations, Title 21, Part 121, Washington, D.C., U.S. GPO 1967, p. 1092.

Resorcinolic Grout for Injecting Sandy Foundations[a]

Closure by Arvind V. Shroff[4] and Dhananjay L. Shah[5]

The writers would like to thank James for his interest in the paper and for his valuable comments.

The discusser has described Alkaline catalyzed RF grouts. From the experimental results of the writers (25), it is found that although the alkaline RF grouts possess low viscosities of about 2 cp at 20° C and gel times ranging from about 20 min to a few hours, they exhibit low gel strength and 5%–10% synerisis, which is not with acid RF grouts developed by the writers. Moreover, exothermic characteristics of acid catalyzed RF grout are 30%–40% less than alkaline catalysed RF grout.

As the writer's work is limited to academic interest, the efficacy of grouts for strengthening granular soils with zones of low permeability, such as fine silts and clayey silts in the field, has not been examined.

The effect of leached water from the grouted sand sample with resorcinolic grouts on fish life and the potability of water could be examined to conform with the relevant standards.

While the corrosion effect on the conventional grout pumps should be examined, currently, anticorrosion chemical pumps are widely employed in industry.

Appendix.—Reference

25. Shah, D., "Characteristics of Resorcinolic Formaldehyde Grouts," thesis presented to M.S. University of Baroda, at Baroda, India, in 1980 in partial fulfilment of the requirements for the degree of Master of Engineering.

[a]October, 1980, by Arvind V. Shroff and Dhananjay L. Shah (Proc. Paper 15724).
[4]Reader, Applied Mechanics Dept., Faculty of Tech. & Engrg., M.S. Univ., Baroda, India.
[5]Jr. Engr., Gujarat Engrg. Research Inst., Baroda, India.

Strength Anisotropy of Layered Soil System[a]

Errata

The following correction should be made to the original paper:

Page 1143, Paragraph 3, last line: Should read ". . . and sampling are . . ." instead of ". . . and sampling which are . . ."

[a]October, 1980, by M. Krishna Murthy, T. S. Nagaraj, and A. Sridharan (Proc. Paper 15724).

Technical Papers

Original papers should be submitted in triplicate to the Manager of Technical and Professional Publications, ASCE, 345 East 47th Street, New York, N.Y. 10017. Authors must indicate the Technical Division or Council, Technical Committee, Subcommittee, and Task Committee (if any) to which the paper should be referred. Those who are planning to submit material will expedite the review and publication procedures by complying with the following basic requirements:

1. Titles must have a length not exceeding 50 characters and spaces.

2. The manuscript (an original ribbon copy and two duplicate copies) should be double-spaced on one side of 8-1/2-in. (220-mm) by 11-in. (280-mm) paper. Three copies of all figures and tables must be included.

3. Generally, the maximum length of a paper is 10,000 word-equivalents. As an *approximation*, each full manuscript page of text, tables or figures is the equivalent of 300 words. If a particular subject cannot be adequately presented within the 10,000-word limit, the paper should be accompanied by a rationale for the overlength. This will permit rapid review and approval by the Division or Council Publications and Executive Committees and the Society's Committee on Publications. Valuable contributions to the Society's publications are not intended to be discouraged by this procedure.

4. The author's full name, Society membership grade, and a footnote stating present employment must appear on the first page of the paper. Authors need not be Society members.

5. All mathematics must be typewritten and special symbols must be identified properly. The letter symbols used should be defined where they first appear, in figures, tables, or text, and arranged alphabetically in an appendix at the end of the paper titled Appendix.—Notation.

6. Standard definitions and symbols should be used. Reference should be made to the lists published by the American National Standards Institute and to the *Authors' Guide to the Publications of ASCE*.

7. Figures should be drawn in black ink, at a size that, with a 50% reduction, would have a published width in the *Journals* of from 3 in. (76 mm) to 4-1/2 in. (110 mm). The lettering must be legible at the reduced size. Photographs should be submitted as glossy prints. Explanations and descriptions must be placed in text rather than within the figure.

8. Tables should be typed (an original ribbon copy and two duplicates) on one side of 8-1/2-in. (220-mm) by 11-in. (280-mm) paper. An explanation of each table must appear in the text.

9. References cited in text should be arranged in alphabetical order in an appendix at the end of the paper, or preceding the Appendix.—Notation, as an Appendix.—References.

10. A list of key words and an information retrieval abstract of 175 words should be provided with each paper.

11. A summary of approximately 40 words must accompany the paper.

12. A set of conclusions must end the paper.

13. Dual units, i.e., U.S. Customary followed by SI (International System) units in parentheses, should be used throughout the paper.

14. A practical applications section should be included also, if appropriate.